

Hierarchical Non-Archimedean Stability of Finite Discrete Dynamical Systems: A Variational Theory over Coordinate Orderings

J. Rogelio Pérez-Buendía^{1*} and Víctor Nopal-Coello²

^{1*}SECIHTI-CIMAT, Unidad Mérida, Mérida, Yucatán, Mexico.

²Universidad Autónoma del Estado de Hidalgo, Pachuca, Hidalgo, Mexico.

*Corresponding author(s). E-mail(s): rogelio.perez@cimat.mx;
Contributing authors: victor_nopal@uaeh.edu.mx;

Abstract

We develop a non-Archimedean reading of finite discrete dynamical systems in which the order chosen on the coordinates is itself a dynamical observable. For a map $\mathbf{f}: \mathbb{F}_p^N \rightarrow \mathbb{F}_p^N$, an ordering embeds the phase space into the p -adic integers, so that agreement in the first n coordinates means membership in a common ball of radius p^{-n} . Realizing \mathbf{f} as a compatible family of ball-level maps over \mathbb{C}_p , we attach to each fixed point scale-resolved indices of expansion, attraction, and invariance. We prove that these indices are computable from the finite data alone, the rational interpreter serving only as a theoretical device. The expansion index μ_E is a function on the symmetric group S_N , and minimizing it gives a variational principle that selects a coordinate hierarchy intrinsic to \mathbf{f} . On the Boolean *Arabidopsis thaliana* floral network ($N = 13$, $p = 2$) the minimizing ordering recovers the eight documented key regulators with Spearman $\rho = 1$, and an exact branch-and-bound search over all $13!$ orderings certifies the global optimum and its four symmetric minimizers. The resulting *A/E/I* words separate canalized cell fates from transient developmental states, a non-Archimedean analogue of Waddington's landscape.

Keywords: finite discrete dynamical systems, non-Archimedean dynamics, p -adic stability, multiscale dynamics, coordinate orderings, gene regulatory networks

MSC Classification: 11S82 , 37P20 , 37N25 , 92B05

1 Introduction

The classical descriptors of stability for a finite discrete dynamical system $f: \mathbb{F}_p^N \rightarrow \mathbb{F}_p^N$, such as topological entropy, Lyapunov exponents, and sensitivity coefficients, are invariant under permutations of the coordinates. Renaming the variables leaves them unchanged, so none of them can say which components govern the coarsest splittings of the state space and which only refine outcomes within an already committed regime. Many finite systems carry exactly this structure, an ordering of the variables into coarse and fine, layered or observed at different resolutions. The natural mathematical question is whether there exists an ordering-dependent stability functional on finite discrete dynamics whose minimizer is intrinsic to the map alone.

We answer this question through the non-Archimedean geometry of the p -adic integers. A choice of ordering π embeds \mathbb{F}_p^N into \mathbb{Z}_p by base- p expansion, so that two configurations agreeing in their first n ordered coordinates lie in a common ball of radius p^{-n} . The same map f acquires different multiscale behavior under different orderings, because the ultrametric decides which coordinates label the coarsest splittings. Realized through rational interpreters $\phi \in \mathbb{C}_p(z)$, whose existence rests on the ε -gluing of [1], the finite map becomes the level- N trace of a hierarchy of ball-level maps F_0, \dots, F_N , and each ball inherits an expanding, attracting, or isometric type from genuine non-Archimedean dynamics. The field \mathbb{C}_p is not optional here. Without it one could still define the common-prefix length $M_{n,m}$ as a combinatorial statistic, but there would be no reason to call $M_{n,m} < n$ expanding, nor to connect it to repelling dynamics. The discrete quantities are the computable shadow of a non-Archimedean structure that gives them their dynamical meaning.

We prove two results. First, although the stability indices are defined through the dynamics over \mathbb{C}_p , they are computable from the discrete data (f, ι) alone, the interpreter being a theoretical device rather than a computational requirement (Theorem 6.8). Second, the expansion index μ_E is a function on the symmetric group S_N , and minimizing it selects a coordinate hierarchy intrinsic to f , a variational principle over orderings.

We illustrate the content of μ_E on a minimal example. For elementary cellular automata on $N = 8$ cells with periodic boundary, the index μ_E is constant at its maximum value $(N-1)2^N$ across all $8!$ orderings for rules 30, 90, and 150, and strictly below it for rules 110 and 184 (exhaustive computation, Remark 6.4). Constancy at the maximum says the dynamics admits no intrinsic hierarchy, since every ball expands at every scale. Note that chaos does not predict saturation here: rule 30 is chaotic and saturates, while the Turing-complete rule 110 does not. Characterizing the boundary between the two regimes remains an open question.

Main results.

For every finite discrete dynamical system $f: \mathbb{F}_p^N \rightarrow \mathbb{F}_p^N$ with p prime, the stability measure $\mu = (\mu_E, \mu_A, \mu_I)$ and the ball-level A/E/I classification of fixed points are computable from the discrete data (f, ι) alone (Theorem 6.8). The associated variational problem

$$\text{Opt}(f) := \arg \min_{\pi \in S_N} \mu_E(\pi)$$

¹ selects an ordering π^* determined by the dynamics through the stability functional. On the *A. thaliana* floral GRN ($N = 13$, $p = 2$), this selected ordering agrees with the documented master-regulator ranking compiled in Table 4, with Spearman $\rho = 1$, and the four-scale A/E/I prefix separates floral organs (IEAA) from inflorescence (IEEE).

These conclusions rest on two structural results, proved in Sections 4–6:

- (T1) (*Computability from discrete data*; Theorem 6.8.) The triple (μ_E, μ_A, μ_I) and the ball-level classification of fixed points are intrinsic to (f, ι) : although defined analytically through rational interpreters $\phi \in \mathbb{C}_p(z)$ (Section 4), they are computable directly from the transition data without constructing any interpreter explicitly. The expansion functional admits the Haar-integral expression $\mu_E(\pi) = p^N \int_{\mathbb{Z}_p} \Phi_\pi d\lambda_H$ (Remark 6.12), where λ_H is the normalized Haar measure on \mathbb{Z}_p (the unique translation-invariant Borel probability measure, Section 2, Lemma 2.2) and $\Phi_\pi: \mathbb{Z}_p \rightarrow \mathbb{Z}_{\geq 0}$ counts the scales at which a state lies in an expanding ball under π .
- (T2) (*Level partition and the μ_E/μ_A trade-off*; Lemmas 6.2 and 6.3.) The A/E/I trichotomy partitions the p^n balls at every level, $E_\pi(n) + A_\pi(n) + I_\pi(n) = p^n$ (with $E_\pi(n)$, $A_\pi(n)$, $I_\pi(n)$ the number of expanding, contracting, and isometric balls at scale n under π , Section 6), so the three weighted scores share a fixed budget $\mu_E(\pi) + \mu_A(\pi) + \mu_I(\pi) = (N-1)p^N$. This budget is a bookkeeping constant set by N and p alone, the same for every map and every ordering, useful as a check on the computed scores. Its one substantive consequence is a trade-off: under the fixed budget, minimizing μ_E is equivalent to maximizing $\mu_A + \mu_I$, not to maximizing μ_A alone.

The scale-resolved word and the worked example.

The A/E/I classification assigns each fixed point a word in $\{A, E, I\}^{N-1}$ recording its local geometry across resolutions, and this partition assembles into a discrete p -adic analogue of Waddington’s landscape (Remark 6.13), in which canalized fates lie in contracting ball chains. This scale-resolved stability word is the genuinely new object, and no permutation-invariant or single-scale descriptor of the network produces it. On the Boolean *A. thaliana* floral network ($N = 13$, $p = 2$), the μ_E -minimizing ordering recovers the documented master-regulator hierarchy from the dynamics alone, with Spearman $\rho = 1$ (Section 7), a consistency check that the functional measures regulatory influence, while the A/E/I word separates floral organs (pattern IEAA) from inflorescence states (pattern IEEI). The framework is carried to *C. elegans* and *D. melanogaster*, with basin analysis, in the companion paper [2].

The construction joins three established lines of work, developed in detail in Section 8: non-Archimedean discrete dynamics and automata theory [3, 4], p -adic biology with its reading of balls as observation classes [5–8], and Boolean network theory with its projection and latent-variable readings of regulatory dynamics [9, 10]. Two configurations are indistinguishable at level n precisely when they lie in the same ball,

¹The operator $\arg \min$ returns the set of *arguments* (here orderings π) at which the minimum is attained. In general $\text{Opt}(f)$ is a set with $|\text{Opt}(f)| \geq 1$ (four elements for *A. thaliana*), and π^* denotes any chosen representative.

so the p -adic embedding equips the finite dynamics with a hierarchy of observational scales. Boolean models for *A. thaliana* [11, 12] provide the empirical benchmark. Main notation is collected in Table 1 (Section 2).

Outline.

The paper develops the framework in three movements. Sections 2–3 fix the minimal p -adic language (ultrametric balls, fixed-point theory, ε -approximation) and the discrete model on \mathbb{F}_p^N with the base- p encoding ι . Sections 4–6 build the apparatus: rational interpreters and their hierarchical approximations F_0, \dots, F_N , the ball-level $A/E/I$ classification of fixed points (§4), a worked toy example with $p = 2$, $N = 4$ in closed form (§5), and the stability measure μ together with the variational principle over orderings, including the cellular-automaton saturation analysis (§6). Section 7 carries the machinery to the *A. thaliana* floral GRN ($N = 13$), where π^* recovers the documented master-regulator hierarchy and the $A/E/I$ profile separates floral organs from inflorescence. Section 8 discusses scope, limitations, and comparison with existing methods. Section 9 summarizes.

2 Mathematical Preliminaries

The framework rests on the following p -adic foundations; standard references are [13–15]. Throughout, \mathbb{C}_p is the ambient field, complete and algebraically closed; it plays the role of \mathbb{C} in complex analysis, the canonical large field over which rational dynamics and fixed-point theory are available.

We recall the construction of \mathbb{Q}_p and \mathbb{C}_p , beginning from the rationals \mathbb{Q} . A *non-Archimedean absolute value* on \mathbb{Q} is a map $|\cdot|: \mathbb{Q} \rightarrow \mathbb{R}_{\geq 0}$ satisfying: $|x| = 0$ if and only if $x = 0$; $|xy| = |x||y|$; and the *strong triangle inequality* $|x + y| \leq \max(|x|, |y|)$. The *p -adic absolute values*, where p is a prime, are important examples: $|0|_p = 0$, and for $x \neq 0$ write $x = p^n \cdot (s/t)$ with s, t coprime to p ; then $|x|_p = p^{-n}$. This defines a non-Archimedean absolute value on \mathbb{Q} . For example, with $p = 2$ one has $|1|_2 = 1$, $|2|_2 = 1/2$, $|1/2|_2 = 2$, and $|3|_2 = 1$ (since 3 is coprime to 2, its 2-adic valuation is 0, so $|3|_2 = 2^0 = 1$); the 2-adic distance between 1 and 3 is $|1 - 3|_2 = |-2|_2 = 1/2$.

Any such absolute value induces a *metric* by $d(x, y) = |x - y|_p$; the strong triangle inequality implies that d is an *ultrametric*: every triangle is isosceles, with the two longest sides equal (see the “Ultrametric properties” paragraph below, or [13, 14]).

The *field of p -adic numbers* \mathbb{Q}_p is the completion of \mathbb{Q} with respect to $|\cdot|_p$. The *ring of p -adic integers* \mathbb{Z}_p is the closed ball of radius 1 and center 0 in \mathbb{Q}_p ; equivalently, $\mathbb{Z}_p = \{x \in \mathbb{Q}_p : |x|_p \leq 1\}$. Note that \mathbb{Z}_p is a commutative ring with unity and a subring of \mathbb{Q}_p . The field \mathbb{C}_p , the completion of the algebraic closure of \mathbb{Q}_p , serves as the p -adic analogue of \mathbb{C} ; its construction is recalled in the “Completions and \mathbb{C}_p ” paragraph below. (Throughout this paper, \mathbb{Z}_p denotes the ring of p -adic integers, *not* the cyclic group $\mathbb{Z}/p\mathbb{Z}$; for the finite field with p elements we write \mathbb{F}_p .)

Every $x \in \mathbb{Q}_p$ has a unique expansion $x = \sum_{i=N}^{\infty} a_i p^i$ with $a_i \in \{0, \dots, p - 1\}$ (for $x = 0$ one takes $N = 0$). In particular, every element of \mathbb{Z}_p has an expansion $x = \sum_{i \geq 0} x_i p^i$. The usual integers \mathbb{Z} embed into \mathbb{Z}_p via base- p expansion. For $p = 2$,

the “Boolean” values 0 and 1 lie in \mathbb{Z}_2 and \mathbb{Q}_2 , which connects with the Boolean network models used in the worked example (Section 7).

Topology of non-Archimedean fields.

We write $\mathfrak{B}_r(a) := \{x \in \mathbb{C}_p : |x - a|_p \leq r\}$ for the *closed ball* of radius r centered at a , and $\mathfrak{D}_r(a) := \{x \in \mathbb{C}_p : |x - a|_p < r\}$ for the *open disk* (additional notation, including balls in \mathbb{Z}_p , is collected in the “Balls, disks, and notation” paragraph below). In any field equipped with a non-Archimedean absolute value, balls are *clopen* (each closed ball is also topologically open, and vice versa). In particular, this holds in \mathbb{Q}_p , \mathbb{Z}_p , and \mathbb{C}_p .² Any point of a ball may serve as its center (by the strong triangle inequality), and the topology is *totally disconnected*. These properties follow from the ultrametric inequality; see [13, 14].

Ultrametric properties.

Four consequences of the strong triangle inequality (proofs in [16]). (i) *Every triangle is isosceles*: the two largest of $|x - y|_p, |y - z|_p, |x - z|_p$ are equal. (ii) *Every point of a ball is a center*: $z \in \mathfrak{B}_r(a)$ implies $\mathfrak{B}_r(a) = \mathfrak{B}_r(z)$. (iii) *Two balls that meet are nested*: one contains the other. (iv) *Disjoint balls $\mathfrak{B}_r(c)$ and $\mathfrak{B}_s(d)$ satisfy $|c - d|_p > \max\{r, s\}$* , and then $|x - y|_p = |c - d|_p$ for all $x \in \mathfrak{B}_r(c)$ and $y \in \mathfrak{B}_s(d)$. Property (iv), the distance between two points of disjoint balls equalling the distance between their centers, is the one used quantitatively below.

Completions and \mathbb{C}_p .

The field \mathbb{Q}_p is complete with respect to $|\cdot|_p$ but is not algebraically closed. Its algebraic closure $\overline{\mathbb{Q}_p}$ is not complete. The *completion of the algebraic closure* of \mathbb{Q}_p is denoted by \mathbb{C}_p ; it is complete and algebraically closed, and serves as the p -adic analogue of \mathbb{C} . The following diagram displays the completions of \mathbb{Q} ; the lower branch represents one completion for each prime p :

$$\begin{array}{ccc}
 & & \mathbb{R} \xrightarrow{\text{alg. cl.}} \mathbb{C} \\
 & \nearrow \text{compl. } |\cdot|_\infty & \\
 \mathbb{Z} \hookrightarrow \mathbb{Q} & & \vdots \\
 & \searrow \text{compl. } |\cdot|_p & \\
 & & \mathbb{Q}_p \xrightarrow{\text{alg. cl.}} \overline{\mathbb{Q}_p} \xrightarrow{\text{compl.}} \mathbb{C}_p
 \end{array} \tag{1}$$

By Ostrowski’s theorem, every non-trivial absolute value on \mathbb{Q} is equivalent to $|\cdot|_\infty$ or to $|\cdot|_p$ for some prime p ; for distinct primes $p \neq q$, $\mathbb{Q}_p \not\cong \mathbb{Q}_q$ as fields. As fields, \mathbb{C}_p

²In \mathbb{C}_p the value group $|\mathbb{C}_p^*| = p^{\mathbb{Q}}$ is dense in $\mathbb{R}_{>0}$. For any radius $r \notin p^{\mathbb{Q}}$ (i.e., with $\log_p r$ irrational), no element of \mathbb{C}_p has absolute value exactly r , so the open and closed balls of radius r centered at a coincide as sets. This phenomenon cannot occur in \mathbb{Q}_p , where the value group $p^{\mathbb{Z}}$ is discrete; there, an equality of open and closed balls requires shifted radii, e.g., $\{x : |x - a|_p < p^{-n}\} = \{x : |x - a|_p \leq p^{-(n+1)}\}$.

and \mathbb{C} are isomorphic [16], but not as valued fields or as topological fields: \mathbb{C}_p carries the ultrametric inherited from \mathbb{Q}_p , and we work in \mathbb{C}_p so that rational functions and p -adic dynamics (e.g. fixed-point theory) are available [13]. The discrete observables $\{0, \dots, p-1\}^N$ embed naturally in $\mathbb{Z}_p \subset \mathbb{Q}_p \subset \mathbb{C}_p$ via the base- p expansion, and the nested-ball structure of \mathbb{Z}_p provides the hierarchical resolution that has no direct analogue in \mathbb{R} (Figure 1).

Balls, disks, and notation.

Recall the notation $\mathfrak{B}_r(a)$ and $\mathfrak{D}_r(a)$ introduced above; the same definitions apply in \mathbb{Q}_p with the subscript p understood. For $a \in \mathbb{Z}_p$, the intersection $\mathfrak{B}_r(a) \cap \mathbb{Z}_p$ is a closed ball in \mathbb{Z}_p ; we denote it $B_r(a) := \mathfrak{B}_r(a) \cap \mathbb{Z}_p$. In particular, the closed ball of radius 1 in \mathbb{C}_p centered at 0, intersected with \mathbb{Q}_p , equals \mathbb{Z}_p (and any point of that ball is a center). The *diameter* of a set S is $\text{diam}(S) := \sup\{|x-y|_p : x, y \in S\}$; in an ultrametric space the diameter of a closed ball equals its radius.

Remark 2.1 (Hierarchical Partition and Nested Balls). *We call the points of \mathbb{Z}_p the observable points: the states the model resolves, sitting inside the ambient analytic field \mathbb{C}_p . The observable ball associated to a \mathbb{C}_p -ball $\mathfrak{B}_r(a)$ is its trace on the observable points, namely $\mathfrak{B}_r(a) \cap \mathbb{Z}_p$. When $a \in \mathbb{Z}_p$ this trace is the \mathbb{Z}_p -ball $B_r(a)$, and it remains a \mathbb{Z}_p -ball even when the center lies outside \mathbb{Z}_p : in the ultrametric every point of a ball is a center, so whenever $\mathfrak{B}_r(a) \cap \mathbb{Z}_p \neq \emptyset$ one may choose $b \in \mathfrak{B}_r(a) \cap \mathbb{Z}_p$, and then $\mathfrak{B}_r(a) \cap \mathbb{Z}_p = B_r(b)$. Conversely, every ball of \mathbb{Z}_p is observable, being $B_r(b) = \mathfrak{B}_r(b) \cap \mathbb{Z}_p$. In particular $\mathbb{Z}_p = \mathfrak{B}_1(0) \cap \mathbb{Z}_p$ is itself the observable unit ball. The nonemptiness condition above is genuine, since a \mathbb{C}_p -ball may miss \mathbb{Z}_p entirely (for instance $\mathfrak{B}_{1/p}(\sqrt{p})$, all of whose points have absolute value $p^{-1/2}$, not of the form p^{-k}). Throughout this paper the balls that arise are centered at integers, so their traces on \mathbb{Z}_p are never empty and every observable ball is a genuine ball of \mathbb{Z}_p . For any $x \in \mathbb{Z}_p$ and $n \geq 1$, there exists a unique $m \in \{0, \dots, p^n - 1\}$ such that $x \in B_{1/p^n}(m)$, where $m = \alpha_0 + \alpha_1 p + \dots + \alpha_{n-1} p^{n-1}$ corresponds to the first n terms of the p -adic expansion of x . Thus:*

$$B_{1/p^n}(m) = \{x \in \mathbb{Z}_p : x = m + p^n y, y \in \mathbb{Z}_p\}.$$

This gives a hierarchical partition of \mathbb{Z}_p : balls at finer scales nest within coarser balls; each $B_{1/p^n}(m)$ is the disjoint union of p sub-balls $B_{1/p^{n+1}}(m + kp^n)$, $k = 0, \dots, p-1$. Any two balls are either disjoint or one contains the other (or equal if same radius; see Figure 1). In the inverse-limit picture $\mathbb{Z}_p = \varprojlim_k \mathbb{Z}/p^k\mathbb{Z}$, the ball $B_{1/p^n}(m)$ corresponds to the residue class $\{x \in \mathbb{Z}_p : x \equiv m \pmod{p^n}\}$.

Lemma 2.2 (Ball-truncation equivalence). *For each $n \geq 1$ and $m \in \{0, \dots, p^n - 1\}$, the ball $B_{1/p^n}(m)$ consists of exactly those $x \in \mathbb{Z}_p$ whose p -adic expansion agrees with m in the first n digits (i.e., $x \equiv m \pmod{p^n}$). Hence $B_{1/p^n}(m)$ has normalized Haar measure³ $\lambda_{\text{H}}(B_{1/p^n}(m)) = p^{-n}$.*

³Since \mathbb{Z}_p is a compact abelian topological group, it carries a unique translation-invariant Borel probability measure, the *normalized Haar measure*, which we denote λ_{H} ; see e.g. [14].

Proof The equality $B_{1/p^n}(m) = \{x \in \mathbb{Z}_p : x \equiv m \pmod{p^n}\}$ is the content of the p -adic expansion and the definition of the ball. For the measure value: the p^n residue classes $\{x \in \mathbb{Z}_p : x \equiv m' \pmod{p^n}\}$ for $m' = 0, \dots, p^n - 1$ are pairwise disjoint, partition \mathbb{Z}_p , and are translates of $p^n\mathbb{Z}_p = B_{1/p^n}(0)$. By translation invariance of $\lambda_{\mathbb{H}}$ they share the same measure; since they partition \mathbb{Z}_p and $\lambda_{\mathbb{H}}(\mathbb{Z}_p) = 1$, each has measure $1/p^n$. \square

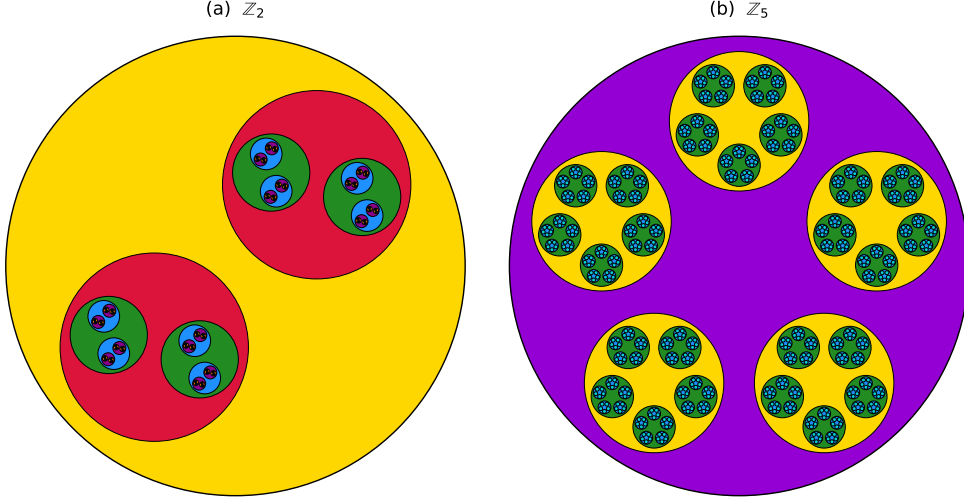


Figure 1: Fractal structure of \mathbb{Z}_2 (left, 7 levels) and \mathbb{Z}_5 (right, 4 levels). Each ball at level n is subdivided into p sub-balls at level $n + 1$; the same pattern repeats at every scale, so passing from a coarser to a finer resolution simply reveals more detail within the same self-similar structure (Remark 2.1). Colors indicate depth.

Rational functions, dynamics, and approximation.

The *projective line* over \mathbb{C}_p is $\mathbb{P}^1(\mathbb{C}_p) = \mathbb{C}_p \cup \{\infty\}$, i.e., \mathbb{C}_p with one point at infinity adjoined (formally: the set of equivalence classes $[z : w]$ with $(z, w) \in \mathbb{C}_p^2 \setminus \{(0, 0)\}$ under $(z, w) \sim (\lambda z, \lambda w)$ with $\lambda \neq 0$; we identify \mathbb{C}_p with $[z : 1]$ and ∞ with $[1 : 0]$). A *ball* in $\mathbb{P}^1(\mathbb{C}_p)$ is either a closed ball in \mathbb{C}_p (as defined above) or the complement in $\mathbb{P}^1(\mathbb{C}_p)$ of an open disk in \mathbb{C}_p , that is, a set of the form $\mathbb{P}^1(\mathbb{C}_p) \setminus \mathfrak{D}_r(a)$, which is a neighborhood of ∞ . Thus the balls in $\mathbb{P}^1(\mathbb{C}_p)$ are exactly the images of closed balls in \mathbb{C}_p under the Möbius transformations that identify charts around ∞ .

Let $\phi \in \mathbb{C}_p(z)$ be a rational function.

Proposition 2.3 (Proposition 3.25 in [13]). *Let \mathfrak{B} be a ball in \mathbb{C}_p and $\phi \in \mathbb{C}_p(z)$ nonconstant. Then $\phi(\mathfrak{B})$ is either $\mathbb{P}^1(\mathbb{C}_p)$ or a ball in $\mathbb{P}^1(\mathbb{C}_p)$.*

Thus rational functions map balls to balls (in $\mathbb{P}^1(\mathbb{C}_p)$); this underlies the interpretation of discrete dynamics in Section 4.

Observable image of a rational map.

For a nonconstant $\phi \in \mathbb{C}_p(z)$ and a ball $\mathfrak{B}_r(a)$ that meets \mathbb{Z}_p , two images must be distinguished. The *pointwise image* $\phi(\mathfrak{B}_r(a) \cap \mathbb{Z}_p)$ is the literal image of the observable points of the ball, and it need not consist of observable points, since ϕ may carry points off \mathbb{Z}_p . The *observable image* $\phi(\mathfrak{B}_r(a)) \cap \mathbb{Z}_p$ is the trace on \mathbb{Z}_p of the image ball. By Proposition 2.3 that image is a ball, so the observable image is again an observable ball whenever it is nonempty. The pointwise image lies inside the image ball, so the observable points it contains lie in the observable image, but the two sets differ in general. The constructions of Section 4 track the observable image, not the pointwise one.

Recall that a point x is a *fixed point* if $\phi(x) = x$. The *multiplier* $\lambda = \phi'(x)$, where ϕ' denotes the formal derivative of the rational function ϕ evaluated at x , classifies x as:

- *Attracting* if $|\lambda|_p < 1$
- *Repelling* if $|\lambda|_p > 1$
- *Indifferent* if $|\lambda|_p = 1$

Remark 2.4 (Terminology: Fixed points vs. “attractors” in the literature). *In discrete dynamics and in Boolean or directed-network models (Section 3), configurations a with $f(a) = a$ are often called attractors or stable states. Here we reserve fixed point for that combinatorial notion and attracting, repelling, and indifferent for the classification by the multiplier $|\phi'(x)|_p$ in \mathbb{C}_p (as above). The distinction between fixed points and their classification at the ball level is discussed in Section 4.5 once the relevant notions are introduced.*

Proposition 2.5 (Theorem 4.18 in [13]). *Let $U = \mathfrak{D}_r(a)$ and $\phi \in \mathbb{C}_p(z)$ with $\phi(U)$ a disk.*

- (a) *If $\phi(U) \subsetneq U$, there is a unique attracting fixed point in U . (In p -adic dynamics this strict inclusion plays the role of a contraction: it implies that iterates converge to the fixed point; no separate metric contraction hypothesis is required.)*
- (b) *If $\phi(U) \supsetneq U$ and ϕ is injective on U^4 , there is a unique repelling fixed point in U .*
- (c) *If $\phi : U \rightarrow U$ is bijective, any fixed points in U are indifferent.*

The ball-level analogue of this classification is given in Definition 4.21 (Section 4.5).

A subtle point: Proposition 2.5 is stated for open disks $\mathfrak{D}_r(a) \subset \mathbb{C}_p$, while our constructions in Section 4 live on closed balls $\mathfrak{B}_r(a)$. The two sets coincide for irrational radii $r \notin p^{\mathbb{Q}}$ (cf. the footnote in the Topology paragraph above), so the proposition transfers directly there. The radii $r = p^{-n}$ that arise in our setting lie in $p^{\mathbb{Q}}$; for them the bridge is density of the value group: a strict-inclusion contraction $F_n(\mathfrak{B}_r(a)) \subsetneq \mathfrak{B}_r(a)$ bounds the image in some $\mathfrak{B}_{r'}(a)$ with $r' < r$, and density of $p^{\mathbb{Q}}$ in $\mathbb{R}_{>0}$ supplies an intermediate $s \in p^{\mathbb{Q}}$ with $r' < s < r$. The open disk $\mathfrak{D}_s(a)$ of *slightly smaller* radius is

⁴This is the injectivity hypothesis of [13, Theorem 4.18].

then an admissible input to Proposition 2.5: F_n maps it into itself, and the resulting unique attracting fixed point lies in $\mathfrak{D}_s(a) \subsetneq \mathfrak{B}_r(a)$. The repelling case is the mirror image: a strict expansion $F_n(\mathfrak{B}_r(a)) \supsetneq \mathfrak{B}_r(a)$ has image radius $r'' > r$, and density of $p^\mathbb{Q}$ in $\mathbb{R}_{>0}$ supplies $s \in p^\mathbb{Q}$ with $r < s < r''$; on the open disk $\mathfrak{D}_s(a)$ of *slightly larger* radius, $F_n(\mathfrak{D}_s(a)) \supsetneq \mathfrak{D}_s(a)$ and F_n is injective, so Proposition 2.5(b) yields the unique repelling fixed point in $\mathfrak{D}_s(a)$.

ε -Approximations.

The following theorem from [1] is fundamental to the construction in Section 4: it provides a “gluing” technique that builds a global rational function from prescribed local dynamics on disjoint balls.

Theorem 2.6 (ε -approximation; Theorem 4.2 in [1]). *Let $g_1, \dots, g_n \in \mathbb{C}_p(z)$ and let $B := \bigcup_{i=1}^n \mathfrak{B}_{r_i}(a_i)$ be a union of pairwise disjoint closed balls in \mathbb{C}_p . Suppose that $g_i(\mathfrak{B}_{r_i}(a_i)) = \mathfrak{B}_{t_i}(b_i)$ for each i , and that $g_i(B) \subset \mathfrak{B}_1(0)$ for all $i = 1, \dots, n$. Then for any $\varepsilon > 0$ there exists $F_\varepsilon \in \mathbb{C}_p(z)$ such that:*

1. $F_\varepsilon(\mathfrak{B}_{r_i}(a_i)) = \mathfrak{B}_{t_i}(b_i)$ for each i (the image of each input ball equals the prescribed target ball in \mathbb{C}_p),
2. $|F_\varepsilon(z) - g_i(z)|_p < \varepsilon$ for all $z \in \mathfrak{B}_{r_i}(a_i)$.

One explicit construction is $F_\varepsilon(z) = \sum_i g_i(z)h_i(z)$ with $h_i(z) = (1 - ((z - a_i)/c_i)^{\kappa_i})^{-1}$ for appropriate c_i and even exponents κ_i ; details are in [1, Section 4].

Table 1 collects the main notation used in the paper; symbols introduced in later sections are defined there and summarized here for reference.

| Symbol | Meaning |
|--|--|
| \mathcal{C} | Configuration space (Section 3); $ \mathcal{C} = p^N$. |
| N | Number of vertices (coordinates). |
| p | Prime; each coordinate takes values in $\{0, \dots, p-1\}$. |
| $\mathbb{Z}_p, \mathbb{Q}_p, \mathbb{C}_p$ | Ring of p -adic integers; field of p -adic numbers; completion of the algebraic closure of \mathbb{Q}_p (Section 2). |
| $\mathfrak{D}_r(a)$ | Open disk of radius r centered at a in \mathbb{C}_p (Definition in Section 2). |
| m_a | Integer center $m_a = \sum_{i=0}^{N-1} a_i p^i \in \{0, \dots, p^N - 1\}$ of the configuration a , induced by the coordinate ordering π (Section 6). |
| ι | Coarse embedding $\mathcal{C} \xrightarrow{\sim} \mathbb{Z}_p/p^N \mathbb{Z}_p$, $\iota(a) = m_a + p^N \mathbb{Z}_p = B_{1/p^N}(m_a)$: the residue class of m_a , equivalently the closed ball of radius $1/p^N$ centered at the point m_a . The dynamics lifts via the interpreter, $\phi(\mathfrak{B}(a)) \subseteq \mathfrak{B}(f(a))$ (Section 3). |
| π | Ordering of the N coordinates; element of S_N . |
| ϕ | Rational interpreter $\phi \in \mathbb{C}_p(z)$ of f ; satisfies $\phi(\mathfrak{B}(a)) \subseteq \mathfrak{B}(f(a))$ (Section 4). |
| $\text{trunc}_n(z)$ | $z \bmod p^n \in \{0, \dots, p^n - 1\}$ for $z \in \mathbb{Z}_p$; for a configuration, $\text{trunc}_n(a) = m_a \bmod p^n$, the index of the ball containing a at level n . |
| $B(a)$ | The configuration ball $\iota(a) = B_{1/p^N}(m_a) \subset \mathbb{Z}_p$ centered at the point m_a (shorthand introduced in Section 3.2; the subscripted form $B_r(x)$ denotes the ball of radius r centered at a point $x \in \mathbb{Z}_p$). |
| $\mathfrak{B}(a)$ | Ball $\mathfrak{B}_{1/p^N}(m_a)$ in \mathbb{C}_p centered at the same point m_a ; $B(a) = \mathfrak{B}(a) \cap \mathbb{Z}_p$ (Section 4). |
| $\phi(\mathfrak{B}) \cap \mathbb{Z}_p$ | <i>Observable image</i> of a ball under $\phi \in \mathbb{C}_p(z)$: the image ball met with \mathbb{Z}_p , again an observable ball; distinct from the pointwise image $\phi(\mathfrak{B} \cap \mathbb{Z}_p)$, which may leave \mathbb{Z}_p (Section 2). |
| \mathcal{U} | Affinoid domain (finite union of disjoint rational closed balls in \mathbb{C}_p ; see [13]) $\bigcup_{a \in \mathcal{C}} \mathfrak{B}(a)$; $\mathbb{Z}_p \subset \mathcal{U} \subset \mathfrak{B}_1(0)$ (Section 4). |
| n | Resolution level; $n \in \{0, 1, \dots, N\}$. |
| F_n | n -th rational approximation of the dynamics (Section 4). |
| $M_{n,m}$ | Maximum common prefix length of image p -adic expansions in ball m at level n ; $t_{n,m} = 1/p^{M_{n,m}}$ (Section 6). |
| $t_{n,m}$ | Image radius $1/p^{M_{n,m}}$ of the ball $B_{1/p^n}(m)$; defined from (f, ι) (Section 6); equals the radius of the analytic image $F_n(B_{1/p^n}(m))$ (interpreters always exist). |
| $\Lambda_{n,m}$ | Coarse multiplier $p^n t_{n,m} = p^{n-M_{n,m}}$; ball-level analogue of the classical multiplier (Section 6). |
| $E(n)$ | Level set of expanding ball indices at level n ($M_{n,m} < n$, i.e. $t_{n,m} > 1/p^n$); $A(n)$, $I(n)$ likewise for contracting and isometric (Section 6). |
| μ_E, μ_A, μ_I | Weighted counts of expanding, contracting, and isometric balls across levels; $\mu := \mu_E = \sum_{n=1}^{N-1} E(n) \cdot p^{N-n}$ (Section 6). Control identity: Lemma 6.3. |

Table 1: Main notation.

3 Finite Discrete Dynamical Systems on \mathbb{F}_p^N

The framework developed below applies to any finite system equipped with an identification of its state space with \mathbb{F}_p^N for some prime p and integer N . Gene regulatory networks are one instance; cellular automata over prime alphabets, lattice spin systems on finite graphs, and arbitrary endomorphisms of \mathbb{F}_p^N are equally amenable. We fix notation and recall the structural properties used in subsequent sections.

3.1 Configuration Space and Transition Functions

Let p be a prime and let $N \geq 1$. A *configuration* is a tuple $a = (a_0, a_1, \dots, a_{N-1})$ with $a_i \in \{0, 1, \dots, p-1\}$; the *configuration space* has p^N elements:

$$\mathcal{C} = \{(a_0, a_1, \dots, a_{N-1}) \mid a_i \in \{0, 1, \dots, p-1\} \text{ for all } i\}. \quad (2)$$

A *discrete dynamical system* on \mathcal{C} is any map $f : \mathcal{C} \rightarrow \mathcal{C}$. We study iterates f^n and long-term behavior: fixed points, periodic points, and the basins they generate.

Scope.

The constructions below place no biological or graph-theoretic hypothesis on f : the only structural requirement is the product decomposition $\mathcal{C} \cong \mathbb{F}_p^N$. Concretely, the framework applies to:

- *Boolean networks* ($p = 2$): gene regulatory networks (the worked example of this paper; see Section 7), Hopfield-type binary networks, Ising spin systems on finite graphs, discrete neural networks [11, 17–23].
- *Cellular automata* over a prime alphabet of size p , with \mathcal{C} the state at a fixed time step on N cells.
- *Polynomial endomorphisms* of \mathbb{F}_p^N , including linear maps given by matrices over \mathbb{F}_p .
- *Finite-state machines* and synchronous logical circuits with N memory cells each of p states.

State spaces of cardinality $\prod_i k_i$ with mixed k_i , or non-prime-power cardinality, require working over the profinite ring $\prod_i \mathbb{Z}_{k_i}$ rather than \mathbb{Z}_p ; this is an extension to which the constructions of Sections 4–6 adapt naturally, but which we leave outside the present scope.

3.2 Embedding Configurations as p -Adic Balls

Extending the discrete dynamics f to a continuous setting requires care. Polynomial interpolation over finite fields, for instance, involves p^N coefficients, is far from unique, and the resulting high-degree maps offer little control over the dynamics; they can create fixed points or attractors absent from the original system. The p -adic integers offer a natural alternative [5, 6, 13] that:

- Respects any hierarchical structure among the N coordinates,
- Provides a natural multi-scale analysis,
- Enables controlled approximation of dynamics,
- Reveals latent stability patterns not evident in flat combinatorial models.

These properties are developed in Sections 4 and 6; Theorem 2.6 provides the approximation tool.

We embed \mathcal{C} into \mathbb{Z}_p as a system of balls, through the standard identification of p -adic balls with residue classes. To each $a = (a_0, \dots, a_{N-1}) \in \mathcal{C}$ associate the integer *center*

$$m_a := \sum_{i=0}^{N-1} a_i p^i \in \{0, \dots, p^N - 1\}, \quad (3)$$

its base- p value, a representative of a class in $\mathbb{Z}/p^N\mathbb{Z}$ (here $|\mathcal{C}| = p^N$). Under the embedding $\mathbb{Z} \hookrightarrow \mathbb{Z}_p$ and the canonical isomorphism $\mathbb{Z}/p^N\mathbb{Z} \cong \mathbb{Z}_p/p^N\mathbb{Z}_p$, the class of m_a is the coset

$$\iota(a) := m_a + p^N\mathbb{Z}_p = B_{1/p^N}(m_a), \quad (4)$$

which is exactly the closed ball of radius $1/p^N$ centered at the point m_a : a coset of $p^N\mathbb{Z}_p$ and such a ball are the same object, since $z \in m_a + p^N\mathbb{Z}_p$ if and only if $|z - m_a|_p \leq 1/p^N$. The map

$$\iota: \mathcal{C} \xrightarrow{\sim} \mathbb{Z}_p/p^N\mathbb{Z}_p$$

is therefore a bijection of the p^N configurations onto the p^N residue classes, equivalently the p^N balls of radius $1/p^N$; we call it the *coarse embedding* and write $B(a) := \iota(a)$. A configuration is identified not with a point but with the class of all p -adic integers sharing its first N digits. The embedding carries the dynamics, not merely the states: the rational interpreter ϕ of Section 4 realizes f on these classes, mapping the ball of a into the ball of $f(a)$ (Definition 4.1), so each transition $a \mapsto f(a)$ of the functional graph lifts to an inclusion of balls.

Then $\mathbb{Z}_p = \bigsqcup_{a \in \mathcal{C}} B(a)$ (disjoint union; Figure 1): p^N balls of radius $1/p^N$, one per configuration. The expansion (3) encodes hierarchy: coordinates at lower powers of p have greater influence on p -adic distance. The multiscale geometry depends on the chosen ordering of the coordinates (the genes, in the GRN application); the role of this ordering and the variational principle over it are developed in Sections 4–6.

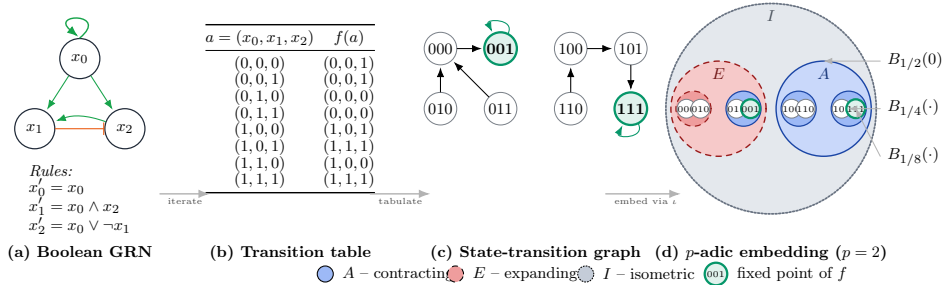


Figure 2: From a Boolean network to a p -adic ball partition ($p = 2$, $N = 3$). (a) Tiny 3-node GRN with one feedback edge and update rules. (b) The synchronous transition table $a \mapsto f(a)$. (c) The state-transition graph: two fixed points (highlighted in green), 001 and 111, are reached from distinct basins. (d) The embedding $a \mapsto B_{1/p^N}(\sum a_i p^i)$ partitions \mathbb{Z}_2 into eight leaf-balls, grouped into four level-2 and two level-1 balls; the coloring shows an illustrative A/E/I label (A = contracting, E = expanding, I = isometric; defined formally in Definition 4.21) assigned to each ball by the level-wise dynamics developed in Section 4. The labels are shown here only to preview that classification, which is constructed in the following section.

4 Hierarchical p -Adic Ball Dynamics

Throughout this section we work with the embedding $\mathcal{C} \hookrightarrow \mathbb{Z}_p$ of Section 3 (Eqs. (2)–(4)). The fractal structure of \mathbb{Z}_p (nested balls at scales $1/p^n$; see Figure 1) is used to model the discrete dynamics $f: \mathcal{C} \rightarrow \mathcal{C}$ via rational approximations $F_0, F_1, \dots, F_N \in \mathbb{C}_p(z)$, each capturing behavior at one scale, with Theorem 2.6 providing the analytic backbone.

4.1 Recap: rational interpreters of finite discrete dynamics

Before constructing the multi-scale dynamics F_0, \dots, F_N , we briefly recall the construction that lets us realize any finite map $f: \mathcal{C} \rightarrow \mathcal{C}$ as the trace of a p -adic rational function. This subsection is self-contained; the reader familiar with the gluing construction of [1] may skip directly to Section 4.5 for the ball-level classification.

The embedding.

Recall from Section 3 that each configuration $a \in \mathcal{C} = \mathbb{F}_p^N$ has integer center $m_a = \sum_{i=0}^{N-1} a_i p^i$ and is identified with the closed ball $\mathfrak{B}(a) := \mathfrak{B}_{1/p^N}(m_a)$, with coarse embedding $\iota(a) = m_a + p^N \mathbb{Z}_p = \mathfrak{B}(a) \cap \mathbb{Z}_p$. The p^N balls $\{\mathfrak{B}(a)\}_{a \in \mathcal{C}}$ are pairwise disjoint, and their union $\mathcal{U} := \bigsqcup_a \mathfrak{B}(a)$ is the *affinoid domain* of f (Section 3.2). The embedding carries the dynamics because the interpreter ϕ below satisfies $\phi(\mathfrak{B}(a)) \subseteq \mathfrak{B}(f(a))$ (Definition 4.1), so each edge $a \rightarrow f(a)$ of the functional graph lifts to an inclusion of balls.

The role of the ordering.

The center m_a , and hence the embedding ι , depends on a choice of *ordering* of the N coordinates: a permutation $\pi \in S_N$ specifies which coordinate occupies the p^0 -place, the p^1 -place, etc. Different orderings yield different embeddings ι_π and hence different multi-scale views of the same dynamics f . This freedom is the new ingredient exploited in Section 6: among the $N!$ orderings, the variational principle selects those that minimize the expansive measure μ_E . The worked example of Section 5 develops the closed-form construction in a small case ($p = 2, N = 4$).

Interpreting discrete dynamics.

The *projection* $\text{proj}_{\mathcal{U}}: \mathcal{U} \rightarrow \mathcal{C}$ sends each $x \in \mathcal{U}$ to the unique $a \in \mathcal{C}$ such that $x \in \mathfrak{B}(a)$.

Definition 4.1. Let $\phi \in \mathbb{C}_p(z)$ be a rational function. We say that ϕ interprets the dynamics of f if

$$\phi(\mathfrak{B}(a)) \subseteq \mathfrak{B}(f(a)) \quad \text{for all } a \in \mathcal{C}.$$

Equivalently, ϕ maps \mathcal{U} to itself and the following diagram commutes:

$$\begin{array}{ccc} \mathcal{U} & \xrightarrow{\phi} & \mathcal{U} \\ \text{proj}_{\mathcal{U}} \downarrow & & \downarrow \text{proj}_{\mathcal{U}} \\ \mathcal{C} & \xrightarrow{f} & \mathcal{C} \end{array}$$

Since each $\mathfrak{B}(a)$ is clopen, $\text{proj}_{\mathcal{U}}$ is locally constant, hence a *semi-conjugacy* from (\mathcal{U}, ϕ) to (\mathcal{C}, f) that preserves the projected transition structure, including periodic orbits at the level of the finite quotient. In this sense ϕ is a rational extension of the finite dynamics f , recovered as its shadow under $\text{proj}_{\mathcal{U}}$.

Existence of rational interpreters.

Existence of a rational interpreter (Definition 4.1) is the analytic backbone of the framework and is a direct consequence of the ε -approximation theorem (Theorem 2.6, Section 2).

Theorem 4.2 (Existence of rational interpreters; cf. Theorem 4.2 of [1]). *For every $f: \mathcal{C} \rightarrow \mathcal{C}$ and every embedding ι as above, there exists $\phi \in \mathbb{C}_p(z)$ that interprets f .*

The interpreter is not unique; Section 4.2 below uses this freedom to build a hierarchy of approximations F_0, \dots, F_N at each resolution level (see also Remark 4.4).

Remark 4.3 (Explicit construction of an interpreter). *An explicit interpreter can be built as*

$$\phi(z) = \sum_{a \in \mathcal{C}} g_a(z) h_a(z), \quad g_a(z) = A_a(z - m_a) + m_{f(a)}, \quad |A_a|_p = 1,$$

where the h_a are partition-of-unity rational functions of the form $h_a(z) = (1 - ((z - m_a)/c_a)^{M_a})^{-1}$ for constants c_a, M_a controlling the approximation radius; see [1, Theorem 4.2] for the full construction and (18) below for the analogous formula at each resolution level.

Downstream requirements.

The remainder of the paper requires only three ingredients from this construction:

1. that ϕ exists (Theorem 4.2);
2. that the radii of its images on balls $B_{1/p^n}(m) \subset \mathbb{Z}_p$ (at level n) depend only on (f, ι) (Remark 4.8, below); and
3. the standard fixed-point dichotomy for non-Archimedean rational dynamics on a closed ball (Proposition 2.5, Section 2).

In particular, *no explicit construction of ϕ is needed to study the ball-level dynamics or to compute the stability invariants defined in Section 6*: the interpreter is a theoretical device that supplies dynamical meaning to combinatorial quantities computed from (f, ι) .

Remark 4.4 (Non-uniqueness of interpreters). *The interpreter ϕ is not unique; the construction in Theorem 2.6 does not optimize degree. The inclusion condition $\phi(\mathfrak{B}(a)) \subseteq \mathfrak{B}(f(a))$ suffices for all results in this paper.*

Definition 4.5 (Exact interpreter). *An interpreter ϕ of f is exact if the inclusion of Definition 4.1 is an equality:*

$$\phi(\mathfrak{B}(a)) = \mathfrak{B}(f(a)) \quad \text{for all } a \in \mathcal{C}.$$

Proposition 4.6 (Existence of an exact interpreter). *For every $f: \mathcal{C} \rightarrow \mathcal{C}$ and every embedding ι there exists an exact interpreter.*

Proof We obtain one exact interpreter from the explicit construction of Remark 4.3 by taking each local piece g_a to be an isometry, $|A_a|_p = 1$. Then g_a carries the source ball $\mathfrak{B}(a)$ onto $\mathfrak{B}(f(a))$ with the same radius, and the gluing of [1, Theorem 4.2 and Remark 4.4] realizes the equality globally. The argument upgrading the ε -approximation to an exact image-ball equality proceeds in two steps:

- (i) Theorem T1 of [1] (ε -approximation) produces a rational $\phi \in \mathbb{C}_p(z)$ satisfying $\sup_{z \in \mathfrak{B}(a)} |\phi(z) - g_a(z)|_p < \varepsilon$ on each source ball; the bound ε controls pointwise distance, not the image radius.
- (ii) Choose any $\varepsilon < 1/p^N$, the common image-ball radius of the local isometries g_a . Since each g_a is a bijection $\mathfrak{B}(a) \rightarrow \mathfrak{B}(f(a))$ and $\phi - g_a$ has sup norm strictly below $1/p^N$, the image-ball perturbation lemma [1, Lemma 3.5] forces $\phi(\mathfrak{B}(a)) = \mathfrak{B}(f(a))$ exactly, with ϕ bijective on each source ball.

The equality of balls is therefore exact, not approximate. Non-injectivity of f is no obstruction: distinct source balls may share a common image ball. \square

Proposition 4.7 (Invariance of $t_{n,m}$). *If ϕ and ψ both interpret the same discrete dynamics $f : \mathcal{C} \rightarrow \mathcal{C}$, then they produce the same values $t_{n,m}$ for all balls $B_{1/p^n}(m)$. In particular, the ball-level classification (contracting, expanding, or isometric) of every ball is the same for both interpreters.*

Proof Immediate from Remark 4.8: $t_{n,m}$ is computed from the transition data f alone, without reference to ϕ . \square

4.2 Hierarchical Rational Approximations

Let $\phi \in \mathbb{C}_p(z)$ interpret f . We construct approximations $F_0, \dots, F_N \in \mathbb{C}_p(z)$ with $|F_n(z) - \phi(z)|_p \leq 1/p^m$ for some $m \in \{0, \dots, N\}$ and all $z \in \mathbb{Z}_p$ (Proposition 4.15); in particular $|F_N(z) - \phi(z)|_p \leq 1/p^N$. The F_n yield stability and periodic structure (Section 4.5).

For $n \geq 0$, $\mathbb{Z}_p = \bigsqcup_{m=0}^{p^n-1} B_{1/p^n}(m)$; write $B_{n,m} := B_{1/p^n}(m) \subset \mathbb{Z}_p$, so $B_{N,m} = B(m) = B_{1/p^N}(m)$. Each $a \in \mathcal{C}$ has center $m_a = \sum_{i=0}^{N-1} a_i p^i$; thus $\mathfrak{B}(a) = \mathfrak{B}_{1/p^N}(m_a)$ and $\iota(a) = B(a) = B_{1/p^N}(m_a)$. For any $z \in \mathbb{Z}_p$ and $n \leq N$, the n -digit truncation is $\text{trunc}_n(z) := z \bmod p^n \in \{0, \dots, p^n - 1\}$. For a configuration $a \in \mathcal{C}$, we write $\text{trunc}_n(a)$ as shorthand for $\text{trunc}_n(m_a)$, where $m_a \in \mathbb{Z}$ is the integer center of $\mathfrak{B}(a)$; then $z \in B_{n,m}$ if and only if $\text{trunc}_n(z) = m$.

For each ball $B_{n,m}$, we define

$$t_{n,m} = \max \left(\{1/p^N\} \cup \{|\phi(x) - \phi(y)|_p : x, y \in B_{n,m}\} \right); \quad (5)$$

when ϕ is an exact interpreter (Definition 4.5), this equals the diameter of the image $\phi(B_{n,m}) \subset \mathbb{C}_p$; for a generic interpreter, $t_{n,m}$ provides an upper bound. As Remark 4.8 below shows, $t_{n,m}$ depends only on (f, ι) and coincides with the canonical definition given in Section 6.

Remark 4.8 (Computation of $t_{n,m}$ from Discrete Data). *The values $t_{n,m}$ do not depend on the choice of interpreter ϕ ; they can be computed directly from the discrete transition data $f : \mathcal{C} \rightarrow \mathcal{C}$, without explicit knowledge of ϕ . This follows from:*

1. For any configuration $a \in \mathcal{C}$ with $\mathfrak{B}(a) \subset B_{n,m}$, the image $\phi(\mathfrak{B}(a))$ is contained in $\mathfrak{B}(f(a))$, and the target ball is determined by the discrete dynamics $f(a)$.
2. The p -adic distance $|\phi(x) - \phi(y)|_p$ for $x \in \mathfrak{B}(a)$ and $y \in \mathfrak{B}(b)$ (with $a, b \in \mathcal{C}$) depends only on the first differing digit between $f(a)$ and $f(b)$:

$$|\phi(x) - \phi(y)|_p = \begin{cases} \leq 1/p^N, & \text{if } f(a) = f(b), \\ 1/p^j, & \text{if } f(a) \neq f(b), \end{cases} \quad (6)$$

where j is the smallest index at which the p -adic digits of $m_{f(a)}$ and $m_{f(b)}$ differ; equivalently, $|m_{f(a)} - m_{f(b)}|_p = 1/p^j$.

3. Therefore, $t_{n,m}$ can be computed algorithmically as follows:
 - (a) Enumerate all configurations $a \in \mathcal{C}$ such that $\mathfrak{B}(a) \subset B_{n,m}$.

- (b) Compute their images $f(a)$ and their corresponding integers $m_a = \sum_{i=0}^{N-1} (f(a))_i p^i$.
- (c) Compute $t_{n,m} = \max\{1/p^N\} \cup \{|m_a - m_b|_p : a, b \text{ such that } \mathfrak{B}(a), \mathfrak{B}(b) \subseteq B_{n,m}\}$.

The entire analysis (classification of Definition 4.21 and the stability measure μ of Section 6) therefore depends only on f , not on ϕ .

Lemma 4.9. *There exists $M \in \{0, 1, \dots, N\}$ such that $t_{n,m} = 1/p^M$. Equivalently, $t_{n,m} \in \{1, 1/p, 1/p^2, \dots, 1/p^N\}$. We call this integer the canonical exponent of $t_{n,m}$ and denote it $M_{n,m}$, so $t_{n,m} = 1/p^{M_{n,m}}$.*

Proof By Remark 4.8, $t_{n,m} = \max(\{1/p^N\} \cup \{|m_{f(a)} - m_{f(b)}|_p : a, b \in \mathcal{C}, \text{trunc}_n(a) = \text{trunc}_n(b) = m\})$. Since $m_{f(a)}, m_{f(b)} \in \{0, \dots, p^N - 1\}$, their p -adic distance is either 0 (when $f(a) = f(b)$) or $1/p^j$ for some $j \in \{0, \dots, N-1\}$. The maximum over such distances and $1/p^N$ is therefore $1/p^M$ for some $M \in \{0, \dots, N\}$. \square

Lemma 4.10 (Monotonicity of $t_{n,m}$). *If $B_{1/p^{n+1}}(m') \subseteq B_{1/p^n}(m)$, then $t_{n+1,m'} \leq t_{n,m}$.*

Proof By equation (5), $t_{n,m} = \max(\{1/p^N\} \cup \{|\phi(x) - \phi(y)|_p : x, y \in B_{n,m}\})$ and $t_{n+1,m'} = \max(\{1/p^N\} \cup \{|\phi(x) - \phi(y)|_p : x, y \in B_{n+1,m'}\})$. Since $B_{n+1,m'} \subseteq B_{n,m}$, every pair (x, y) in $B_{n+1,m'}$ lies in $B_{n,m}$, so the set over which the maximum is taken for $t_{n+1,m'}$ is contained in the set for $t_{n,m}$. Hence $t_{n+1,m'} \leq t_{n,m}$. \square

Standing assumption for Definition 4.11 and the propositions that follow. From this point through the end of Section 4, ϕ denotes an exact interpreter (Definition 4.5), which exists for every f by Proposition 4.6, so that $\phi(\mathfrak{B}(a)) = \mathfrak{B}(f(a))$.

Definition 4.11 (n -th approximation). *An n -th approximation of f is a rational function $F_n \in \mathbb{C}_p(z)$ such that, for each $m \in \{0, \dots, p^n - 1\}$, there exists a center $\beta_{n,m} \in \mathbb{C}_p$ with*

$$F_n(\mathfrak{B}_{1/p^n}(m)) = \mathfrak{B}_{t_{n,m}}(\beta_{n,m}) \quad \text{as balls in } \mathbb{C}_p,$$

where $t_{n,m}$ is given by (5).

The equality of balls in Definition 4.11 is exact and already holds for any finite $\varepsilon < \min_m t_{n,m}$ in the construction of Theorem 4.12, not merely in the limit $\varepsilon \rightarrow 0$: by the strong triangle inequality a rational map whose sup-norm distance to the exact local affine on $\mathfrak{B}_{1/p^n}(m)$ is below $t_{n,m}$ has the same image ball, and the balls-to-balls property ([13, Prop. 3.25]) makes that image a ball of radius exactly $t_{n,m}$. The argument uses only the strict bound $\varepsilon < t_{n,m}$ and the strong triangle inequality, not the discreteness of the value group, so it remains valid for the analytic image in \mathbb{C}_p .

The standing assumption isolates the sharp statements below from the generic case of Remark 6.9, where the equality weakens to the inclusion \subseteq . For generic interpreters merely satisfying Definition 4.1, the propositions go through with \subseteq in place of $=$ in their hypotheses, since the proofs use only the upper bounds $|F_n(z) - \phi(m)|_p \leq 1/p^M$. When ϕ is the underlying interpreter, $\beta_{n,m}$ may be taken to be the integer center $m_{f(a_m)} \in \mathbb{Z}_p$ (any point of a ball serves as a center). The combinatorial $t_{n,m}$ of (5) (the diameter of $\phi(B_{n,m}) \subset \mathbb{C}_p$, computable from (f, ι) alone) coincides with the radius of the analytic image ball $F_n(\mathfrak{B}_{1/p^n}(m)) = \mathfrak{B}_{t_{n,m}}(\beta_{n,m})$ given by Definition 4.11 (in a non-Archimedean ball, radius and diameter coincide). A single quantity $t_{n,m}$ thus serves both the combinatorial role (diameter of $\phi(B_{n,m})$) and the analytic role (radius of the F_n -image ball).

For a generic interpreter the analytic image is only *contained* in $\mathfrak{B}_{t_{n,m}}(\beta_{n,m})$ and can be strictly smaller, e.g. when f is constant on $B_{n,m}$ (where the floor in (5) forces $t_{n,m} = 1/p^N$ while the actual image may be a single point); the combinatorial $t_{n,m}$ and the scores μ_E, μ_A, μ_I are unaffected (Theorem 6.8, Remark 6.9).

Theorem 4.12 (Existence of hierarchical approximations). *Let $f : \mathcal{C} \rightarrow \mathcal{C}$ be a discrete dynamical system. For each resolution level $n \in \{0, \dots, N\}$, there exists a rational function $F_n \in \mathbb{C}_p(z)$ satisfying Definition 4.11; that is, $F_n(\mathfrak{B}_{1/p^n}(m)) = \mathfrak{B}_{t_{n,m}}(\beta_{n,m})$ is a ball of radius $t_{n,m}$ for every m .*

Strategy of the proof. For each m we exhibit a local rational piece \hat{g}_m that satisfies the hypotheses (H1)–(H3) of Theorem 2.6. The bare affine suffices when the image radius does not exceed the source radius ($t_{n,m} \leq 1/p^n$, the non-expanding case); when $t_{n,m} > 1/p^n$ (expanding case) we localise it with a rational gluing factor of degree 2 whose pole sphere has half-integer radius, hence misses \mathbb{Z}_p . Theorem 2.6 then produces a global F_n within ε of each \hat{g}_m on its own ball, and [1, Lemma 3.5] closes the image-ball equality and injectivity.

Proof Fix $0 \leq n \leq N$. For $n = 0$ the partition is the single ball \mathbb{Z}_p and $F_0(z) := A_0 z + \beta_{0,0}$ with $|A_0|_p = t_{0,0}$ is one affine map onto $\mathfrak{B}_{t_{0,0}}(\beta_{0,0})$; assume $n \geq 1$ below. For each $m \in \{0, \dots, p^n - 1\}$ choose $a_m \in \mathcal{C}$ with $\text{trunc}_n(m_{a_m}) = m$, set $\beta_{n,m} := m_{f(a_m)} \in \mathbb{Z}_p$ (so $|\beta_{n,m}|_p \leq 1$), and write $\Lambda := t_{n,m} p^n$. The balls $\{\mathfrak{B}_{1/p^n}(m)\}_{m=0}^{p^n-1}$ are pairwise disjoint (Section 3.2).

We exhibit a family $\{\hat{g}_m\}_{m=0}^{p^n-1} \subset \mathbb{C}_p(z)$ satisfying:

- (H1) \hat{g}_m maps $\mathfrak{B}_{1/p^n}(m)$ bijectively onto $\mathfrak{B}_{t_{n,m}}(\beta_{n,m})$;
- (H2) for every $m' \neq m$, $\hat{g}_m(\mathfrak{B}_{1/p^n}(m')) \subset \mathfrak{B}_1(0)$;
- (H3) \hat{g}_m has no pole on \mathbb{Z}_p .

These are the hypotheses of Theorem 2.6: each \hat{g}_m is rational on the affinoid $\mathcal{U} \subset \mathfrak{B}_1(0)$, with image in the unit ball.

Case A: $\Lambda \leq 1$ (non-expanding ball). Take the bare affine $\hat{g}_m(z) := A_m(z - m) + \beta_{n,m}$ with $|A_m|_p = \Lambda$. (H3) is immediate. For $z \in \mathfrak{B}_{1/p^n}(m)$, $|\hat{g}_m(z) - \beta_{n,m}|_p = \Lambda |z - m|_p$ attains $\Lambda \cdot p^{-n} = t_{n,m}$ on the boundary and is strictly smaller in the interior; the affine map is bijective, giving (H1). For z in any other source ball, $|\hat{g}_m(z)|_p \leq \max\{\Lambda |z - m|_p, |\beta_{n,m}|_p\} \leq 1$ since $\Lambda \leq 1$, $|z - m|_p \leq 1$, and $|\beta_{n,m}|_p \leq 1$, giving (H2).

Case B: $t_{n,m} > 1/p^n$ (expanding ball). The bare affine violates (H2): on a distinct ball $|A_m(z-m)|_p$ reaches $\Lambda > 1$. Localize with a rational gluing factor of degree 2:

$$\hat{g}_m(z) := \frac{A_m(z-m)}{1 - ((z-m)/c_m)^2} + \beta_{n,m}, \quad |A_m|_p = \Lambda, \quad |c_m|_p = p^{1/2-n}. \quad (7)$$

The formula uses only c_m^2 ; choose the representative $c_m^2 := p^{2n-1} \in \mathbb{Q}_p$, of integer valuation $2n-1$ (equivalently $|c_m^2|_p = p^{1-2n}$, consistent with $|c_m|_p = p^{1/2-n}$). Then $\hat{g}_m \in \mathbb{Q}_p(z)$, although its poles, the two square roots of c_m^2 , lie in the ramified extension $\mathbb{Q}_p(\sqrt{p})$. The poles sit on the sphere $|z-m|_p = p^{1/2-n}$, of half-integer radius; since every $\zeta \in \mathbb{Z}_p$ has $|\zeta-m|_p \in p^{\mathbb{Z}_{\leq 0}}$ (equivalently, $|\zeta-m|_p \in \{p^{-k} : k \in \mathbb{Z}_{\geq 0}\}$, of integer exponent), no point of \mathbb{Z}_p lies on that sphere of half-integer exponent, giving (H3).

For $z \in \mathfrak{B}_{1/p^n}(m)$, $|z-m|_p \leq p^{-n}$ and $|c_m|_p = p^{1/2-n}$ give $|(z-m)/c_m|_p^2 \leq p^{-1} < 1$, so by the strong triangle inequality $|1 - ((z-m)/c_m)^2|_p = 1$ and

$$\hat{g}_m(z) - \beta_{n,m} = A_m(z-m) (1-u)^{-1}, \quad u := ((z-m)/c_m)^2, \quad |u|_p \leq 1/p.$$

The geometric expansion $(1-u)^{-1} = 1+u+u^2+\dots$ converges in \mathbb{C}_p since $|u|_p < 1$, so $\hat{g}_m(z) - \beta_{n,m} = A_m(z-m) + r(z)$ with $\sup_{\mathfrak{B}_{1/p^n}(m)} |r|_p \leq |A_m(z-m)|_p \cdot |u|_p \leq t_{n,m}/p < t_{n,m}$. The bare affine $z \mapsto A_m(z-m) + \beta_{n,m}$ is bijective from $\mathfrak{B}_{1/p^n}(m)$ onto $\mathfrak{B}_{t_{n,m}}(\beta_{n,m})$, and the rational perturbation has sup norm strictly below the image radius. By [1, Lemma 3.5], \hat{g}_m maps $\mathfrak{B}_{1/p^n}(m)$ onto the same ball $\mathfrak{B}_{t_{n,m}}(\beta_{n,m})$ and is injective there, giving (H1).

For z in any other source ball, $|z-m|_p \geq p^{1-n}$, so $|(z-m)/c_m|_p^2 \geq p > 1$ and $|1 - ((z-m)/c_m)^2|_p = |(z-m)/c_m|_p^2$. Hence

$$\begin{aligned} \left| \hat{g}_m(z) - \beta_{n,m} \right|_p &= \frac{|A_m|_p |c_m|_p^2}{|z-m|_p} = \frac{(t_{n,m} p^n) \cdot p^{1-2n}}{|z-m|_p} = \frac{t_{n,m} p^{1-n}}{|z-m|_p} \\ &\leq \frac{t_{n,m} p^{1-n}}{p^{1-n}} = t_{n,m} \leq 1, \end{aligned} \quad (8)$$

so $|\hat{g}_m(z)|_p \leq \max\{|\hat{g}_m - \beta_{n,m}|_p, |\beta_{n,m}|_p\} \leq 1$, giving (H2).

The family $\{\hat{g}_m\}_{m=0}^{p^n-1}$ satisfies (H1)–(H3). By Theorem 2.6, for every $\varepsilon > 0$ there exists $F_n^{(\varepsilon)} \in \mathbb{C}_p(z)$ with $\sup_{z \in \mathfrak{B}_{1/p^n}(m)} |F_n^{(\varepsilon)}(z) - \hat{g}_m(z)|_p < \varepsilon$ for every m , and $F_n^{(\varepsilon)}(\mathbb{Z}_p) \subset \mathfrak{B}_1(0)$. Choose any $\varepsilon < \min_m t_{n,m}$ and set $F_n := F_n^{(\varepsilon)}$. On each $\mathfrak{B}_{1/p^n}(m)$,

$$\sup_{z \in \mathfrak{B}_{1/p^n}(m)} |F_n(z) - \hat{g}_m(z)|_p < \varepsilon < t_{n,m}, \quad (9)$$

the image radius of \hat{g}_m , which is bijective onto $\mathfrak{B}_{t_{n,m}}(\beta_{n,m})$. By [1, Lemma 3.5], F_n maps $\mathfrak{B}_{1/p^n}(m)$ onto the same image ball $\mathfrak{B}_{t_{n,m}}(\beta_{n,m})$ and is injective there. \square

Remark 4.13. *The image-ball equality of Definition 4.11 and the injectivity of F_n on each source ball hold for any $\varepsilon < \min_m t_{n,m}$, by [1, Lemma 3.5]; the repelling case of Proposition 2.5(b) uses the injectivity. All steps are uniform in p . The combinatorial quantities $t_{n,m}$, $M_{n,m}$, $\Lambda_{n,m}$ and the scores μ_E, μ_A, μ_I are determined by (f, ι) alone (Theorem 6.8), independently of the choice of A_m and c_m .*

This yields a finite sequence F_0, F_1, \dots, F_N satisfying Definition 4.11; the approximation bound $|\phi(z) - F_n(z)|_p \leq t_{n,m}$ for $z \in \mathfrak{B}_{1/p^n}(m)$ is given by Proposition 4.15 below. Non-uniqueness and invariance of classification are in Proposition 4.16 and Section 6.

4.3 Properties of the Approximation Sequence

Three properties of $\{F_n\}$ are established next, under the standing assumption stated before Definition 4.11: ϕ is the exact interpreter of Theorem 4.2 (so Definition 4.11 reads as the equality $F_n(\mathfrak{B}_{1/p^n}(m)) = \mathfrak{B}_{t_{n,m}}(\phi(m))$), and the $M_{n,m}$ appearing in the hypotheses is the canonical exponent with $t_{n,m} = 1/p^{M_{n,m}}$.

Proposition 4.14. *Let F_n, F_{n+1} be two approximations with $0 \leq n < n+1 \leq N$, and let $m \in \{0, 1, \dots, p^n - 1\}$, writing $M_{n,m} \in \{0, 1, \dots, N\}$ for the exponent with $t_{n,m} = 1/p^{M_{n,m}}$ (Lemma 4.9). Then:*

$$|F_n(z) - F_{n+1}(z)|_p \leq \frac{1}{p^{M_{n,m}}} \quad \text{for all } z \in B_{1/p^n}(m). \quad (10)$$

Proof Let $z \in B_{1/p^n}(m)$. By the standing assumption, $F_n(\mathfrak{B}_{1/p^n}(m)) = \mathfrak{B}_{1/p^{M_{n,m}}}(\phi(m))$, so $F_n(z) \in \mathfrak{B}_{1/p^{M_{n,m}}}(\phi(m))$ and $|F_n(z) - \phi(m)|_p \leq 1/p^{M_{n,m}}$.

Since $z \in B_{1/p^n}(m)$, there exist $a \in \mathcal{C}$ and $m_2 \in \{0, 1, \dots, p^{n+1} - 1\}$ such that $z \in \mathfrak{B}(a) \subset \mathfrak{B}_{1/p^{n+1}}(m_2) \subset \mathfrak{B}_{1/p^n}(m)$. By the standing assumption at level $n+1$, $F_{n+1}(\mathfrak{B}_{1/p^{n+1}}(m_2)) = \mathfrak{B}_{t_{n+1,m_2}}(\phi(m_2))$, so $|F_{n+1}(z) - \phi(m_2)|_p \leq t_{n+1,m_2}$.

To bound $|\phi(m) - \phi(m_2)|_p$, observe that both m and m_2 are integer representatives in $B_{1/p^n}(m)$ (the center m itself and m_2 , which lies in its own sub-ball $B_{1/p^{n+1}}(m_2) \subset B_{1/p^n}(m)$). By the definition of $t_{n,m}$ in equation (5) as the supremum of $|\phi(x) - \phi(y)|_p$ over pairs $(x, y) \in B_{n,m}^2$, taking $(x, y) = (m, m_2)$ gives $|\phi(m) - \phi(m_2)|_p \leq t_{n,m} = 1/p^{M_{n,m}}$.

Finally, by the strong triangle inequality,

$$\begin{aligned} |F_n(z) - F_{n+1}(z)|_p &= |(F_n(z) - \phi(m)) + (\phi(m) - \phi(m_2)) + (\phi(m_2) - F_{n+1}(z))|_p \\ &\leq \max\{|F_n(z) - \phi(m)|_p, |\phi(m) - \phi(m_2)|_p, |F_{n+1}(z) - \phi(m_2)|_p\} \\ &\leq 1/p^{M_{n,m}}, \end{aligned} \quad (11)$$

where we used $t_{n+1,m_2} \leq t_{n,m} = 1/p^{M_{n,m}}$ from Lemma 4.10 for the last term. \square

The rational functions F_n approximate ϕ along the finite refinement (as n increases toward the final resolution N), in the following precise sense.

Proposition 4.15. *Let F_n be an n -th approximation and let $m \in \{0, \dots, p^n - 1\}$, with $M_{n,m}$ the canonical exponent ($t_{n,m} = 1/p^{M_{n,m}}$). Then:*

$$|\phi(z) - F_n(z)|_p \leq \frac{1}{p^{M_{n,m}}} \quad \text{for all } z \in B_{1/p^n}(m). \quad (12)$$

Proof Let $z \in B_{1/p^n}(m)$. By the standing assumption, $F_n(\mathfrak{B}_{1/p^n}(m)) = \mathfrak{B}_{1/p^{M_{n,m}}}(\phi(m))$, so $|F_n(z) - \phi(m)|_p \leq 1/p^{M_{n,m}}$.

For any configuration $a \in \mathcal{C}$ with $\text{trunc}_n(a) = m$, the interpreter maps $\phi(\mathfrak{B}(a)) \subset \mathfrak{B}(f(a)) \subset \mathfrak{B}_{1/p^{M_{n,m}}}(\phi(m))$, since $m_{f(a)}$ lies in the image ball at level n . Covering $B_{1/p^n}(m)$ by such micro-balls gives $|\phi(z) - \phi(m)|_p \leq 1/p^{M_{n,m}}$ for all $z \in B_{1/p^n}(m)$.

Combining by the strong triangle inequality:

$$|\phi(z) - F_n(z)|_p \leq \max\{|\phi(z) - \phi(m)|_p, |\phi(m) - F_n(z)|_p\} \leq \frac{1}{p^{M_{n,m}}}. \quad (13)$$

□

Proposition 4.16. *Let $F_n \in \mathbb{C}_p(z)$ be an n -th approximation, and write $\hat{M} = \max_{0 \leq m \leq p^n - 1} M_{n,m}$. Let $h \in \mathbb{C}_p(z)$ be a rational function such that:*

$$|h(z)|_p < \frac{1}{p^{\hat{M}}}, \quad \text{for all } z \in \bigsqcup_{m=0}^{p^n-1} \mathfrak{B}_{1/p^n}(m). \quad (14)$$

Then $F'_n := F_n + h \in \mathbb{C}_p(z)$ is also an n -th approximation.

Proof It is sufficient to prove that $F'_n(\mathfrak{B}_{1/p^n}(m)) = F_n(\mathfrak{B}_{1/p^n}(m))$ for every $m \in \{0, \dots, p^n - 1\}$.

Fix m . By the standing assumption, F_n maps $\mathfrak{B}_{1/p^n}(m)$ onto the ball $\mathfrak{B}_{1/p^{M_{n,m}}}(\phi(m))$ of radius $1/p^{M_{n,m}}$. By (14) the perturbation satisfies $|h(z)|_p < 1/p^{\hat{M}} \leq 1/p^{M_{n,m}}$ for every $z \in \mathfrak{B}_{1/p^n}(m)$, so its sup norm on the ball is strictly below the image radius. By [1, Lemma 3.5], $F'_n = F_n + h$ then maps $\mathfrak{B}_{1/p^n}(m)$ onto the same ball $\mathfrak{B}_{1/p^{M_{n,m}}}(\phi(m))$. Hence F'_n is an n -th approximation. □

4.4 Explicit Construction of Approximations

The existence of n -th approximations is guaranteed by Theorem 4.12 (from the ε -approximation theorem, [1, Theorem 4.2]). Let $0 \leq n \leq N$.

First, for each $m = 0, 1, \dots, p^n - 1$, we choose an auxiliary rational function g_m such that

$$g_m(\mathfrak{B}_{1/p^n}(m)) = \mathfrak{B}_{t_{n,m}}(\phi(m)). \quad (15)$$

A simple and computationally efficient choice is the affine function:

$$g_m(z) = A_m(z - m) + \beta_m, \quad (16)$$

where:

- $\beta_m = \phi(m) \bmod p^M$, with $M \in \mathbb{N}$ chosen so that $t_{n,m} = 1/p^M$;
- $A_m \in \mathbb{C}_p$ is chosen to satisfy $|A_m|_p = t_{n,m} \cdot p^n$.

Coefficients lie in \mathbb{C}_p ; integrality (e.g. in \mathbb{Z}_p) is not required for the construction. The existence of such A_m is guaranteed by standard arguments in ultrametric analysis (see [1, Section 4] for the explicit construction).

Second, to combine the local functions g_m into a global rational function, we use “gluing” functions h_m that act as a non-Archimedean partition of unity. As detailed

in [1, Section 4], we can take:

$$h_m(z) = \frac{1}{1 - \left(\frac{z-m}{c_m}\right)^{\kappa_m}} \quad (17)$$

for appropriate choices of $c_m \in \mathbb{C}_p$ and an even exponent $\kappa_m \in \mathbb{N}$.

Remark 4.17 (Local gluing parameters in the expanding case). *Following the proof of [1, Theorem 4.2], set $r_m = 1/p^n$ (the ball radius) and $\delta_m = \min_{m' \neq m} |m - m'|_p = 1/p^{n-1}$ (the minimal separation between distinct centres, so $\delta_m > r_m$). In Case B of Theorem 4.12 the gluing parameter is $c_m \in \mathbb{C}_p$ with $|c_m|_p = \sqrt{\delta_m r_m} = p^{1/2-n}$, the geometric mean of separation and radius. The squared parameter c_m^2 has integer valuation $2n - 1$ (so that $|c_m^2|_p = p^{1-2n}$) and may be taken in \mathbb{Q}_p , so the local pieces \hat{g}_m live in $\mathbb{Q}_p(z)$ even though their poles lie in the ramified extension $\mathbb{Q}_p(\sqrt{p})$; the half-integer pole sphere is the analytic reason the present construction descends to $\mathbb{Q}_p(z)$ only after squaring, while its poles unavoidably leave \mathbb{Q}_p . Writing $u = (z - m)/c_m$, on the home ball $|u|_p \leq p^{-1/2} < 1$, whence $|1 - u^{\kappa_m}|_p = 1$, while on each other source ball $|u|_p \geq p^{1/2} > 1$, whence $|1 - u^{\kappa_m}|_p = |u|_p^{\kappa_m} > 1$. The exponent κ_m is taken even, so that $c_m^{\kappa_m} = (c_m^2)^{\kappa_m/2} \in \mathbb{Q}_p$ and the construction descends to $\mathbb{Q}_p(z)$ as noted above. The home and away regimes then separate for every even $\kappa_m \geq 2$, but separation alone gives only $|h_m - 1|_p \leq p^{-\kappa_m/2}$ on the home ball, not yet below the image radius $t_{n,m}$. The sharper bound $\sup_{\mathfrak{B}_{1/p^n}(m)} |F_n - g_m|_p < t_{n,m}$, used in Section 6 to obtain the exact slope $|F'_n|_p = \Lambda_{n,m}$ through [1, Lemma 3.5], requires in addition $\kappa_m > 2(N + 1)$, the binding case being the nearest neighbouring ball. The construction therefore uses an even exponent $\kappa_m > 2(N + 1)$ (for instance $\kappa_m = 2N + 4$). All steps are uniform in p .*

Lemma 4.18 (Properties of gluing functions; [1, Lemma 4.1]). *This is Lemma 4.1 of [1], stated here for the specific gluing functions h_m of equation (17) used in our construction. Let h_m be defined as in equation (17). Given any $\varepsilon > 0$, the parameters $c_m \in \mathbb{C}_p$ and the even exponent $\kappa_m \in \mathbb{N}$ can be chosen (see [1, Thm. 4.2 and Rem. 4.4] and Remark 4.17) so that:*

- (i) $|h_m(z) - 1|_p < \varepsilon$ for all $z \in B_{1/p^n}(m)$ (local approximation of unity).
- (ii) $|h_m(z)|_p < \varepsilon$ for all $z \in B_{1/p^n}(m')$ with $m' \neq m$ (decay on the complementary balls).
- (iii) h_m is rational on \mathbb{C}_p with poles confined to the sphere $\{z : |z - m|_p = |c_m|_p\}$, which lies strictly outside $B_{1/p^n}(m)$; hence h_m is well-defined and continuous on the complement of that sphere.

The functions $\{h_m\}$ form a non-Archimedean partition of unity in the ε -approximate sense: they are not exactly 1 on $B_{1/p^n}(m)$, but the deviation from 1 on the central ball and from 0 on each complementary ball can be made smaller than any prescribed $\varepsilon > 0$.

Proof Items (i)–(ii) are [1, Lemma 4.1] applied to the present h_m (with $|c_m|_p > p^{-n}$, Remark 4.17); item (iii) places the poles on the sphere $|z - m|_p = |c_m|_p > p^{-n}$, outside $B_{1/p^n}(m)$, and the well-definedness it asserts is the content of Remark 4.19. See [1, Thm. 4.2] for the full construction. \square

Remark 4.19 (On the impossibility of $h_m \equiv 1$ on a ball). *A rational function h that satisfies $h(z) = 1$ on an entire ball $B_{1/p^n}(m) \subset \mathbb{C}_p$ (which contains infinitely many points) must equal 1 identically on \mathbb{C}_p , since \mathbb{C}_p is algebraically closed; in particular h cannot have poles. The h_m in (17) have poles on the sphere $|z - m|_p = |c_m|_p$, so the best one can hope for, and what Lemma 4.18 (i) provides, is approximation to within any prescribed ε .*

Third, using Theorem 4.12 (which relies on Theorem 2.6 from [1]), we construct the n -th approximation as:

$$F_n(z) = \sum_{m=0}^{p^n-1} g_m(z) \cdot h_m(z). \quad (18)$$

By Theorem 2.6 together with the ε -control of Lemma 4.18, this construction yields, for any $\varepsilon > 0$, a rational function $F_n^{(\varepsilon)}$ satisfying Definition 4.11. Under the standing assumption (exact interpreter) and for any finite $\varepsilon < \min_m t_{n,m}$, this is the analytic equality $F_n(\mathfrak{B}_{1/p^n}(m)) = \mathfrak{B}_{t_{n,m}}(\beta_{n,m})$ in \mathbb{C}_p , by the strong triangle inequality and the balls-to-balls property ([13, Prop. 3.25]; see the proof of Theorem 4.12), not only in the limit $\varepsilon \rightarrow 0$. For a generic interpreter (Remark 6.9), it holds only as the inclusion \subseteq .

Remark 4.20. *The choice of auxiliary functions g_m affects the explicit form of F_n but not the overall conclusions. Simpler choices, such as $g_m(z) = A_m(z - m) + \beta_m$, are preferred for computational efficiency. This non-uniqueness is a fundamental feature of the approximation process: different choices of g_m and h_m can produce different rational functions that satisfy the same mapping properties, as formalized in Proposition 4.16.*

4.5 Classification of Ball-Level Dynamics

Definition 4.21. *Let $f : \mathcal{C} \rightarrow \mathcal{C}$ be a dynamical system with affinoid domain $\mathcal{U} = \bigcup_{a \in \mathcal{C}} \mathfrak{B}(a)$, and let $t_{n,m}$ be as in equation (5). For $m \in \{0, \dots, p^n - 1\}$, the coarse multiplier of the ball $\mathfrak{B}_{1/p^n}(m)$ is the ratio of image radius to domain radius,*

$$\Lambda_{n,m} := \frac{t_{n,m}}{1/p^n} = p^n t_{n,m} = p^{n-M_{n,m}},$$

the non-Archimedean ball-level analogue of the classical multiplier $|\phi'(x_0)|_p$ at a fixed point (the comparison is made precise in Section 6). We say that the dynamics of f in $\mathfrak{B}_{1/p^n}(m)$ is

- n -contracting if $\Lambda_{n,m} < 1$ (equivalently $t_{n,m} < 1/p^n$);
- n -expanding if $\Lambda_{n,m} > 1$ (equivalently $t_{n,m} > 1/p^n$);
- n -isometric if $\Lambda_{n,m} = 1$ (equivalently $t_{n,m} = 1/p^n$).

The value $t_{n,m}$ captures the dynamical spread within $B_{1/p^n}(m)$: if all configurations in the ball map to the same configuration, $t_{n,m} = 1/p^n$ (minimal spread); if they map to different configurations, $t_{n,m} > 1/p^n$. The classification depends on this spread, and refinement from F_n to F_{n+1} can reveal sub-balls with different stability types.

Remark 4.22 (Set-inclusion form of the classification). *Since an n -approximation F_n always exists (Theorem 4.12), the classification of Definition 4.21 coincides with the set-inclusion formulation whenever the image ball lies in the same ball chain as $\mathfrak{B}_{1/p^n}(m)$: $F_n(\mathfrak{B}_{1/p^n}(m)) \subsetneq \mathfrak{B}_{1/p^n}(m)$ for contracting, \supsetneq for expanding, and $=$ for isometric.*

Remark 4.23 (Invariance of the classification). *Let F_n and $F'_n = F_n + h$ be two n -th approximations as in Proposition 4.16. Since $F'_n(\mathfrak{B}_{1/p^n}(m)) = F_n(\mathfrak{B}_{1/p^n}(m))$ for every m (Proposition 4.16), the classification of each ball as n -contracting, n -expanding, or n -isometric is invariant under the choice of approximation F_n , and hence under the choice of interpreter ϕ . In particular, the stability measure μ (Section 6) is invariant under all perturbations satisfying the bound in Proposition 4.16.*

The terms “contracting,” “expanding,” and “isometric” denote a ball-level classification (behavior of F_n on the partition balls) and depend on the gene ordering (Remark 4.26); the classification may change as resolution or ordering changes.

Remark 4.24 (Ball-Level Classification and \mathbb{Z}_p). *The classification of Definition 4.21 is read on the observable balls $B_{1/p^n}(m) \cap \mathbb{Z}_p$, through the observable image of F_n (Section 2), and not on all of \mathbb{C}_p . Each $F_n \in \mathbb{C}_p(z)$ is rational on all of \mathbb{C}_p and the construction uses its ball-to-ball geometry there, but we observe only its action on the observable points. In particular, a fixed point guaranteed by a contraction on a \mathbb{C}_p -ball need not be observable, that is need not lie in \mathbb{Z}_p , while the ball-level label, formulated on the observable image, is unambiguous.*

The classification “ n -expanding” indicates that the image radius $t_{n,m}$ is strictly larger than the ball radius $1/p^n$ (in particular, when the image ball intersects the domain ball, it properly contains it); it does not guarantee that a classical repelling fixed point exists in the ball in the sense of having $|\phi'(x)|_p > 1$. The terminology reflects ball-level dynamics (expansion of the image), not point-level multipliers.

Remark 4.25 (n -quasi-attractors and n -quasi-repellers). *Call a ball $\mathfrak{B}_{1/p^n}(m)$ that is n -contracting and contains its own image, $F_n(\mathfrak{B}_{1/p^n}(m)) \subsetneq \mathfrak{B}_{1/p^n}(m)$, an n -quasi-attractor. The gluing construction places the poles of F_n outside $\mathfrak{B}_{1/p^n}(m)$, so F_n is continuous there, and the strict inclusion makes it a contraction, so by Proposition 2.5(a) it has a unique attracting fixed point in the ball. Call a ball that is*

n -expanding and contained in its own image an n -quasi-repeller. Since F_n is injective on each ball (Theorem 4.12, by [1, Lemma 3.5]), Proposition 2.5(b) then gives it a unique repelling fixed point. These are ball-level objects, the analogues at resolution n of an attracting or repelling point. A small image radius alone does not suffice: an n -contracting ball whose image lies in a different ball is no n -quasi-attractor, carries no fixed point, and feeds contractively into another basin. The fixed points here are those of the analytic map F_n . They lie in the \mathbb{C}_p -ball and need not be observable (Remark 4.24). The observable point an n -quasi-attractor carries is the discrete fixed configuration of f , and one configuration may be an n -quasi-attractor at one scale and a transient ball at another.

Remark 4.26 (Scope and dependence on gene ordering). *The conclusions below concern the action of F_n on the observable balls of \mathbb{Z}_p , through the observable image of Remark 4.24, and not the full dynamics of F_n on \mathbb{C}_p . Stability and optimal-ordering statements are made for a fixed resolution N and a fixed map f . With N and f fixed, the ball partition and the stability measure μ (Section 6) are well-defined and independent of the choice of approximants F_n (Remark 4.23).*

All derived quantities depend on the gene ordering x_0, x_1, \dots, x_{N-1} . Changing the order alters the embedding into \mathbb{Z}_p : genes at lower powers of p have more influence on p -adic distances and hence on the ball-level classification. Different orderings produce different sequences F_0, \dots, F_N and may yield different classifications. Section 6 introduces a stability measure μ that quantifies this dependence and identifies optimal orderings.

5 Illustrative Example: A Toy Model

We illustrate the framework with $p = 2$, $N = 4$: we construct F_0, F_1, F_2, F_3 explicitly and show how hierarchical analysis reveals stability structure. In this toy model all balls turn out to be n -contracting (Definition 4.21), so the expansion measure μ_E (defined in Section 6) vanishes and the A/E/I classification reduces to a single letter (A). By contrast, the richer mix of contracting, expanding, and isometric behavior across scales appears in the *A. thaliana* application of Section 7.

Take $p = 2$, $N = 4$ (genes x_0, x_1, x_2, x_3); \mathcal{C} has 16 elements. Configurations (a_0, a_1, a_2, a_3) correspond to $m = a_0 + 2a_1 + 4a_2 + 8a_3 \in \{0, \dots, 15\}$. The dynamics f is given by:

Interpolated over \mathbb{F}_2 , the component update functions of f are the multilinear polynomials

$$x'_0 = x_0, \quad x'_1 = 0, \quad x'_2 = x_1 + x_0x_1, \quad x'_3 = x_0x_1 + x_0x_2, \quad (19)$$

equivalently $x'_2 = \neg x_0 \wedge x_1$ and $x'_3 = x_0 \wedge (x_1 \oplus x_2)$ in Boolean form. The variable that each output polynomial depends on, read off from (19), gives the dependency graph of Figure 3(a).

Let $\phi \in \mathbb{C}_2(z)$ interpret f (Definition 4.1); then $\phi(\mathfrak{B}(a)) \subseteq \mathfrak{B}(f(a))$, and in our construction equality holds (ϕ is an exact interpreter, Definition 4.5). Example: $a =$

| Config (x_0, x_1, x_2, x_3) | m | $f(x_0, x_1, x_2, x_3)$ | m' |
|-------------------------------|-----|-------------------------|------|
| (0, 0, 0, 0) | 0 | (0, 0, 0, 0) | 0 |
| (1, 0, 0, 0) | 1 | (1, 0, 0, 0) | 1 |
| (0, 1, 0, 0) | 2 | (0, 0, 1, 0) | 4 |
| (1, 1, 0, 0) | 3 | (1, 0, 0, 1) | 9 |
| (0, 0, 1, 0) | 4 | (0, 0, 0, 0) | 0 |
| (1, 0, 1, 0) | 5 | (1, 0, 0, 1) | 9 |
| (0, 1, 1, 0) | 6 | (0, 0, 1, 0) | 4 |
| (1, 1, 1, 0) | 7 | (1, 0, 0, 0) | 1 |
| (0, 0, 0, 1) | 8 | (0, 0, 0, 0) | 0 |
| (1, 0, 0, 1) | 9 | (1, 0, 0, 0) | 1 |
| (0, 1, 0, 1) | 10 | (0, 0, 1, 0) | 4 |
| (1, 1, 0, 1) | 11 | (1, 0, 0, 1) | 9 |
| (0, 0, 1, 1) | 12 | (0, 0, 0, 0) | 0 |
| (1, 0, 1, 1) | 13 | (1, 0, 0, 1) | 9 |
| (0, 1, 1, 1) | 14 | (0, 0, 1, 0) | 4 |
| (1, 1, 1, 1) | 15 | (1, 0, 0, 0) | 1 |

Table 2: Transition table for the toy example with $N = 4$ genes. Each configuration (x_0, x_1, x_2, x_3) maps to its image under f . The integer representation m is computed as $m = x_0 + 2x_1 + 4x_2 + 8x_3$.

$(0, 1, 0, 1)$ gives $m = 10$, $\mathfrak{B}(a) = \mathfrak{B}_{1/16}(10)$; $f(a) = (0, 0, 1, 0)$ gives $m' = 4$, so $\phi(\mathfrak{B}_{1/16}(10)) = \mathfrak{B}_{1/16}(4)$.

Construction of Hierarchical Approximations.

We compute F_0, F_1, F_2, F_3 following Section 4. Throughout this subsection, we abbreviate $\mathfrak{B}_{n,m} := \mathfrak{B}_{1/p^n}(m)$ for the closed ball in \mathbb{C}_p at level n with index m .

Construction of F_0 .

The entire configuration space satisfies $\mathfrak{B}(a) \subset \mathfrak{B}_1(0)$ for all $a \in \mathcal{C}$, and direct inspection of Table 2 gives:

$$t_{0,0} = \max\{|\phi(x) - \phi(y)|_2 : x, y \in B_{0,0}\} = 1, \quad (20)$$

and that $\beta_0 = 0$.

Since $t_{0,0} = 1$, the image radius equals the domain radius, so the required mapping property $F_0(\mathfrak{B}_1(0)) = \mathfrak{B}_1(0)$ is satisfied by the identity:

$$F_0(z) = z. \quad (21)$$

Construction of F_1 .

At level $n=1$, the two balls are $\mathfrak{B}_{1,0} = \mathfrak{B}_{1/2}(0)$ and $\mathfrak{B}_{1,1} = \mathfrak{B}_{1/2}(1)$.

If $a, b \in \mathcal{C}$ with $\mathfrak{B}(a) \subset \mathfrak{B}_{1,0}$ and $f(a) = b$, then $a = (0, a_1, a_2, a_3)$ for some $a_1, a_2, a_3 \in \{0, 1\}$; that is, the configuration has first digit 0, so the corresponding integer m is in $\{0, 2, 4, 6, 8, 10, 12, 14\}$.

Examining the transition table, the images of these configurations are $(0, 0, 0, 0)$ and $(0, 0, 1, 0)$, corresponding to integers 0 and 4 only. Computing, the 2-adic distance between these two images is $|0 - 4|_2 = 1/4$. We have, then, all images of configurations in $\mathfrak{B}_{1,0}$ lying within a ball of radius $1/4$, and we can take $\mathfrak{B}_{1/4}(0)$ as the containing ball. Thus $t_{1,0} = 1/4$.

Analogously, if $a, b \in \mathcal{C}$ with $\mathfrak{B}(a) \subset \mathfrak{B}_{1,1}$ and $f(a) = b$, then $a = (1, a_1, a_2, a_3)$ and $b = (1, 0, 0, b_1)$ for some $a_1, a_2, a_3, b_1 \in \{0, 1\}$. Hence, $\mathfrak{B}(b) \subset \mathfrak{B}_{1/8}(1)$.

One verifies that $t_{1,0} = \frac{1}{4}$, $t_{1,1} = \frac{1}{8}$, $\beta_0 = 0$ and $\beta_1 = 1$.

The 1-approximation is a rational function $F_1 \in \mathbb{C}_2(z)$ such that $F_1(\mathfrak{B}_{1/2}(0)) = \mathfrak{B}_{\frac{1}{4}}(0)$ and $F_1(\mathfrak{B}_{1/2}(1)) = \mathfrak{B}_{\frac{1}{8}}(1)$.

In this case, we can construct a 1-approximation F_1 using the auxiliary functions:

$$g_0(z) = 2z \quad \text{and} \quad g_1(z) = 4(z - 1) + 1. \quad (22)$$

Then using the gluing technique from [1, Section 4] we construct:

$$F_1(z) = \frac{2z}{1 - \left(\frac{z}{c_0}\right)^{\kappa_0}} + \frac{4(z - 1) + 1}{1 - \left(\frac{z-1}{c_1}\right)^{\kappa_1}}, \quad (23)$$

for some $c_0, c_1 \in \mathbb{C}_2$ and even exponents $\kappa_0, \kappa_1 \in \mathbb{N}$ chosen appropriately.

Since $F_1(\mathfrak{B}_{1/2}(0)) = \mathfrak{B}_{\frac{1}{4}}(0) \subsetneq \mathfrak{B}_{1/2}(0)$, the dynamics of f is 1-contracting in $\mathfrak{B}_{1/2}(0)$, which therefore contains its own image and is a 1-quasi-attractor. By Remark 4.25, the rational function F_1 has an attracting fixed point in $\mathfrak{B}_{\frac{1}{4}}(0)$.

On the other hand, since $F_1(\mathfrak{B}_{1/2}(1)) = \mathfrak{B}_{\frac{1}{8}}(1) \subsetneq \mathfrak{B}_{1/2}(1)$, the dynamics of f is 1-contracting in $\mathfrak{B}_{1/2}(1)$, a 1-quasi-attractor, and the rational function F_1 thus has an attracting fixed point in $\mathfrak{B}_{\frac{1}{8}}(1)$.

Construction of F_2 .

At level $n=2$ the balls are $\mathfrak{B}_{2,m} = \mathfrak{B}_{1/4}(m)$ with $m = 0, 1, 2, 3$. Reading off the transition table, $t_{2,0} = t_{2,2} = \frac{1}{16}$, $t_{2,1} = t_{2,3} = \frac{1}{8}$, $\beta_0 = 0$, $\beta_1 = \beta_3 = 1$ and $\beta_2 = 4$.

A 2-approximation $F_2 \in \mathbb{C}_2(z)$ should satisfy:

$$\begin{aligned} F_2(\mathfrak{B}_{2,0}) &= \mathfrak{B}_{\frac{1}{16}}(0), & F_2(\mathfrak{B}_{2,1}) &= \mathfrak{B}_{\frac{1}{8}}(1), \\ F_2(\mathfrak{B}_{2,2}) &= \mathfrak{B}_{\frac{1}{16}}(4), & F_2(\mathfrak{B}_{2,3}) &= \mathfrak{B}_{\frac{1}{8}}(1). \end{aligned} \quad (24)$$

All four level-2 balls are 2-contracting: each image radius ($t_{2,0} = t_{2,2} = 1/16$, $t_{2,1} = t_{2,3} = 1/8$) is strictly smaller than the domain radius $1/4$. By Remark 4.25, a contracting ball carries a fixed point only when it also contains its own image, that is when it is a 2-quasi-attractor. This holds for $\mathfrak{B}_{2,0}$, where $F_2(\mathfrak{B}_{2,0}) = \mathfrak{B}_{1/16}(0) \subseteq \mathfrak{B}_{2,0}$, and for $\mathfrak{B}_{2,1}$, where $F_2(\mathfrak{B}_{2,1}) = \mathfrak{B}_{1/8}(1) \subseteq \mathfrak{B}_{2,1}$. Both are 2-quasi-attractors, each carrying a unique attracting fixed point of F_2 in its \mathbb{C}_p -ball, the analytic counterpart

of the discrete fixed configurations 0 and 1 respectively. These fixed points lie in the \mathbb{C}_p -ball and need not be observable. The other two balls are contracting but map away from themselves: $F_2(\mathfrak{B}_{2,2}) = \mathfrak{B}_{1/16}(4)$ and $F_2(\mathfrak{B}_{2,3}) = \mathfrak{B}_{1/8}(1)$ are disjoint from their own domains (their centres lie at 2-adic distance $1/2$ from 2 and 3 respectively), so $\mathfrak{B}_{2,2}$ and $\mathfrak{B}_{2,3}$ are not 2-quasi-attractors, carry no fixed point, and instead feed contractively into the basins of 0 and 1.

Construction of F_3 .

At level $n=3$ the balls are $\mathfrak{B}_{3,m} = \mathfrak{B}_{1/8}(m)$ with $m = 0, \dots, 7$. A further transition-table enumeration yields $t_{3,i} = \frac{1}{16}$ for $i = 0, \dots, 7$, $\beta_0 = \beta_4 = 0$, $\beta_1 = \beta_7 = 1$, $\beta_2 = \beta_6 = 4$ and $\beta_3 = \beta_5 = 9$.

Therefore, a 3-approximation $F_3 \in \mathbb{C}_2(z)$ should satisfy:

$$\begin{aligned}
 F_3(\mathfrak{B}_{3,0}) &= \mathfrak{B}_{\frac{1}{16}}(0), & F_3(\mathfrak{B}_{3,1}) &= \mathfrak{B}_{\frac{1}{16}}(1), \\
 F_3(\mathfrak{B}_{3,2}) &= \mathfrak{B}_{\frac{1}{16}}(4), & F_3(\mathfrak{B}_{3,3}) &= \mathfrak{B}_{\frac{1}{16}}(9), \\
 F_3(\mathfrak{B}_{3,4}) &= \mathfrak{B}_{\frac{1}{16}}(0), & F_3(\mathfrak{B}_{3,5}) &= \mathfrak{B}_{\frac{1}{16}}(9), \\
 F_3(\mathfrak{B}_{3,6}) &= \mathfrak{B}_{\frac{1}{16}}(4), & F_3(\mathfrak{B}_{3,7}) &= \mathfrak{B}_{\frac{1}{16}}(1).
 \end{aligned} \tag{25}$$

At level 3 the picture is the same: all eight balls are 3-contracting ($t_{3,m} = 1/16 < 1/8$ for every m), but only $\mathfrak{B}_{3,0}$ and $\mathfrak{B}_{3,1}$ contain their own image, $F_3(\mathfrak{B}_{3,0}) = \mathfrak{B}_{1/16}(0)$ and $F_3(\mathfrak{B}_{3,1}) = \mathfrak{B}_{1/16}(1)$, so these are the only two 3-quasi-attractors, carrying the discrete fixed configurations 0 and 1 at the finest scale. The remaining six balls map contractively into these two. Note that the discrete map f then has two attracting fixed points, $(0, 0, 0, 0)$ and $(1, 0, 0, 0)$, as Table 2 confirms; many configurations converge to them. The example is inspired by $z^2 \in \mathbb{C}_2(z)$, which has attracting fixed points 0 and 1 in $\mathfrak{B}_1(0)$; the F_n recover this structure from discrete data, illustrating that hierarchical approximation infers continuous dynamics from a finite set. All quantities are computed from f alone (Remark 4.8).

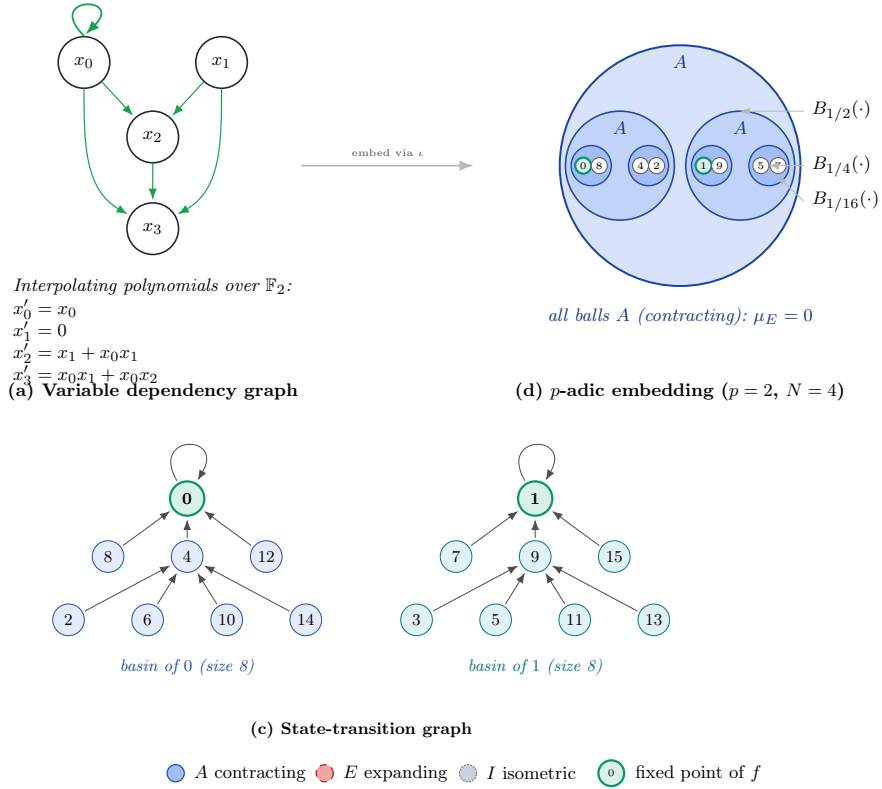


Figure 3: The toy example ($p = 2, N = 4$) across three views, mirroring Figure 2. Panel (b) of that figure, the transition table, appears here separately as Table 2, so the panel letters below skip from (a) to (c). **(a)** Variable dependency graph: an edge $x_i \rightarrow x_j$ marks that x_i appears in the interpolating polynomial x'_j over \mathbb{F}_2 of equation (19), shown inset. Here x_0 self-activates and drives the cascade, x_3 is a pure sink, and x_1 becomes constant. **(c)** State-transition graph of the map f of Table 2: two attracting fixed points, $m = 0$ (configuration $(0, 0, 0, 0)$) and $m = 1$ (configuration $(1, 0, 0, 0)$), shown in green with self-loops, with disjoint basins, each containing eight of the sixteen configurations (the basin of 0 in blue, of 1 in teal, both attracting), reached in at most two iterations through the intermediate states $m = 4$ and $m = 9$. **(d)** The p -adic embedding ι with the $A/E/I$ color code: here every ball is n -contracting (A) at every resolution, so $\mu_E = 0$; the two leaves 0 and 1 carry the fixed points. The richer mix of $A/E/I$ behavior appears instead in the *A. thaliana* application of Section 7. The ball-cascade view of this same dynamics, with $A/E/I$ labels at each resolution, appears in Figure 4.

6 Stability Measure and Optimal Ordering

The gene ordering fixes the partition and, with it, the stability classification (Remark 4.26). This section defines a *stability measure* μ on orderings: it quantifies how much expanding behavior appears across scales. Orderings that minimize μ then correspond to the most stable hierarchical organization.

Motivation.

If the network is organized hierarchically so that coarse-scale dynamics are stable, then a suitable ordering should yield few expanding balls. μ makes this idea quantitative; minimizing μ singles out orderings that expose that latent hierarchy.

Encoding convention and canonical definitions.

All quantities below depend only on (f, ι) . We fix the following convention.

Remark 6.1 (Convention: encoding induced by the gene ordering). *Recall from Sections 2 and 3 that the coordinate ordering fixes the integer center $m_a = \sum_{i=0}^{N-1} a_i p^i$, the embedding $\iota(a) = B_{1/p^N}(m_a)$, and the truncation $\text{trunc}_n(z) = z \bmod p^n$. Since trunc_n acts on \mathbb{Z}_p , for a configuration $a \in \mathcal{C}$ we abbreviate $\text{trunc}_n(a) := \text{trunc}_n(m_a)$, the truncation of its integer center. Throughout this section we index the ball $B_{1/p^n}(m)$ by $m = \text{trunc}_n(a)$, and write $a \equiv b \pmod{p^n}$ when $\text{trunc}_n(a) = \text{trunc}_n(b)$.*

For $n \in \{1, \dots, N-1\}$, $m \in \{0, \dots, p^n - 1\}$, and $k \in \{0, 1, \dots, N\}$, define the set of image truncations at level k in the block indexed by m :

$$S_n^{(k)}(m) := \{m_{f(a)} \bmod p^k : a \in \mathcal{C}, \text{trunc}_n(a) = m\} \subseteq \{0, \dots, p^k - 1\}$$

(since $a \bmod 1 = 0$ for every integer a , we have $|S_n^{(0)}(m)| = 1$ for all n, m). The canonical exponent $M_{n,m}$ of $t_{n,m}$ (Lemma 4.9) coincides with the *maximum common prefix length* of these image truncations,

$$M_{n,m} = \max\{k \in \{0, \dots, N\} : |S_n^{(k)}(m)| = 1\}.$$

Since $|S_n^{(0)}(m)| = 1$ always, this maximum is over a nonempty set, so $M_{n,m} \in \{0, \dots, N\}$. Equivalently (Lemma 4.9), the radius $t_{n,m}$ is

$$t_{n,m} = \frac{1}{p^{M_{n,m}}},$$

providing a combinatorial interpretation: $M_{n,m}$ is the number of shared leading p -adic digits among the images $f(a)$ with a in the ball $B_{1/p^n}(m)$; the larger $M_{n,m}$, the more concentrated the image in a small ball. The coarse multiplier $\Lambda_{n,m}$ (Definition 4.21) is

$$\Lambda_{n,m} = p^n t_{n,m} = p^{n-M_{n,m}}.$$

At level n , the domain ball has radius $1/p^n$ and the image (under an interpreter) has radius $t_{n,m} = 1/p^{M_{n,m}}$; the ratio $\Lambda_{n,m} = t_{n,m}/(1/p^n) = p^{n-M_{n,m}}$ is the expansion factor and plays the role of the classical multiplier $|\phi'(x_0)|_p$ in dynamics (cf. [13, Proposition 3.20]). For an analytic function that is injective on the ball, this ratio equals $|\phi'|_p$ at any point of the ball. The local affine pieces $g_m(z) = A_m(z - m) + \beta_m$ of (16) satisfy $|g'_m(z)|_p = |A_m|_p = \Lambda_{n,m}$ exactly: this is the affine (degree-one) case, in which the multiplier is literally the slope. For an exact interpreter (Definition 4.5), once the gluing exponent satisfies $\kappa_m > 2(N+1)$, so that $\sup_{\mathfrak{B}_{1/p^n}(m)} |F_n - g_m|_p < t_{n,m}$ (Theorem 4.12), the same value transfers to the glued approximant: by [1, Lemma 3.5], F_n is a bijection of $\mathfrak{B}_{1/p^n}(m)$ onto $\mathfrak{B}_{t_{n,m}}(\beta_m)$, so $|F_n(x) - F_n(y)|_p = \Lambda_{n,m} |x - y|_p$ on the ball and $|F'_n(z)|_p = \Lambda_{n,m}$ for every z there ([13, Proposition 3.20] together with [1, Lemma 3.4]), without passing to the limit $\varepsilon \rightarrow 0$. For a generic (non-exact) interpreter the pointwise slope of the glued $F_n = \sum_{m'} g_{m'} h_{m'}$ need not equal $\Lambda_{n,m}$, because the partition-of-unity factors $h_{m'}$ enter the derivative through the product rule; we do not rely on any such pointwise identity, since $\Lambda_{n,m} = p^{n-M_{n,m}}$ is by definition the ratio of image radius to domain radius and is unaffected by the choice of interpreter or of ε . Classification by ball: $\Lambda_{n,m} > 1$ (expanding), $\Lambda_{n,m} = 1$ (isometric), $\Lambda_{n,m} < 1$ (contracting). Equivalently (Definition 4.21), $M_{n,m} < n \Leftrightarrow$ expanding, $M_{n,m} = n \Leftrightarrow$ isometric, $M_{n,m} > n \Leftrightarrow$ contracting. The level sets are

$$E(n) := \{m : M_{n,m} < n\}, \quad I(n) := \{m : M_{n,m} = n\}, \quad A(n) := \{m : M_{n,m} > n\},$$

so that $|E(n)| + |I(n)| + |A(n)| = p^n$. The letters E, A, I stand for expansion, attraction, and invariance: geometrically the E -balls are expanding, the A -balls contracting (hence attracting at the fixed-point level, Proposition 2.5), and the I -balls isometric, and we use the two vocabularies interchangeably. The three stability scores are

$$\begin{aligned} \mu_E &:= \sum_{n=1}^{N-1} |E(n)| \cdot p^{N-n}, \\ \mu_A &:= \sum_{n=1}^{N-1} |A(n)| \cdot p^{N-n}, \\ \mu_I &:= \sum_{n=1}^{N-1} |I(n)| \cdot p^{N-n}. \end{aligned}$$

The sum runs over the interior scales $1 \leq n \leq N-1$. The endpoints are degenerate and carry no expansion: at $n=0$ the partition is the single ball \mathbb{Z}_p , so $E(0) = 0$, and at $n=N$ every ball is a single configuration with $M_{N,m} = N$, hence isometric. The interior range is also what yields the constant $(N-1)p^N$ in Lemma 6.3.

Lemma 6.2 (Level-wise partition). *For each resolution level $n \in \{1, \dots, N-1\}$,*

$$|E(n)| + |A(n)| + |I(n)| = p^n.$$

Proof The p^n balls $\{B_{1/p^n}(m)\}_{m=0}^{p^n-1}$ form a partition of \mathbb{Z}_p (Section 2). Each ball belongs to exactly one of the three classes of Definition 4.21 according to whether $M_{n,m} < n$ (expanding), $M_{n,m} = n$ (isometric), or $M_{n,m} > n$ (contracting). Summing the indicators yields p^n . \square

Lemma 6.3 (Control identity). $\mu_E + \mu_A + \mu_I = (N - 1)p^N$.

Proof By Lemma 6.2, $\sum_{n=1}^{N-1} (|E(n)| + |A(n)| + |I(n)|) p^{N-n} = \sum_{n=1}^{N-1} p^n \cdot p^{N-n} = (N - 1)p^N$. \square

The identity makes the three stability types partition the weighted multiscale ball tree at each level and exhibits the variational problem as a redistribution of a fixed budget across A/E/I. The two identities are conceptually distinct: Lemma 6.2 is a *combinatorial* statement (the three A/E/I classes partition the p^n balls at each level), while Lemma 6.3 is its weighted aggregation across levels with the multiplicative weight p^{N-n} (Remark 6.12). The constancy of $\mu_E + \mu_A + \mu_I$ across S_N is the structural reason why the variational problem $\pi^* = \arg \min_{\pi} \mu_E$ is not equivalent to maximizing μ_A alone (Remark 6.5).

Remark 6.4 (Saturated dynamics). *When μ_E takes its maximum value $(N-1)p^N$ on every ordering, the variational principle is uninformative. All balls are expanding at every level, and the dynamics admits no exploitable hierarchical decomposition. For the elementary one-dimensional cellular automata on $N = 8$ cells with periodic boundary, exhaustive computation over all $8! = 40320$ orderings shows that Wolfram’s rule 30 (chaotic; [24]), rule 90 (XOR/Sierpinski), and rule 150 (linear over \mathbb{F}_2) saturate, each giving $\mu_E(\pi) = (N-1)2^N = 1792$ for every ordering π , while the Turing-complete rule 110 and the traffic rule 184 never reach the maximum, attaining at most 1744 and 1728 respectively (reproducibility script and full scores in the Zenodo bundle). In fact, saturation does not coincide with chaos: rule 30 is chaotic and saturates, whereas the Turing-complete rule 110 does not. A characterization of the boundary between the saturated and unsaturated regimes is left open. In every saturated case the constancy of μ_E across S_N is itself a meaningful diagnostic, signaling the absence of an intrinsic coordinate hierarchy.*

Remark 6.5 (Multi-objective trade-off). *Since $\mu_E + \mu_A + \mu_I$ is constant, minimizing μ_E is equivalent to maximizing $\mu_A + \mu_I$, not to maximizing μ_A alone. In particular, the set of orderings that minimize μ_E and the set that maximize μ_A can be, and in general are, disjoint. Empirical comparison of the two criteria on the *A. thaliana* network, and the resulting trade-off, are treated separately in [2].*

Definition of Stability Measure.

Definition 6.6. *Let $(x_{\alpha_0}, \dots, x_{\alpha_{N-1}})$ be an ordering of the N genes in the GRN and let ι , $M_{n,m}$, $t_{n,m}$ be as in Section 6. For each resolution level n with $1 \leq n \leq N - 1$,*

the set of expanding balls at level n is

$$E(n) = \{m \in \{0, 1, \dots, p^n - 1\} : M_{n,m} < n\} = \{m : t_{n,m} > 1/p^n\}. \quad (26)$$

The stability measure μ of the ordering is

$$\mu(x_{\alpha_0}, \dots, x_{\alpha_{N-1}}) = \sum_{n=1}^{N-1} |E(n)| \cdot p^{N-n} = \mu_E. \quad (27)$$

Proposition 4.7 (Section 4) can now be restated: if ϕ and ψ both interpret f , we have the same set $E(n)$ and the same stability measure μ . As noted in Remark 4.23, μ is also invariant under the perturbations of the approximations F_n that satisfy the bound in Proposition 4.16: the values $t_{n,m}$ (and thus the sets $E(n)$) are invariant under different constructions of F_n .

Remark 6.7 (Compatibility with diameter formulation). *An interpreter ϕ and approximants F_n always exist (Section 4), and for them $t_{n,m}$ equals the diameter $\text{diam}(F_n(B_{n,m}))$ of the image: $\phi(B_{n,m})$ meets each micro-ball $\mathfrak{B}(f(a))$ with $\text{trunc}_n(a) = m$, and any two disjoint such balls of radius $1/p^N$ are at mutual distance equal to the distance of their centres (Section 2). Since $E(n)$ collects the expanding balls, those with $t_{n,m} > 1/p^n$, this gives $E(n) = \{m : \text{diam}(F_n(B_{1/p^n}(m))) > 1/p^n\}$. The discrete definition is adopted for Theorem 6.8.*

Theorem 6.8 (Intrinsic nature of μ_*). *The quantities $M_{n,m}$, $t_{n,m} = 1/p^{M_{n,m}}$, $\Lambda_{n,m} = p^{n-M_{n,m}}$, the level sets $E(n)$, $A(n)$, $I(n)$, and the scores μ_E , μ_A , μ_I are defined explicitly from (f, ι) by the combinatorial formulae of Section 6, with no reference to any rational interpreter ϕ or approximant F_n . For every rational interpreter ϕ of f (Definition 4.1) and every n -th approximation F_n in the sense of Definition 4.11, the bound*

$$\text{diam}(\phi(B_{n,m})) \leq t_{n,m}, \quad \text{diam}(F_n(B_{n,m})) \leq t_{n,m} \quad (28)$$

holds for every $n \in \{0, \dots, N\}$ and $m \in \{0, \dots, p^n - 1\}$, with equality whenever ϕ is the exact interpreter of Theorem 4.2 (the local pieces g_a are isometries with $|A_a|_p = 1$). In particular $t_{n,m}$ is the combinatorial supremum over $B_{n,m}^2$ and is independent of the choice of ϕ and of the approximants F_n .

Proof The first claim, that $M_{n,m}$, $t_{n,m}$, $\Lambda_{n,m}$, $E(n)$, $A(n)$, $I(n)$, and the three μ_* are defined as functions of (f, ι) alone, is immediate from Section 6: $M_{n,m}$ is the cardinality threshold of the truncated image sets $S_n^{(k)}(m)$, and all subsequent quantities are explicit functions of $M_{n,m}$.

For the second claim, fix ϕ interpreting f , $n \in \{0, \dots, N\}$, and $m \in \{0, \dots, p^n - 1\}$. By definition of the diameter,

$$\text{diam}(\phi(B_{n,m})) = \sup\{|\phi(x) - \phi(y)|_p : x, y \in B_{n,m}\}.$$

Let $x \in \mathfrak{B}(a) \cap \mathbb{Z}_p$ and $y \in \mathfrak{B}(b) \cap \mathbb{Z}_p$ with $a, b \in \mathcal{C}$ and $\text{trunc}_n(a) = \text{trunc}_n(b) = m$. Since ϕ interprets f , $\phi(x) \in \mathfrak{B}(f(a))$ and $\phi(y) \in \mathfrak{B}(f(b))$. If $f(a) = f(b)$, both images lie in a single

ball of radius $1/p^N$, so $|\phi(x) - \phi(y)|_p \leq 1/p^N$. If $f(a) \neq f(b)$, the disjoint-balls property (see (6) in Remark 4.8) gives

$$|\phi(x) - \phi(y)|_p = |m_{f(a)} - m_{f(b)}|_p = 1/p^j,$$

where j is the smallest index at which the p -adic digits of $m_{f(a)}$ and $m_{f(b)}$ differ. Taking the supremum over a, b with $\text{trunc}_n(a) = \text{trunc}_n(b) = m$ produces at most $1/p^{M_{n,m}} = t_{n,m}$, with equality precisely when the supremum is realized by a pair (x, y) for which $f(a) \neq f(b)$ (the realized case for the exact interpreter of Theorem 4.2, since then g_a acts as an isometry on $\mathfrak{B}(a)$). When f is constant on $B_{n,m}$ (so the floor $1/p^N$ in (5) dominates) and ϕ contracts within the common target ball $\mathfrak{B}(f(a))$, the supremum may be strictly smaller than $t_{n,m}$; this is the only source of strict inequality in (28).

The bound for F_n follows from Definition 4.11, which makes $F_n(\mathfrak{B}_{1/p^n}(m))$ a ball of radius at most $t_{n,m}$ (equality for an exact interpreter). \square

Remark 6.9 (Exact versus generic interpreters). *For an exact interpreter (Definition 4.5) the inclusion $\phi(\mathfrak{B}(a)) \subseteq \mathfrak{B}(f(a))$ is an equality, the local pieces g_a are isometries with $|A_a|_p = 1$, and the analytic image radius in \mathbb{C}_p coincides with $t_{n,m}$, so (28) holds with equality. For a generic interpreter, satisfying only the inclusion of Definition 4.1, the analytic image radius may be strictly smaller, for instance when f is constant on $B_{n,m}$. In both cases the combinatorial $t_{n,m}$ and the scores μ_E, μ_A, μ_I are fixed by (f, ι) alone (Theorem 6.8), so the A/E/I labels carry the semantic content of ϕ while the scores do not depend on its choice.*

Theorem 6.8 is a *computability result*: the stability invariants, originally defined through the dynamics of rational functions over \mathbb{C}_p , turn out to be evaluable from the discrete data (f, ι) . The theory of non-Archimedean dynamics over \mathbb{C}_p is not an auxiliary convenience but a mathematical necessity; three ingredients of the framework require \mathbb{C}_p specifically:

- (i) *Existence of interpreters and approximations* (Theorem 4.2, Theorem 4.12). The ε -approximation technique of [1] builds global rational functions from local data on disjoint balls; the gluing functions h_m (equation (17)) require parameters c_m whose p -adic valuation is non-integral ($|c_m|_p = p^{1/2}/p^n$; Remark 4.17). No element of \mathbb{Q}_p has half-integral valuation (the value group of \mathbb{Q}_p is $p^{\mathbb{Z}}$), so these coefficients exist in \mathbb{C}_p but not in \mathbb{Q}_p .
- (ii) *Balls to balls* (Proposition 2.3). That a nonconstant rational function maps every ball to a ball is a result in \mathbb{C}_p [13, Prop. 3.25]; it relies on the algebraic closure of the ground field. This property is what guarantees that the image $\phi(\mathfrak{B}_{1/p^n}(m))$ is a well-defined ball of radius $t_{n,m}$, the starting point of the classification.
- (iii) *Fixed-point theory* (Proposition 2.5). The label A records that the image radius is strictly smaller than the source radius. When the image ball lies inside the same ball, $F_n(\mathfrak{B}_{1/p^n}(m)) \subsetneq \mathfrak{B}_{1/p^n}(m)$, the classical non-Archimedean fixed-point theorem [13, Thm. 4.18] gives a unique attracting fixed point in the corresponding \mathbb{C}_p -ball; the analogous statement for E -balls under injectivity gives a unique repelling one. This fixed point need not lie in \mathbb{Z}_p ; the observable classification remains attached to the ball determined by (f, ι) . This is what gives the contracting/expanding/isometric classification its dynamical content: it extends the

attracting/repelling/indifferent trichotomy of Proposition 2.5 from individual fixed points to entire balls.

The radius $t_{n,m}$ coincides with the image radius under any n -th approximation F_n (equation (5), Theorem 4.12); the coarse multiplier $\Lambda_{n,m}$ is the ball-level analogue of a classical multiplier, equal to the pointwise slope $|F'_n|_p$ of the linear (constructive) approximation and shared by all n -th approximations, which is what justifies the name; and the classification (Definition 4.21) extends the classical trichotomy to ball-level dynamics. Without \mathbb{C}_p , one could still define $M_{n,m}$ as a combinatorial statistic (the maximum common prefix length of images), but there would be no mathematical reason to call $M_{n,m} < n$ “expanding” or to connect it to repelling dynamics. The discrete formulae of Theorem 6.8 are thus not *ad hoc* combinatorial definitions but the computable shadow of a richer analytical structure.

Integral formulation of μ .

Let $B_{n,m} = m + p^n \mathbb{Z}_p \subset \mathbb{Z}_p$ denote the ball at resolution p^{-n} .

Remark 6.10 (Coarse multiplier and compatibility). *When an interpreter exists, the diameter $\text{diam}(F_n(B_{n,m}))$ of the analytic image equals the canonical $t_{n,m}$, and $\Lambda_{n,m} = p^n t_{n,m}$ accordingly (Remark 6.7). The classification sequence of a fixed point is the word in $\{A, E, I\}$ at levels $n = 1, \dots, N - 1$ ($A =$ contracting, $E =$ expanding, $I =$ isometric), e.g. IEAA, IEE. The letter A is chosen for contracting because contraction together with the self-containment condition $F_n(\mathfrak{B}_{1/p^n}(m)) \subsetneq \mathfrak{B}_{1/p^n}(m)$ makes the ball an n -quasi-attractor, carrying a unique attracting fixed point of F_n in the corresponding \mathbb{C}_p -ball (Remark 4.25). The E -balls on which F_n is injective are the n -quasi-repellers. We keep the $A/E/I$ notation as the per-scale label, reserving the n -quasi-attractor and n -quasi-repeller names for the ball-level objects, to avoid confusion with the point-level attracting/repelling/indifferent trichotomy of ϕ in \mathbb{C}_p .*

Recall that the *normalized Haar measure* on \mathbb{Z}_p (see Section 2 and [14]) is the unique translation-invariant Borel probability measure on \mathbb{Z}_p ; we denote it by λ_H to avoid confusion with the stability measure μ , and it satisfies $\lambda_H(B_{1/p^n}(m)) = p^{-n}$ for each ball of the partition.

Proposition 6.11 (Haar integral form). *Let λ_H denote the normalized Haar measure on \mathbb{Z}_p (so that $\lambda_H(B_{1/p^n}(m)) = p^{-n}$). For $x \in \mathbb{Z}_p$, let $m_n(x) \in \{0, \dots, p^n - 1\}$ be the index of the ball containing x . The indicators*

$$\mathbf{1}_{E,n}(x) = \mathbf{1}_{\{\Lambda_{n,m_n(x)} > 1\}}, \quad \mathbf{1}_{A,n}(x) = \mathbf{1}_{\{\Lambda_{n,m_n(x)} < 1\}}, \quad \mathbf{1}_{I,n}(x) = \mathbf{1}_{\{\Lambda_{n,m_n(x)} = 1\}}$$

are locally constant on balls at level n . Then

$$\mu_* = p^N \sum_{n=1}^{N-1} \int_{\mathbb{Z}_p} \mathbf{1}_{*,n}(x) d\lambda_H(x), \quad * \in \{E, A, I\}.$$

Proof $\mathbf{1}_{*,n}$ is constant on each $B_{1/p^n}(m)$, so $\int_{\mathbb{Z}_p} \mathbf{1}_{*,n} d\lambda_{\mathbb{H}}$ equals the Haar measure of the set $\{x : \Lambda_{n,m_n(x)} * 1\}$, which is the count of balls of that type times p^{-n} . Multiplying by p^N and summing over n yields the weighted counts defining μ_E, μ_A, μ_I . \square

Remark 6.12 (Interpretation of the weight and volume). *The weight p^{N-n} in the definition of μ has two equivalent interpretations. Combinatorial interpretation: the discrete space $\mathcal{C} = \mathbb{F}_p^N$ has p^N configurations, partitioned into p^n balls at level n ; each ball $B_{1/p^n}(m)$ contains exactly p^{N-n} configurations. Thus p^{N-n} is the “mass” of each ball, the number of configurations affected by expanding dynamics at that level; instabilities at coarser scales (small n) contribute more. Measure-theoretic interpretation: let $\lambda_{\mathbb{H}}$ denote the normalized Haar measure on \mathbb{Z}_p . Since $\lambda_{\mathbb{H}}(B_{n,m}) = p^{-n}$, the ratio $|E(n)|/p^n$ equals $\lambda_{\mathbb{H}}(\{x \in \mathbb{Z}_p : \Lambda_{n,m(x)} > 1\})$, i.e., the Haar volume of expanding balls at resolution p^{-n} ; similarly $|A(n)|/p^n$ and $|I(n)|/p^n$ for contracting and isometric balls. Hence $\mu_E(\pi) = p^N \sum_{n=1}^{N-1} \lambda_{\mathbb{H}}(\Lambda_{n,\bullet} > 1)$; the weight p^{N-n} multiplies the count $|E(n)|$, not the fraction $|E(n)|/p^n$. Equivalently, defining the multi-scale roughness functional $\Phi_\pi : \mathbb{Z}_p \rightarrow \mathbb{Z}_{\geq 0}$ by $\Phi_\pi(z) := \#\{1 \leq n \leq N-1 : \Lambda_{n,m_n(z)} > 1\}$, one has*

$$\mu_E(\pi) = p^N \int_{\mathbb{Z}_p} \Phi_\pi(z) d\lambda_{\mathbb{H}}(z). \quad (29)$$

The integrand Φ_π is locally constant on the level- $(N-1)$ balls and, by Theorem 6.8, depends only on (f, ι) : the rational interpreter $\phi \in \mathbb{C}_p(z)$ is not part of the integration data, and the integral lives entirely on the locally compact ring \mathbb{Z}_p (the field \mathbb{C}_p is not locally compact and admits no analogous normalized Haar measure). The variational problem $\pi^ = \arg \min_{\pi \in S_N} \mu_E(\pi)$ is therefore the minimization of a Haar-integral functional under the S_N -action on coordinates. We use variational in this sense, the minimization of a functional over a configuration space, and not in the sense of an Euler–Lagrange or action-extremal structure: the domain S_N is finite and discrete and μ_E is integer-valued, so no gradient flow is implied. Here the averaging is over resolution scales rather than over time: μ_E is a scale-resolved expansion functional that records how the placement of coordinates governs multi-scale stability, the very structure that a single time-averaged Lyapunov exponent, being permutation-invariant, cannot resolve.*

Remark 6.13 (The A/E/I partition as a p -adic Waddington landscape). *The A/E/I partition admits a direct dynamical reading as a discrete, scale-resolved Waddington landscape on \mathbb{Z}_p , summarized in Table 3. The reading rests on three observations.*

(i) Geometric content of the label. *The multiplier $\Lambda_{n,m} = t_{n,m}/(1/p^n) = p^{n-M_{n,m}}$ is the ratio of image radius to domain radius under the rational interpreter ϕ . The label of the ball $B_{1/p^n}(m)$ records this ratio: A when $\Lambda_{n,m} < 1$ (the image is a strictly smaller ball, concentrating the bundle of configurations into a tighter region); I when $\Lambda_{n,m} = 1$ (the image is a ball of the same radius, preserving the bundle); E when $\Lambda_{n,m} > 1$ (the image is a strictly larger ball, dispersing the bundle).*

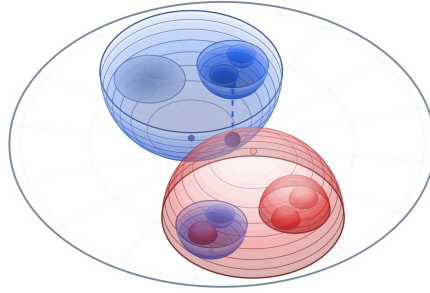
(ii) Local dynamical content. *Within each ball, when the image lies in the same ball chain, Proposition 2.5 converts the geometric content into the existence of a local fixed point of ϕ with explicit type: a unique attracting fixed point in every A-ball (Proposition 2.5(a); iterates of ϕ converge to it), a unique repelling fixed point in every E-ball on which ϕ is injective (Proposition 2.5(b); iterates eject configurations from it), and indifferent fixed points in every I-ball (iterates preserve local neighborhoods). The landscape vocabulary follows: A-balls are valleys where the dynamics carries configurations toward an attracting fixed point; E-balls are ridges from which the dynamics ejects configurations outward; I-balls are plateaus where the dynamics preserves the ball pending finer-scale decision.*

(iii) Multi-scale assembly. *The nested-ball refinement of \mathbb{Z}_p assembles these local dynamics into a tree of resolutions: at scale n , the p^n balls partition the state space into A/E/I regions; at scale $n + 1$, each ball refines into p sub-balls with their own labels (Figure 4). The classification word in $\{A, E, I\}^{N-1}$ that a fixed point inherits at each resolution is its trajectory through the landscape: the type of terrain (valley, plateau, ridge) at every cascade level from coarse to fine.*

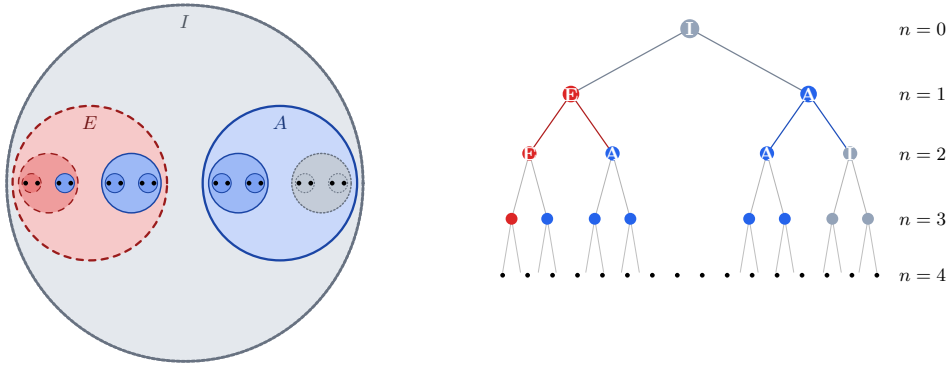
*The classical Waddington landscape has been formalized in continuous settings through quasi-potential constructions for stochastic dynamics and through variational reconstructions of a potential surface from data [25], and in non-Archimedean settings through ultrametric diffusion on hierarchical energy landscapes [26], where the hierarchy is fixed in advance by the energy function. The present reading is structurally different. The landscape is intrinsically discrete and ultrametric, its relief is the geometric content of the radii ratio $\Lambda_{n,m}$ rather than a fitted potential, and it is resolved scale by scale and intrinsic to the coordinate ordering, none of which a single continuous potential surface provides. Section 7 reads this structure off the *A. thaliana* floral network, where canalized organ identities sit in A-rich words and transient inflorescence states in E-rich ones.*

| Ball type | p -adic geometry | Dynamics of ϕ | GRN reading |
|-----------------|--|---------------------------------|------------------------------|
| A (contracting) | image radius < source, $ \lambda _p < 1$ | attracting fixed point (valley) | canalized, robust endpoint |
| E (expanding) | image radius > source, $ \lambda _p > 1$ | repelling fixed point (ridge) | decision or transient state |
| I (isometric) | image radius = source, $ \lambda _p = 1$ | indifferent (plateau) | fate undecided at this scale |

Table 3: The three readings of a ball’s type at a given scale: the p -adic geometry of its image radius, the dynamical content supplied by the rational interpreter ϕ (Remark 6.13), and the reading on a gene regulatory network. The geometric column (A/E/I by image radius) is unconditional. The column “Dynamics of ϕ (the multiplier $|\lambda|_p$ and the attracting/repelling/indifferent reading) is the ball-level analogue under the exact-interpretor normalization and the same-ball-chain hypothesis (Remarks 6.9 and 4.24), not an unconditional point-level equivalence. The assignment is resolution-dependent, so a single fixed point carries one row per scale, giving its A/E/I word.



(a) Hemispherical relief



(b) Schematic cascade ($p = 2, N = 4$): ball view (left), tree view (right)

Figure 4: The p -adic Waddington landscape, read two ways. **(a)** Hemispherical relief (here $p = 2$, drawn to depth 3): the ambient ball is \mathbb{Z}_p , and the relief encodes the action of the rational interpreter ϕ on each ball (Remark 6.13). Contracting balls (A) are concave blue *valleys* where iterates of ϕ converge to an attracting fixed point, expanding balls (E) are convex red *ridges* from which ϕ ejects configurations, and isometric balls (I) are flat slate-gray *plateaus*. The blue marble descends into a contracting level-2 sub-ball toward its attracting fixed point. **(b)** A schematic ball/tree cascade ($p = 2, N = 4$) illustrating how the $A/E/I$ labeling is assembled and how μ_E counts expanding nodes with the weights p^{N-n} , shown combinatorially. *Left:* \mathbb{Z}_2 decomposes at levels $n = 0, \dots, 4$ into 2^n balls, each labeled $A/E/I$ via the multipliers $\Lambda_{n,m}$ (Section 4.5). The color code is the same in both panels: blue marks A (contracting, $|\lambda|_p < 1$), red marks E (expanding, $|\lambda|_p > 1$), and slate-gray marks I (isometric, $|\lambda|_p = 1$). *Right:* the same balls as a rooted binary tree, where μ_E counts the red nodes weighted by p^{N-n} , so coarse expansion (high in the tree) is penalized more than fine expansion. This panel is schematic, not the toy model of Section 5, in which every ball is contracting and $\mu_E = 0$; the toy's state-transition graph is Figure 3. The actual cascade of the *A. thaliana* floral network is Figure 6 in Section 7.

Properties of the Stability Measure.

The sum in (27) runs from $n = 1$ to $N - 1$: at $n = 0$ there is only one ball (\mathbb{Z}_p itself), so no hierarchical information is available; levels $n = 1$ to $N - 1$ capture the full stratification from coarsest to finest. The bounds $0 \leq \mu \leq (N - 1)p^N$ are immediate from $|E(n)| \in [0, p^n]$; the upper bound is achieved only when every ball is expanding at every level.

We adopt μ_E as the primary optimization criterion throughout this paper. Expanding dynamics at coarse scales signals that configurations agreeing in the most influential genes (those occupying the leading p -adic positions) diverge under f ; this is a direct obstruction to hierarchical stability. Contraction at fine scales records local convergence among configurations that already differ in high-level regulators (Remark 6.12); the weight p^{N-n} in μ_E therefore prioritizes coarse-scale information about the regulatory hierarchy. The complementary criterion of maximizing μ_A is governed by the same trade-off (Lemma 6.3, Remark 6.5).

Definition 6.14. *Let $(x_{\alpha_0}, \dots, x_{\alpha_{N-1}})$ and $(x_{\beta_0}, \dots, x_{\beta_{N-1}})$ be two different orderings of the same N genes.*

We say that the ordering $(x_{\alpha_0}, \dots, x_{\alpha_{N-1}})$ is more stable than the ordering $(x_{\beta_0}, \dots, x_{\beta_{N-1}})$ if:

$$\mu(x_{\alpha_0}, \dots, x_{\alpha_{N-1}}) < \mu(x_{\beta_0}, \dots, x_{\beta_{N-1}}). \quad (30)$$

The measure μ induces a total preorder on the set of orderings. Different orderings give different $|E(n)|$ at each level; the minimizers are those that concentrate stability at coarse scales. In applications, orderings that place master regulators early often achieve low μ , consistent with their stabilizing role.

Finding optimal orderings.

The mathematical problem is to minimize μ over the $N!$ orderings. For a given ordering, μ is determined by (f, ι) alone (Remark 4.8); no construction of F_n or ϕ is required. Algorithm 1 gives the explicit procedure.

The cost of evaluating μ for one ordering is $O(N \cdot p^N)$, which is feasible for $N \leq 15$. For small N (e.g. $N \leq 8$) minimization over all $N!$ orderings can be done by exhaustive enumeration. For $N = 13$, the μ_E -minimizer reported here is one of four global minimizers, certified by branch-and-bound over all $13!$ orderings, with the certification logs in the reproducibility bundle [27]. A genetic algorithm (with Algorithm 1 as fitness function) independently recovers the same optimum and serves as a general-purpose method for networks where branch-and-bound may not scale.

Algorithm 1 Evaluation of μ from (f, ι)

Require: Discrete dynamical system $f : \mathcal{C} \rightarrow \mathcal{C}$; gene ordering (encoding ι)**Ensure:** Stability measure $\mu = \mu_E$

```
1: Initialize  $\mu := 0$ 
2: for each resolution level  $n = 1, \dots, N - 1$  do
3:    $E(n) := \emptyset$ 
4:   for each ball index  $m = 0, \dots, p^n - 1$  do
5:     Compute  $M_{n,m} := \max\{k \in \{0, \dots, N\} : |\{m_{f(a)} \bmod p^k : a \in \mathcal{C}, \text{trunc}_n(a) = m\}| = 1\}$ 
6:     if  $M_{n,m} < n$  then add  $m$  to  $E(n)$   $\triangleright$  expanding:  $t_{n,m} = 1/p^{M_{n,m}} > 1/p^n$ 
7:   end for
8:    $\mu := \mu + |E(n)| \cdot p^{N-n}$ 
9: end for
10: return  $\mu$ 
```

7 Worked example: *Arabidopsis thaliana* floral GRN

This section develops the framework of Sections 4–6 on the floral development network of *A. thaliana*, a well-studied Boolean GRN. The aim here is twofold: to make the constructions of the previous sections concrete on a non-trivial $N = 13$ instance, and to exhibit the consistency check that the μ_E -minimizer recovers a documented master-regulator hierarchy. A separate body of work, the companion paper [2], addresses cross-organism validation (*A. thaliana* $N = 13$, *C. elegans* $N = 8$, *D. melanogaster* $N = 6$), basin analysis, robustness under mutants and noise, and the extension to periodic attractors via iterated maps.

Remark 7.1 (The embedding as a biological model cut). *The coarse embedding $a \mapsto \iota(a) = B_{1/p^N}(m_a)$ has a natural biological reading that makes the present application particularly transparent. A Boolean GRN on N genes selects N regulatory components from a much larger biological state space: the modeled genes fix the first N digits of the p -adic expansion, and the unresolved tail $g_N g_{N+1} \dots$ stands for factors the model has chosen not to resolve (additional regulatory genes, epigenetic marks, environmental variables). The completion \mathbb{C}_p provides the analytic framework for the rational interpreter ϕ ; its role is analogous to the use of \mathbb{C} in classical modeling, where the apparatus is the natural one even when individual complex coordinates lack direct interpretation. This reading extends to Boolean regulatory dynamics two complementary traditions: the ball-as-equivalence-class formalization developed by Khrennikov for mental categories [7] and by Khrennikov–Yurova for protein conformational states [8], where observable states are obtained by factorizing a much larger ontic state space into ultrametric balls, and the Boolean-network treatment of unmeasured genes, proteins, and environmental factors as latent variables in the probabilistic framework of Shmulevich et al. [9]. The present framework realizes both traditions geometrically and deterministically, with the A/E/I partition recording the dynamical action on each equivalence class. The deeper biological justification of this reading is developed in the companion paper [2].*

The *A. thaliana* floral development network has a well-established Boolean model [11, 12] (cell fate, robustness, agreement with expression data), extended to the full flowering transition pathway in [28], and is a standard benchmark in GRN analysis [17]; we use it here to illustrate the measure μ , the classification of fixed points, and the role of ordering. We adopt the standard ABC model nomenclature for organ identities (Sepal, Petal, Stamen, Carpel, Inflorescence) and gene names (AP1, AP2, AG, PI, AP3, etc.) as in [11, 12], consistently throughout. The optimal gene ordering is not assumed from experiment; it is derived by minimizing μ from the dynamics f alone (the Boolean model does not prescribe an order; our framework selects it from the discrete map).

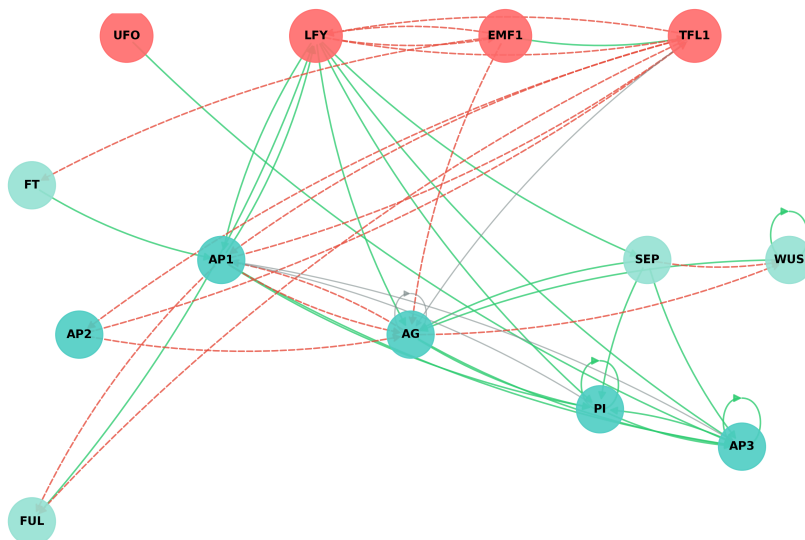


Figure 5: *A. thaliana* floral development network ($N = 13$ genes). Node colors: red = master regulators (UFO, EMF1, LFY, TFL1), dark teal = organ identity genes (AP1, AP2, AG, PI, AP3), light teal = other regulatory genes (FT, FUL, WUS, SEP). Edge styles: solid green arrows = activation, dashed red = repression, solid gray = regulation with context-dependent effect. Network topology and interaction types from [11, 12].

The regulatory network (Figure 5) and the transition table defining f are taken from [11, 12]. In those articles, the authors report the fixed points (attractors) of the network and identify each with a floral organ identity: inflorescence, sepal, petal, stamen, or carpel (the correspondence under our ordering π^* is given in Table 5). The gene order used in the reference to write the state vector is the *original-model ordering*; we compare it with the μ -minimizing ordering in Section 8. The network has $N = 13$ genes with states in $\{0, 1\}$, so \mathcal{C} has 2^{13} configurations; the map $f : \mathcal{C} \rightarrow \mathcal{C}$ is given by synchronous update of that Boolean model. The object of interest is an ordering that minimizes μ . For $N = 13$, the ordering used here is one of the four μ_E -minimizers over all $13!$ orderings, certified by branch-and-bound (certification logs in

the reproducibility bundle [27]); a genetic algorithm (Algorithm 1 as fitness function, 51 independent runs) independently recovers the same optimum and is a general-purpose method for networks where exhaustive certification is infeasible. Denote this ordering by π^* :

$$\begin{aligned} & (x_0, x_1, x_2, x_3, x_4, x_5, x_6, x_7, x_8, x_9, x_{10}, x_{11}, x_{12}) \\ & \parallel \\ & (\text{UFO}, \text{EMF1}, \text{LFY}, \text{TFL1}, \text{AP2}, \text{FT}, \text{AG}, \text{AP1}, \text{SEP}, \text{AP3}, \text{PI}, \text{WUS}, \text{FUL}). \end{aligned} \tag{31}$$

Under π^* , configurations that differ only in later genes are close in the p -adic metric; those differing in early genes (UFO, EMF1, LFY, ...) are distant. The value $\mu(\pi^*)$ is 26,776 (evaluated from f and ι_{π^*} as in Section 6). Exactly four orderings in S_{13} attain this global minimum, all four sharing the full triple $(\mu_E, \mu_A, \mu_I) = (26,776, 53,880, 17,648)$ (Remark 7.2); their certification as the global μ_E -optima over the full $13!$ permutation space is established by branch-and-bound (certification logs in the reproducibility bundle [27]). We use the value 26,776 throughout this section as the reference scale for the analysis that follows. All results in this section refer to this ordering. It places UFO, EMF1, LFY, TFL1 in the first four positions (EMF1 before LFY); the rank order of these eight regulators matches the biological hierarchy in the literature (Table 4), with Spearman $\rho = 1.0$. The biological ranking of the eight key regulators used for the Spearman comparison is the curated hierarchy supported by the experimental literature [11, 12] (see Table 4). This agreement is a genuine recovery of the biological hierarchy from the dynamics alone, and three features secure it. First, the eight genes and their ranking form an *independent benchmark*: they are the documented master and major regulators of floral identity and timing [11, 12], fixed in advance of the optimization. Second, π^* is *intrinsic to the map*: μ_E is a function of (f, ι) , so the optimal ordering emerges from the transition dynamics themselves. Third, μ_E is *equivariant under relabeling*, so the recovered hierarchy reflects the intrinsic dynamical structure and is the same under any naming of the genes. The Spearman value $\rho = 1$ is therefore a one-shot agreement between an ordering computed purely from the dynamics and an externally fixed biological ranking. The exact probability that a uniformly random ordering of the thirteen genes induces $\rho = 1$ on the same eight key regulators is $1/8! \approx 2.48 \times 10^{-5}$; a Monte Carlo over 2×10^6 random orderings yields tail probabilities $\hat{P}(\rho \geq 0.9) \approx 2.3 \times 10^{-3}$, $\hat{P}(\rho \geq 0.95) \approx 5.5 \times 10^{-4}$, $\hat{P}(\rho = 1) \approx 2.75 \times 10^{-5}$, in agreement with the exact value (verification script V6 in the Zenodo reproducibility bundle). The match obtained by π^* is therefore approximately 1 in 36,000 under the null. Four orderings attain $\mu_E = 26,776$; they differ from π^* by transpositions in two pairs of positions (EMF1,LFY and AP2,FT) and share the same tail (genes in positions 7–13).

Remark 7.2 (The μ_E -optimal set is four-fold degenerate). *The global minimum $\mu_E = 26,776$ is attained by exactly four orderings. They differ from π^* only by transpositions within two pairs of adjacent positions (positions 2–3, EMF1 and LFY; positions 5–6, AP2 and FT), and all four share the full triple $(\mu_E, \mu_A, \mu_I) = (26,776, 53,880, 17,648)$ and the per-ball A/E/I classification at every scale (verified computationally). The*

representative π^* has Spearman $\rho = 1$ with the strict no-ties benchmark of Table 4. With that strict ranking the other three μ_E -minimizers have Spearman values 41/42, 41/42, and 20/21, differing from π^* only by adjacent transpositions within the two dynamically degenerate pairs and sharing the tail in positions 7–13. If those two pairs are treated as interchangeable, all four minimizers realize the same coarse regulatory hierarchy.

| Pos. | Gene | Biological Role | Key phenotype (refs.) |
|------|------|-----------------------------------|-------------------------------------|
| 1 | UFO | Organ identity modulator | Petal/stamen defects |
| 2 | EMF1 | Flowering repressor | <i>emf1</i> : flower early |
| 3 | LFY | Master regulator, floral identity | <i>leafy</i> mutants fail to flower |
| 4 | TFL1 | Inflorescence identity | <i>tfl1</i> : terminal flower |
| 5 | AP2 | Organ identity, represses AG | Homeotic transformations |
| 6 | FT | Flowering promoter | Late flowering mutants |
| 7 | AG | Stamen/carpel identity | No reproductive organs |
| 8 | AP1 | Floral meristem identity | Inflorescence-like structures |

Table 4: Ordering π^* (Eq. 31) vs. biological hierarchy for *A. thaliana*. Model rank = position of each regulator in π^* ; biological rank = order in this table. Spearman ρ on these eight ranks (no ties). Phenotypes from [11, 12].

With this ordering, the partition at each scale and hence the stability classification are fixed (Remark 4.26); the leading positions are occupied by master regulators.

Construction of Hierarchical Approximations.

The rational approximations F_0, \dots, F_4 displayed below encode the dynamics of f at the first four scales, which are the scales used here to separate the fixed-point classes; their construction follows Section 4.

Balls are classified as in Definition 4.21 (Section 6).

Let $\phi \in \mathbb{C}_2(z)$ be a rational function which interprets the dynamics of f . The target image balls at each level are read off from the transition table of f (taken from [11, 12]; the full table is in the reproducibility bundle) as the radii $t_{n,m}$ of Section 6. By definition of ϕ , we need $F_0(\mathfrak{B}_1(0)) = \mathfrak{B}_1(0)$, so we can choose $F_0(z) = z$. For F_1 , any 1-approximation $F_1 \in \mathbb{C}_2(z)$ should satisfy:

$$\begin{aligned} F_1(\mathfrak{B}_{1/2}(0)) &= \mathfrak{B}_{1/2}(0), \\ F_1(\mathfrak{B}_{1/2}(1)) &= \mathfrak{B}_{1/2}(1). \end{aligned} \tag{32}$$

For example, we can take $F_1(z) = z$. Any 2-approximation $F_2 \in \mathbb{C}_2(z)$ should satisfy:

$$\begin{aligned} F_2(\mathfrak{B}_{1/4}(0)) &= \mathfrak{B}_{1/2}(0), & F_2(\mathfrak{B}_{1/4}(1)) &= \mathfrak{B}_{1/2}(1), \\ F_2(\mathfrak{B}_{1/4}(2)) &= \mathfrak{B}_{1/2}(0), & F_2(\mathfrak{B}_{1/4}(3)) &= \mathfrak{B}_{1/2}(1). \end{aligned} \tag{33}$$

Using Theorem 4.12, we can construct the rational function F_2 with the appropriate properties.

Since $F_2(\mathfrak{B}_{1/4}(0)) = \mathfrak{B}_{1/2}(0) \supsetneq \mathfrak{B}_{1/4}(0)$, the dynamics of f is 2-expanding in $\mathfrak{B}_{1/4}(0)$, and similarly in $\mathfrak{B}_{1/4}(1)$, $\mathfrak{B}_{1/4}(2)$ and $\mathfrak{B}_{1/4}(3)$. Any 3-approximation $F_3 \in \mathbb{C}_2(z)$ should satisfy:

$$\begin{aligned} F_3(\mathfrak{B}_{1/8}(0)) &= \mathfrak{B}_{1/16}(6), & F_3(\mathfrak{B}_{1/8}(1)) &= \mathfrak{B}_{1/16}(7), \\ F_3(\mathfrak{B}_{1/8}(2)) &= \mathfrak{B}_{1/4}(2), & F_3(\mathfrak{B}_{1/8}(3)) &= \mathfrak{B}_{1/4}(3), \\ F_3(\mathfrak{B}_{1/8}(4)) &= \mathfrak{B}_{1/16}(4), & F_3(\mathfrak{B}_{1/8}(5)) &= \mathfrak{B}_{1/16}(5), \\ F_3(\mathfrak{B}_{1/8}(6)) &= \mathfrak{B}_{1/4}(0), & F_3(\mathfrak{B}_{1/8}(7)) &= \mathfrak{B}_{1/4}(1). \end{aligned} \tag{34}$$

The dynamics of f is 3-expanding in $\mathfrak{B}_{1/8}(2)$, $\mathfrak{B}_{1/8}(3)$, $\mathfrak{B}_{1/8}(6)$ and $\mathfrak{B}_{1/8}(7)$ (image radius $1/4 > 1/8$), and 3-contracting in $\mathfrak{B}_{1/8}(0)$, $\mathfrak{B}_{1/8}(1)$, $\mathfrak{B}_{1/8}(4)$ and $\mathfrak{B}_{1/8}(5)$ (images $\mathfrak{B}_{1/16}(6)$, $\mathfrak{B}_{1/16}(7)$, $\mathfrak{B}_{1/16}(4)$, $\mathfrak{B}_{1/16}(5)$ respectively). Any 4-approximation $F_4 \in \mathbb{C}_2(z)$ should satisfy:

$$\begin{aligned} F_4(\mathfrak{B}_{1/16}(0)) &= \mathfrak{B}_{1/64}(54), & F_4(\mathfrak{B}_{1/16}(1)) &= \mathfrak{B}_{1/64}(55), \\ F_4(\mathfrak{B}_{1/16}(2)) &= \mathfrak{B}_{1/8}(6), & F_4(\mathfrak{B}_{1/16}(3)) &= \mathfrak{B}_{1/8}(7), \\ F_4(\mathfrak{B}_{1/16}(4)) &= \mathfrak{B}_{1/64}(52), & F_4(\mathfrak{B}_{1/16}(5)) &= \mathfrak{B}_{1/64}(53), \\ F_4(\mathfrak{B}_{1/16}(6)) &= \mathfrak{B}_{1/128}(20), & F_4(\mathfrak{B}_{1/16}(7)) &= \mathfrak{B}_{1/128}(21), \\ F_4(\mathfrak{B}_{1/16}(8)) &= \mathfrak{B}_{1/128}(38), & F_4(\mathfrak{B}_{1/16}(9)) &= \mathfrak{B}_{1/128}(39), \\ F_4(\mathfrak{B}_{1/16}(10)) &= \mathfrak{B}_{1/8}(2), & F_4(\mathfrak{B}_{1/16}(11)) &= \mathfrak{B}_{1/8}(3), \\ F_4(\mathfrak{B}_{1/16}(12)) &= \mathfrak{B}_{1/64}(36), & F_4(\mathfrak{B}_{1/16}(13)) &= \mathfrak{B}_{1/64}(37), \\ F_4(\mathfrak{B}_{1/16}(14)) &= \mathfrak{B}_{1/128}(0), & F_4(\mathfrak{B}_{1/16}(15)) &= \mathfrak{B}_{1/128}(1). \end{aligned} \tag{35}$$

The dynamics of f is 4-contracting in $\mathfrak{B}_{1/16}(4)$ and $\mathfrak{B}_{1/16}(5)$, and 4-expanding in $\mathfrak{B}_{1/16}(10)$ and $\mathfrak{B}_{1/16}(11)$.

Remark 7.3. *With a 3-approximation F_3 , the dynamics of f is 3-contracting in $\mathfrak{B}_{1/8}(4)$ and $\mathfrak{B}_{1/8}(5)$ (images $B_{1/16}(4)$, $B_{1/16}(5)$), and 3-expanding in $\mathfrak{B}_{1/8}(2)$, $\mathfrak{B}_{1/8}(3)$, $\mathfrak{B}_{1/8}(6)$, $\mathfrak{B}_{1/8}(7)$. With a 4-approximation F_4 , the dynamics is 4-expanding in $\mathfrak{B}_{1/16}(10)$ and $\mathfrak{B}_{1/16}(11)$ (images $B_{1/8}(2)$, $B_{1/8}(3)$).*

Since $\mathfrak{B}_{1/16}(10) \subsetneq \mathfrak{B}_{1/8}(2)$ and $\mathfrak{B}_{1/16}(11) \subsetneq \mathfrak{B}_{1/8}(3)$, the n -approximations narrow down, through filtration, the balls that exhibit expanding dynamics (expansion) and that contain the inflorescence fixed points of f . This hierarchical refinement progressively locates unstable configurations (those in expanding balls).

Analogously for attracting points, $\mathfrak{B}_{1/16}(4) \subsetneq \mathfrak{B}_{1/8}(4)$ and $\mathfrak{B}_{1/16}(5) \subsetneq \mathfrak{B}_{1/8}(5)$.

Identification of Attractors and Repellers.

Fixed points of this network and their link to floral organ identities are well established [11, 12, 29]. Here we use *fixed point* for a configuration a with $f(a) = a$, and *contracting/expanding* for the ball-level classification from the p -adic environment (Remark 2.4): the former marks stable (contracting) neighborhoods, the latter expanding ones, giving a finer picture than treating all fixed points as equivalent attractors.

Under the best-known ordering π^* (Eq. 31, Table 4), f has exactly 10 fixed points, grouped in four balls at resolution $n = 4$. Note that configuration indices in this subsection and in Table 5 use the encoding $m = \sum_{k=0}^{N-1} x_{\alpha_k} 2^k$ with π^* ; ball assignment depends on the chosen ordering.

- Contracting $B_{1/16}(4)$: four fixed points (436, 1972, 5492, 6004) with UFO=0, EMF1=0, LFY=1, TFL1=0 (floral identity: Sepal, Carpel, Petal, Stamen in the ABC interpretation).
- Contracting $B_{1/16}(5)$: two fixed points (1973, 6005), UFO=1, EMF1=0, LFY=1, TFL1=0 (Petal and Stamen with UFO active).
- Expanding $B_{1/16}(10)$: two fixed points (10, 2058), inflorescence-like (UFO=0, EMF1=1, LFY=0, TFL1=1); the ball has expanding dynamics (Remark 4.24).
- Expanding $B_{1/16}(11)$: two fixed points (11, 2059), same inflorescence pattern with UFO=1.

Observe that mature organs sit in contracting ball chains (stable endpoints; see Remark 4.25) and inflorescence states in expanding balls (biologically transient, though fixed under f). Indeed, the 10 fixed points and their organ identities match the ABC interpretation of [11, 12]: Sepal 436; Petal 1972, 1973; Stamen 6004, 6005; Carpel 5492; Inflorescence 10, 2058, 11, 2059 (LFY=0).

Figure 6 summarizes this basin layout: $B_{1/16}(4)$ and $B_{1/16}(5)$ hold stable organ fates; $B_{1/16}(10)$ and $B_{1/16}(11)$ hold inflorescence-like fixed configurations, biologically transient and lying in expanding balls. The $A/E/I$ word is attached to the chain of observable balls containing the discrete fixed configuration; it records scale-wise contraction or expansion of the induced observable uncertainty, and when an analytic fixed point exists in the corresponding \mathbb{C}_p -ball, this agrees with the classical attracting/repelling interpretation. The observable classification itself is defined purely from (f, ι) (Theorem 6.8).

Biological Interpretation.

Remark 7.4. *In the Boolean model of [11, 12], the condition $(0, 1, 1, 1, x_4, \dots, x_{12})$ (i.e., UFO=0, EMF1=1, LFY=1, TFL1=1 in the first four positions of π^* , with arbitrary states for the remaining genes) guarantees convergence under iteration of f to the Carpel fixed point $(0, 0, 1, 0, 1, 1, 1, 0, 1, 0, 1, 0, 1)$ (configuration 5492). In the p -adic encoding these 512 configurations form a single ball $B_{1/16}(14)$ (the prefix $(0, 1, 1, 1)$ encodes $m = 0 \cdot 2^0 + 1 \cdot 2^1 + 1 \cdot 2^2 + 1 \cdot 2^3 = 14$), and all of them flow to Carpel: the entire ball lies inside the Carpel basin. The Carpel fixed point itself is not in this ball (it has prefix $(0, 0, 1, 0)$, with EMF1=0 in the second digit, and so sits in a different ball), so $B_{1/16}(14)$ marks a sub-basin that funnels into Carpel, rather than the location of the Carpel state. This is exactly the entry $F_4(B_{1/16}(14)) = B_{1/128}(0)$ in (35), confirming contracting dynamics ($\Lambda_{4,14} = 1/8$).*

In that model, the combination UFO=0, LFY=1, TFL1=1 with EMF1=1 in the encoding (the basin condition) eventually reaches the Carpel fate regardless of the other genes' initial states. Within the Boolean model and its induced discrete dynamics f , the hierarchical analysis thus confirms that these genes, when placed in early positions

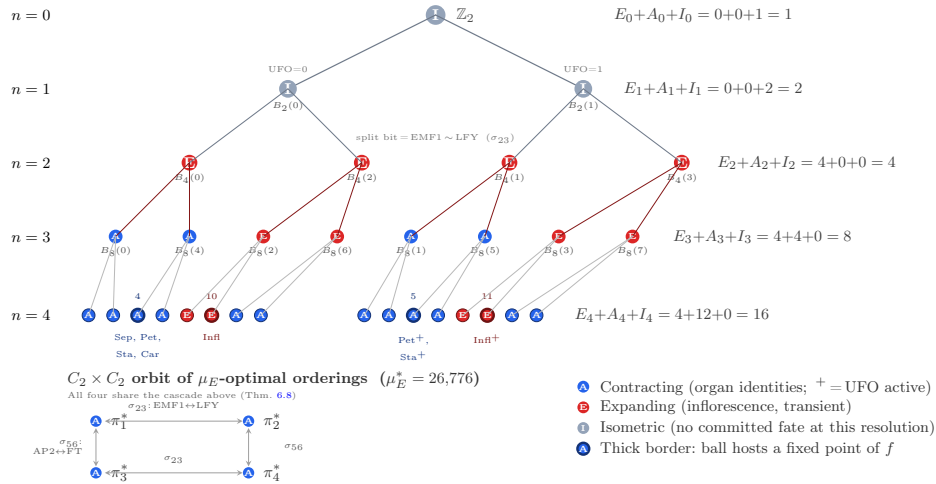


Figure 6: Hierarchical p -adic ball cascade for the *A. thaliana* floral GRN under ordering π^* (Eq. 31). The tree shows the $1 + 2 + 4 + 8 + 16 = 31$ balls at levels $n = 0, \dots, 4$; the four balls at the leaf level that host the ten fixed points of f are highlighted by thicker borders. The color scheme matches Figure 4: **blue** for contracting balls (A , organ identities canalized into stable basins: Sepal, Petal, Stamen, Carpel, with and without UFO), **red** for expanding balls (E , inflorescence states, biologically transient, with persistent expansion at fine scales), **gray** for isometric balls (I , no committed fate at this resolution; refinement deferred to a finer scale). Each fixed point inherits the A/E/I word of its containing chain: floral organs read IEAA, inflorescence reads IEEEE (see Table 5); the level-1 ball labels mark the UFO bit (the leading coordinate of π^*). The intrinsic A/E/I type of each ball depends only on (f, ι) by Theorem 6.8 and is invariant under the four μ_E -optimal orderings (Remark 7.2). Dynamics f from [11, 12].

in the p -adic encoding, have the most significant influence on the network's long-term behavior and act as master regulators.

The ordering that minimizes μ places UFO, EMF1, LFY, and TFL1 in the leading positions, and the ball-level classification separates mature floral organs (contracting) from inflorescence states (expanding). This separation reflects a biological asymmetry: organs are stable developmental endpoints, while inflorescence states, though fixed points of f , lie in expanding balls and are biologically transient developmental intermediates. The four leading genes are established master regulators:

- *LFY* (LEAFY) is a well-established master regulator of floral identity. Mutations in *LFY* produce plants that fail to flower, generating leaf-like structures instead [30, 31]; *LFY* activates the floral organ identity genes (AP1, AP3, AG) and is essential for the transition from inflorescence to floral meristem identity.
- *UFO* (UNUSUAL FLORAL ORGANS) specifies petal and stamen identity. Loss-of-function mutants exhibit homeotic transformations (petals replaced by

sepals, stamens by carpels [32]), consistent with UFO acting as a cofactor whose hierarchical position influences network stability.

- *EMF1* (EMBRYONIC FLOWER 1) represses flowering and maintains the vegetative state. Loss of EMF1 causes premature flowering, supporting its role in developmental timing [33].
- *TFL1* (TERMINAL FLOWER 1) maintains inflorescence meristem identity and antagonizes LFY. *tfl1* mutants produce terminal flowers instead of indeterminate inflorescences [34].

The classification of mature floral organs as lying in *contracting* balls recalls the concept of *canalization* [35]: once a cell commits to a particular fate, it maintains that identity despite minor perturbations. In the framework, this robustness manifests as ball-level contraction at fine scales.

Conversely, inflorescence states lie in *expanding* balls: the image expands beyond the ball radius, reflecting their transient character as developmental intermediates that progress toward organ formation [11]. The contracting/expanding dichotomy parallels the valleys and ridges of Waddington’s *epigenetic landscape* [36], with the p -adic metric providing a quantitative counterpart.

Scale-dependent stability classification.

We propose a scale-dependent classification: for each fixed point, the *sequence* of ball-level types (contracting, expanding, isometric) across resolution levels. The classification (contracting ‘A’, expanding ‘E’, or isometric ‘I’) at levels $n = 1, 2, 3, 4$ yields a 4-character sequence per fixed point, revealing qualitative differences invisible to standard Boolean analysis. This four-scale sequence is the prefix of the full scale-resolved word, which has length $N - 1 = 12$ for the *A. thaliana* network; levels $n = 1, 2, 3, 4$ are the scales at which the organ/inflorescence separation occurs.

| Config | Ball | Seq. | Ball type | State | Key genes |
|--------|----------------|------|-------------|------------|----------------------|
| 436 | $B_{1/16}(4)$ | IEAA | Contracting | Sepal | LFY, AP1 |
| 1972 | $B_{1/16}(4)$ | IEAA | Contracting | Petal | LFY, AP3 |
| 5492 | $B_{1/16}(4)$ | IEAA | Contracting | Carpel | LFY, AG |
| 6004 | $B_{1/16}(4)$ | IEAA | Contracting | Stamen | LFY, AG, AP3 |
| 1973 | $B_{1/16}(5)$ | IEAA | Contracting | Petal+UFO | UFO, LFY |
| 6005 | $B_{1/16}(5)$ | IEAA | Contracting | Stamen+UFO | UFO, LFY, AG |
| 10 | $B_{1/16}(10)$ | IEEE | Expanding | Inflor. | EMF1, TFL1, LFY=0 |
| 2058 | $B_{1/16}(10)$ | IEEE | Expanding | Inflor. | EMF1, TFL1, WUS |
| 11 | $B_{1/16}(11)$ | IEEE | Expanding | Inflor. | EMF1, TFL1, UFO |
| 2059 | $B_{1/16}(11)$ | IEEE | Expanding | Inflor. | EMF1, TFL1, WUS, UFO |

Table 5: Classification sequence of fixed points under the best-known ordering π^* (Table 4). Seq. = classification at levels $n = 1, 2, 3, 4$ (the four-scale prefix of the full length- $(N-1)$ word); level $n = 1$ is I for all balls by (32). Config numbers use the encoding $m = \sum_{k=0}^{N-1} x_{\alpha_k} 2^k$ with that order. A=contracting, E=expanding, I=isometric; computed from $\Lambda_{n,m}$.

(Stamen configurations 6004 and 6005 have AP2=1 in the encoding; this is a property of the Boolean model [11, 12], not an assertion about canonical ABC biology.)

The 10 fixed points partition into two classes by their classification sequences (Table 5). The IEAA pattern (6 fixed points): isometric at level 1, expanding at level 2, then contracting at levels 3–4; these are floral organ identities (LFY=1), and the system *stabilizes* at fine scales by transitioning from expansion to contraction. The IEEI pattern (4 fixed points): isometric at level 1, then expanding at levels 2–4; these are inflorescence states (TFL1=1, LFY=0), where expansion *persists* across all finer scales. The key distinction is whether the system *stabilizes* (transitions from E to A) at fine scales. Standard Boolean network analysis treats all 10 fixed points as equivalent; the framework separates them, matching the observation that inflorescence is a developmental waypoint rather than a terminal state [11].

What the scale-resolved word sees that single-scale stability does not.

The ten fixed points fall into two classes fixed in advance from the biology: six floral-organ identities and four inflorescence states (LFY off). The *A/E/I* word separates them without exception, organs reading IEAA and inflorescence reading IEEI (Table 5). In both, the dynamics expands at level 2, but in an organ the expansion gives way to contraction at finer scales (the transition E→A, the ball-level multiplier crossing 1, the configuration settling into a canalized basin), while in an inflorescence state it persists at every scale. A single-scale stability descriptor does not draw this line. The average Boolean sensitivity $s(a) = N^{-1} \sum_i \mathbf{1}[f(a \oplus e_i) \neq a]$ equals 7/13 for all four inflorescence fixed points, a value that lies inside the organ range [6/13, 11/13]: one organ is strictly less sensitive (6/13) than every inflorescence state and another matches them exactly (7/13), so no threshold on s separates the two classes. The separation is carried by the resolution-by-resolution profile, an object of the ball tree, not by any scalar read at a single scale. The same gap appears in coordinate ranking: UFO has wiring out-degree one (it regulates only AP3) and is ranked last by centrality, yet μ_E places it first, because its leading p -adic position governs the coarsest splitting of the state space. The recovery of the master-regulator hierarchy (Spearman $\rho = 1$) is a sanity check that simpler rankings also pass. The scale-resolved *A/E/I* classification of fixed points is what the construction adds beyond it.

Statistical robustness of the best-known ordering across multiple algorithm runs, comparison with alternative orderings, and the analysis of basins of attraction, mutant frequency, and sensitivity to environmental noise (with applications to biotechnology) are addressed in the companion paper [2], which extends the worked example here to *C. elegans* and *D. melanogaster*.

8 Discussion

We introduced a hierarchical framework that embeds discrete GRN dynamics into \mathbb{Z}_p and uses rational approximations F_0, \dots, F_N to classify ball-level dynamics as n -contracting, n -expanding, or n -isometric at each resolution. The stability measure μ is defined from the discrete data (f, ι) alone (Theorem 6.8) and satisfies $\mu_E + \mu_A + \mu_I = (N-1)p^N$ (Lemma 6.3), so that minimizing expansion is equivalent to maximizing the sum $\mu_A + \mu_I$, not to maximizing μ_A alone (Remark 6.5). Whether the μ_E - and μ_A -minimizing orderings coincide is examined in Part II [2]. The p -adic hierarchy

exposes structure that flat attractor analysis cannot: a minimizing ordering places master regulators first, and ball-level contraction separates developmental outcomes (mature organ identities in contracting balls, inflorescence states in expanding ones), in line with canalization [35] and epigenetic landscape models [36, 37]. The ultrametric encodes this quantitatively: configurations agreeing in master-regulator digits are p -adically close, so downstream variation may converge to one fate while regulator-level differences drive distinct outcomes.

What the framework adds.

Note that Boolean analysis identifies attractors and basins but treats all configurations in a basin alike. Here, μ_E gives a scalar that quantifies how much expanding behavior appears across scales, and it depends on the ordering: in *A. thaliana* the optimal ordering gives $\mu_E(\pi^*) = 26,776$ while the original-model ordering [11, 12] gives $\mu_E = 80,704$ on the same map f . Minimizing $\mu_E(\pi)$ over the $N!$ orderings is precisely what selects the optimal ordering π^* . The ball-level classification separates fixed points by local dynamics: under π^* , the four inflorescence fixed points are carried by the 4-quasi-repellers $B_{1/16}(10)$ and $B_{1/16}(11)$, while the six organ-identity fixed points are carried by the 4-quasi-attractors $B_{1/16}(4)$ and $B_{1/16}(5)$ (Table 5); the decomposition $\mu = \sum_{n=1}^{N-1} |E(n)| p^{N-n}$ shows which levels contribute most (e.g. level $n = 2$ accounts for about 30.6%, identifying the first few positions as a stability bottleneck). The A/E/I sequence over levels (Table 5) separates fixed points that stabilize at fine scales (IEAA, floral organs) from those that remain expanding (IEEE, inflorescence). All of this is computable from (f, ι) alone.

Observational interpretation.

Conceptually, the framework separates microstates from their coarse-grained classes. A configuration corresponds to a finest-scale ball, whereas larger balls encode coarser observation classes. The dynamics therefore acts not only on individual configurations, but also on families of observables across resolutions. From this viewpoint, contracting, expanding, and isometric behavior describe whether one update decreases, increases, or preserves observational uncertainty. This reading is natural for biological systems, where exact microstates are rarely measurable and predictions are made at finite resolution.

Methodological note.

The sole input to the optimization is the transition map $f: \mathcal{C} \rightarrow \mathcal{C}$ from the Boolean model [12, 17]; no gene labels, expression data, or prior ranking enter the computation, and the measure μ_E has no adjustable parameters (equation (27)). That this parameter-free criterion recovers the master-regulator hierarchy established by decades of experimental genetics [11, 31] is a nontrivial consistency check for a $13!$ -ordering search (Section 7, Table 4).

Validation beyond a single network.

The framework applies without modification to any finite system identified with \mathbb{F}_p^N for some prime p . The prime is genuinely free: for the ternary system $X' = Y + Z$,

$Y' = X + Z$, $Z' = Z$ over \mathbb{F}_3 ($N = 3$), exhaustive search over the $3! = 6$ orderings gives $\mu_E^* = 27$, attained at exactly two orderings related by the $X \leftrightarrow Y$ swap, with the same $A/E/I$ classification as in the Boolean case, and the same system over \mathbb{F}_5 returns $\mu_E^* = 125$. Although *A. thaliana* is the example worked in full here, the framework is tested well beyond a single case. The companion paper [2] certifies μ_E -optimal orderings for three developmental networks (*A. thaliana* $N=13$, *C. elegans* $N=8$, *D. melanogaster* $N=6$), with certified $(\mu_E^*, \mu_A^*, \mu_I^*)$ triples, basin analysis, and the extension to periodic attractors via iterated maps.

In each row the control identity of Lemma 6.3 holds exactly, and the leading positions of the μ_E -minimizing ordering coincide with master regulators independently identified in the experimental literature.

Mixed-radix networks.

The single-prime analysis applies to networks all of whose nodes share one prime cardinality p . Multivalued models whose state space factors as $\prod_i \mathbb{F}_{p_i}^{N_i}$ across distinct primes fall outside a single \mathbb{F}_p . When the update is congruence-preserving across primes, the functional graph splits as a direct product (a Dynamic Chinese Remainder Theorem), so the hierarchy analysis is well posed block by block at each prime, while genuinely cross-prime coupling (the smallest witness being an $m = 6$ obstruction) requires a coupled, adelic-style treatment. The full development for composite alphabets is the subject of the companion paper [38].

Context: three traditions joined by the present framework.

The framework sits at the confluence of three established lines of work, each of which independently develops one ingredient of the present construction.

(i) *Non-Archimedean discrete dynamics and automata theory* [3, 39] established the inverse-limit picture $\mathbb{Z}_p = \varprojlim_k \mathbb{Z}/p^k\mathbb{Z}$, in which finite spaces \mathbb{F}_p^N appear as level- N truncations and balls are the natural neighborhoods of states indistinguishable at a given resolution. Non-Archimedean methods for discrete dynamics have a record in nonlinear phenomena, beginning with the p -adic Siegel-disc geometry of [4]. The compatibility of automaton transitions across truncations (including the characterization of 1-Lipschitz maps as those whose first n output digits depend only on the first n input digits) is the algebraic backbone of the present framework. That tradition does not apply this structure to gene regulation nor develop a variational principle over coordinate orderings.

(ii) *p -Adic biology and ball-as-class semantics.* The review [5] synthesizes the broader claim that biological systems are naturally hierarchical, with ultrametric balls as a structural language. The explicit treatment of balls as observational equivalence classes appears in [7] for mental categories, in [8] for protein conformational states, and in [40] for the 2-adic geometry of the genetic code: the (huge) ontic state space is factorized into ultrametric balls, and observable functional states are obtained as equivalence classes. These works supply the conceptual precedent for the ball-as-class reading used here, but address proteins, cognition, and the genetic code rather than Boolean GRNs, and develop no analogue of the variational $A/E/I$ classification we use to read the dynamics.

(iii) *Boolean network theory: projection and latent variables.* The foundational paper [9] motivates probabilistic Boolean networks by three explicit sources of uncertainty: intrinsic biological variability, experimental noise, and latent variables (proteins, environmental factors, unmeasured genes). Subsequent reduction methods preserve attractors under projection [10] or under collapse of equivalence classes of dynamically indistinguishable states [41]. These works treat the smaller model as a projection of a larger latent dynamics, with the uncertainty layer absorbed probabilistically and the reduced dynamics given by transition rules.

Contributions relative to the three traditions.

The present work joins these three strands into a single deterministic geometric framework and adds four specific contributions absent from any of them. *First*, a geometric realization of the Boolean model cut: the coarse embedding $a \mapsto \iota(a) = B_{1/p^N}(m_a)$ identifies each modeled configuration with the equivalence class of all p -adic integers agreeing in the first N digits, and the rational interpreter $\phi \in \mathbb{C}_p(z)$ supplies the dynamical continuation, replacing the probabilistic uncertainty layer of [9] with an analytic one. *Second*, a new structural invariant for finite discrete systems: the ordering-dependent stability measure $\mu = (\mu_E, \mu_A, \mu_I)$ and the ball-level $A/E/I$ classification, both intrinsic to (f, ι) alone (Theorem 6.8); no analogue of this Lyapunov-type ball-level trichotomy appears in [3] (which treats individual fixed-point dynamics of the lifted map) or in [7, 8] (which use balls as equivalence classes without dynamical classification). *Third*, a variational principle on S_N : $\text{Opt}(f) := \arg \min_{\pi} \mu_E(\pi)$. This optimization over coordinate orderings has no precedent in the three traditions cited. *Fourth*, a concrete biological readout: on the *A. thaliana* floral GRN, π^* places the documented master regulators in the leading positions and matches the experimentally established hierarchy of eight key regulators with Spearman $\rho = 1$, recovered from the transition map alone.

Comparison with related modeling traditions.

Beyond the three lines above, three further comparisons are worth making explicit. Topology-based methods focus on structure; the present framework uses the same discrete dynamics f but adds the ultrametric and the measure μ , so that stability is quantified and orderings can be compared. Differential-equation models need kinetic parameters and yield continuous dynamics; here the dynamics remain discrete and the p -adic side is used for the multi-scale classification. Epigenetic landscape approaches [25, 29], most recently a topological analysis of the same network’s basins as an epigenetic forest [42], study hierarchical developmental structure on this floral GRN. The present construction builds hierarchy from the discrete map f and an ordering, and μ measures how stable that hierarchy is.

Position among standard descriptors.

Table 6 places the construction against the standard families of descriptors. Centrality, Boolean sensitivity and canalization, and the hypercube-isometry classification of [43] all rank or group coordinates from the wiring or the truth tables at a single scale. What sets the present framework apart is the combination none of them provides: it is at

once multi-scale and ordering-dependent, so it selects a coordinate ordering intrinsic to the dynamics and, through the $A/E/I$ classification, assigns each fixed point a scale-resolved stability word. The ball-level $A/E/I$ trichotomy is the genuinely new object. Recovering the master-regulator hierarchy is a check that simpler rankings also approach. The scale-resolved stability word that distinguishes canalized organ fates from inflorescence states in expanding balls across resolutions is not (Section 7). The word is also genuinely dynamical rather than a statistic of the wiring graph: under an iterate f^k it generally changes, periodic orbits acquiring $A/E/I$ words of their own [2], whereas every wiring-based descriptor is identical for f and f^k .

| Descriptor | Resolves coordinates | Multi-scale | Intrinsic optimal ordering | Per-fixed-point stability word |
|--|----------------------|-------------|----------------------------|--------------------------------|
| Lyapunov exponent, entropy | – | – | – | – |
| Network centrality [44] | ✓ | – | – | – |
| Boolean sensitivity, canalization [45] | ✓ | – | – | – |
| Fibration symmetry [46] | ✓ | – | – | – |
| CANA input-symmetry [47] | ✓ | – | – | – |
| Hypercube isometry [43] | ✓ | – | – | – |
| μ_E with $A/E/I$ (this work) | ✓ | ✓ | ✓ | ✓ |

Table 6: The ordering-dependent measure against standard descriptors of finite discrete dynamics. Permutation-invariant scalars (Lyapunov exponent, topological entropy) resolve no coordinates; centrality and sensitivity rank or group coordinates but at a single scale; the symmetry methods group nodes from wiring or per-function structure. Only the present construction is simultaneously multi-scale and ordering-dependent, hence selects an ordering intrinsic to f and grades each fixed point by scale.

Relation to canalizing-layer and modular decompositions of Boolean networks.

A separate body of work decomposes each Boolean update function f_i into nested canalizing layers, yielding an algebraic ranking of the inputs of f_i that captures their per-function priority (the decomposition problem is itself NP-hard) [48]. That decomposition is local and syntactic: it operates on each f_i in isolation, from the algebraic structure of its truth table, and produces one ranking per function. The variational ordering π^* of the present framework is global and dynamical: it minimizes a scale-resolved expansion functional μ_E over the joint dynamics of all f_i , and produces a single ordering of the N coordinates shared across the network. The two notions arise from orthogonal principles, algebraic structure of individual f_i versus dynamical contraction at the ball level under joint update, and need not coincide on any given network; a systematic empirical comparison across the three biological networks studied in [2] is the natural place for that experiment. Related modular decompositions of Boolean networks group nodes into modules with intrinsic dynamics [49]; that is again orthogonal to the present coordinate ordering, since modules are subnetworks while π^* ranks individual coordinates.

Dependence on the prime p .

Recall that the definitions of $t_{n,m}$, $\Lambda_{n,m}$, and the classification A/E/I depend on the prime p used in the embedding $\mathbb{F}_p^N \hookrightarrow \mathbb{Z}_p$. For Boolean networks the choice $p = 2$ is canonical (forced by the binary state space); for k -ary networks with k prime, the canonical choice is $p = k$. Networks whose state space is a product $\prod_i \mathbb{Z}/k_i\mathbb{Z}$ with mixed k_i require working over the profinite ring $\prod_i \mathbb{Z}_{k_i}$ (Section 3); the framework adapts, but the resulting measure is not directly comparable across choices of p .

Three modes of use.

The variational problem $\pi^* = \arg \min_{\pi \in S_N} \mu_E(\pi)$ studied here is one of three useful regimes.

- *Diagnostic mode*: for a user-chosen ordering π (e.g. one supplied by experiment, or one in which the suspected master regulators occupy the leading positions), the scale-resolved A/E/I word and the level decomposition of μ_E classify each fixed point as contracting, expanding, or isometric at each resolution. Evaluating the classification for that single ordering costs $O(N p^N)$; no search over the $N!$ orderings is performed in this mode.
- *Constrained-optimization mode*: partial constraints (“fix gene i at position 0, leave the rest free”) reduce the search to a strict sub-permutation set, on which branch-and-bound or a genetic algorithm returns the conditionally optimal completion.
- *Unconstrained mode*: full minimization over S_N , exercised here on *A. thaliana* ($N = 13$, certified by branch-and-bound). For larger networks where unconstrained certification is unaffordable, the diagnostic mode at a literature-grounded ordering, the constrained mode on its neighborhood, and a memetic genetic algorithm (PMX crossover with hill-climbing refinement, using Algorithm 1 as fitness function) cover the practical applications.

The underlying classification and stability measure are unchanged across modes. Systematic comparison with alternative metaheuristics (simulated annealing, tabu search, learned policies) for $\arg \min_{\pi} \mu_E(\pi)$ is a natural direction we have not pursued here.

What recovery of the biological hierarchy actually says.

Whenever the unconstrained mode certifies a global minimum (by exhaustive enumeration or by branch-and-bound), the resulting π^* identifies, by construction, the coordinates whose placement at coarse scales most reduces the multiscale expansion functional μ_E . A different objective on the same ordering space (e.g. maximization of μ_A) would define a different minimizer, identifying the most influential coordinates *for that objective* instead. The empirically striking observation in the *A. thaliana* worked example of Section 7 is that the certified μ_E -minimizer *coincides* with the master regulators identified by decades of experimental genetics, with no biological input to the optimization. At face value this is a consistency check; read more strongly it suggests that, in the stable regimes that support robust development, regulatory architectures sit close to a μ_E -minimum, a chaos-controlled basin of dynamical organization. A complementary identification of master regulators as *order parameters* of

gene-expression states, derived from a Hopfield-type free-energy landscape rather than from a p -adic variational principle, has been obtained independently by Krämer [50]; the two viewpoints converge on the same biological objects through orthogonal formal routes.

Scope and limitations.

The framework applies to any discrete system with $|\mathcal{C}| = p^N$, $f: \mathcal{C} \rightarrow \mathcal{C}$, and a meaningful component order. We use $p = 2$; definitions and results extend to arbitrary primes p . Potential applications include metabolic, signaling, neural, and immune networks. Minimizing μ over $N!$ orderings is combinatorially hard: for $N \leq 8$ exhaustive enumeration is feasible, and for $N = 13$ the ordering reported here was obtained by branch-and-bound certification and independently verified by a genetic-algorithm heuristic.

Remark 8.1 (Open problem: submodularity and a convex structure for μ_E). *The minimization $\pi^* = \arg \min_{\pi} \mu_E$ runs over the finite group S_N and carries no Euler-Lagrange or gradient structure (Remark 6.12). A genuine convex-analytic structure, if present, would live in the dependence of μ_E on which coordinates occupy the leading, coarsest-weighted positions, viewed as a set function. Whether that set function is submodular is open. A positive answer would give a greedy $(1 - 1/e)$ approximation of π^* and exhibit a diminishing-returns law, each further master regulator added to the leading positions contributing less, as the discrete counterpart of the convexity that would underlie the selection. The analogous variable-ordering problem for binary decision diagrams is NP-complete [51], so μ_E -minimization may inherit that hardness or admit a p -adic pruning bound.*

The p -adic embedding and the measure μ yield a quantitative, ordering-dependent view of hierarchical stability that agrees with the known regulatory hierarchy in *A. thaliana* and recovers a partial order on genes from the transition map alone. Part II [2] develops the comparison between μ_{E^-} and μ_A -minimizing orderings, analyzes basin structure and mutant perturbations, and applies the framework to *C. elegans* and *D. melanogaster*.

9 Conclusions

This paper lifts finite discrete dynamical systems $f: \mathbb{F}_p^N \rightarrow \mathbb{F}_p^N$ into continuous non-Archimedean dynamics on the p -adic integers \mathbb{Z}_p , where the ultrametric matches the digit hierarchy of \mathbb{F}_p^N and exposes multi-scale structure that \mathbb{R} -valued embeddings collapse. Within this lift, a hierarchical stability measure μ and a ball-level classification of fixed points are derived from the discrete dynamics f and the coarse embedding ι alone, without constructing the rational interpreter ϕ explicitly (Theorem 6.8); minimizing μ over the symmetric group S_N defines a variational principle whose minimizer is intrinsic to the dynamics. Gene regulatory networks provide the motivating application; *A. thaliana* is the worked example here, with cross-organism application in the companion paper [2].

1. *Stability measure and the score budget.* The scores μ_E, μ_A, μ_I are functions of the ordering $\pi \in S_N$, changing as the coordinates are permuted. The weighted count $\mu_E(\pi) = \sum_{n=1}^{N-1} |E(n)| p^{N-n}$ penalizes expanding balls at coarse scales. The $A/E/I$ trichotomy partitions the p^n balls at every resolution (Lemma 6.2), so the three scores share a fixed budget $\mu_E + \mu_A + \mu_I = (N-1)p^N$ (Lemma 6.3), a constant set by N and p that serves as a numerical check on them. The substantive consequence is that the triple is not independent: minimizing expansion is equivalent to maximizing the sum of contraction and isometry, not to maximizing contraction alone (Remark 6.5).
2. *Optimal ordering and biological hierarchy.* In the *A. thaliana* floral network ($N = 13$), minimizing μ_E over all $13! \approx 6.2 \times 10^9$ orderings places known master regulators (UFO, EMF1, LFY, TFL1) in the leading positions, matching the biological hierarchy of the first eight regulators with Spearman $\rho = 1.0$ (Table 4). Exactly four orderings attain the global minimum $\mu_E = 26,776$; they differ only by transpositions within two pairs of positions (EMF1/LFY and AP2/FT) and share the full triple, recovering the hierarchy equally well (Remark 7.2).
3. *Classification sequences.* The scale-dependent $A/E/I$ classification at levels $n = 1, \dots, 4$ distinguishes floral organ fixed points (IEAA: expansion at level 2, contraction at levels 3–4) from inflorescence fixed points (IEEE: expansion persists at all finer scales). The p -adic classification separates them by scale-dependent behavior and identifies inflorescence as a developmental waypoint.

The two principal contributions.

The hierarchy π^* is the most legible result, but it is not the only one. The ball-level $A/E/I$ classification of fixed points is a *separate* contribution: to our knowledge, no non-Archimedean ball-level analogue of the attracting/repelling/indifferent trichotomy of point-level p -adic dynamics had been developed for finite discrete systems on \mathbb{F}_p^N in the form presented here, and the construction in Sections 4–6 supplies one. At every resolution n each fixed point inherits a label in $\{A, E, I\}$ from its containing ball, producing a word in $\{A, E, I\}^{N-1}$ that summarizes the orbit’s multiscale stability profile. This refines the binary “fixed/not-fixed” partition of standard discrete-dynamics analysis with three biologically meaningful regimes: A -rich profiles mark *robust developmental endpoints* (canalized cell fates); E -rich profiles mark *transient or decision states*; mixed profiles mark *threshold/bifurcation regimes*. Recovering known master regulators is the more striking structural consequence; the $A/E/I$ classification is the more novel mathematical contribution, and the two are conceptually independent.

The framework is general: it applies to any discrete dynamical system $f: \mathbb{F}_p^N \rightarrow \mathbb{F}_p^N$ for an arbitrary prime p , demonstrated for the cases $p = 3$ and $p = 5$ (Section 8), with the application to Boolean GRNs ($p = 2$) as one instance among cellular automata, lattice spin systems, and polynomial endomorphisms of \mathbb{F}_p^N (Section 3).

A variational principle as a Haar-integral functional on S_N .

The stability measure admits the integral expression $\mu_E(\pi) = p^N \int_{\mathbb{Z}_p} \Phi_\pi d\lambda_H$ (Remark 6.12, equation (29)), placing the variational problem $\pi^* = \arg \min_{\pi \in S_N} \mu_E(\pi)$ in the framework of integral functionals minimized under a finite group action on the

labeling of coordinates. The integrand $\Phi_\pi: \mathbb{Z}_p \rightarrow \mathbb{Z}_{\geq 0}$ is determined by (f, ι) , so the integration takes place entirely on the locally compact ring \mathbb{Z}_p with its normalized Haar measure. The construction is the non-Archimedean analogue of variational principles for averaged Lyapunov-type observables in classical ergodic theory [3, 14], with Φ_π as a scale-resolved roughness density and λ_H as the canonical reference measure on the embedded state space.

Outlook.

Characterizing when the variational principle becomes degenerate, the saturation phenomenon of Remark 6.4, is a natural open direction. The companion paper [2] carries the same machinery to the *C. elegans* and *D. melanogaster* developmental networks, compares μ_E - and μ_A -minimizing orderings, and develops basin-of-attraction and mutant-frequency analysis.

Software and reproducibility.

The construction of μ , the search for π^* (exhaustive, branch-and-bound, and genetic-algorithm heuristic), and the ball-level $A/E/I$ classification are bundled in the open implementation **p-GRN-Suite** (Pérez-Buendía, Nopal-Coello, and Cortés-Poza), registered with INDAUTOR. An interactive browser applet that runs the suite on user-supplied transition tables is available at <https://www.cimat.mx/~rogelio.perez/software/padic-grn/padic-balls-animation.html>. The complete reproducibility bundle (transition tables, branch-and-bound logs, analysis scripts, supplementary figures, and source code) is publicly available at Zenodo [27], doi:10.5281/zenodo.20709159.

Declarations

Funding

This work was supported by the project “Modelos matemáticos y computacionales no convencionales para el estudio y análisis de problemas relevantes en Biología” (CF 2019/217367) funded by SECIHTI, and by the Proyecto de Frontera.

Competing interests

The authors declare that they have no competing interests.

Authors’ contributions

J.R.-P.B.: Conceptualization, Methodology, Formal analysis, Software, Validation, Writing – original draft, Writing – review & editing, Funding acquisition, Project administration. **V.N.C.:** Conceptualization, Methodology, Formal analysis, Validation, Writing – review & editing.

Data availability

The transition table for the *A. thaliana* network, the reported optimal orderings (Section 7), the analysis scripts, and the source code are publicly available in the Zenodo reproducibility bundle, [doi:10.5281/zenodo.20709159](https://doi.org/10.5281/zenodo.20709159).

Acknowledgments

We thank the P-adagio working group and the p -adic research group for their support, and Esteban Sánchez Durán for his contributions in the early stages of this project, including the creation of the first models and computational implementations during his period as a research fellow in the Proyecto de Frontera “Modelos matemáticos y computacionales no convencionales para el estudio y análisis de problemas relevantes en Biología” (CF 2019/217367) funded by SECIHTI. The authors acknowledge support from the Supercomputing Center of CIMAT-Mérida “TOOLOK.”

References

- [1] Nopal Coello, V., Pérez-Buendía, J.R.: Gluing dynamics: ε -precision in solving a non-archimedean inverse problem. *Boletín de la Sociedad Matemática Mexicana* **31**(2), 52 (2025) <https://doi.org/10.1007/s40590-025-00730-y>
- [2] Pérez-Buendía, J.R., Nopal-Coello, V., Cortés-Poza, Y.: Regulatory p -Adic Orderings from Stability in Gene Networks: Applications and Validation in Three Developmental Systems. Preprint, Zenodo, [10.5281/zenodo.19426870](https://doi.org/10.5281/zenodo.19426870). (2026)
- [3] Anashin, V., Khrennikov, A.: Applied Algebraic Dynamics. De Gruyter Expositions in Mathematics, vol. 49. Walter de Gruyter, Berlin (2009). <https://doi.org/10.1515/9783110203011>
- [4] Arrowsmith, D.K., Vivaldi, F.: Geometry of p -adic Siegel discs. *Physica D: Nonlinear Phenomena* **71**(3), 222–236 (1994) [https://doi.org/10.1016/0167-2789\(94\)90191-0](https://doi.org/10.1016/0167-2789(94)90191-0)
- [5] Dragovich, B., Khrennikov, A.Y., Kozyrev, S.V., Mišić, N.Ž.: p -adic mathematics and theoretical biology. *Biosystems* **199**, 104288 (2021) <https://doi.org/10.1016/j.biosystems.2020.104288>
- [6] Zúñiga-Galindo, W.A.: Non-archimedean replicator dynamics and eigen’s paradox. *Journal of Physics A: Mathematical and Theoretical* **51**(50), 505601 (2018) <https://doi.org/10.1088/1751-8121/aaebb1>
- [7] Khrennikov, A.: Modelling of psychological behavior on the basis of ultrametric mental space: Encoding of categories by balls. *p-Adic Numbers, Ultrametric Analysis and Applications* **2**(1), 1–20 (2010) <https://doi.org/10.1134/S2070046610010012>

- [8] Khrennikov, A., Yurova, E.: Automaton model of protein: Dynamics of conformational and functional states. *Progress in Biophysics and Molecular Biology* **130**, 2–14 (2017) <https://doi.org/10.1016/j.pbiomolbio.2017.07.001>
- [9] Shmulevich, I., Dougherty, E.R., Kim, S., Zhang, W.: Probabilistic boolean networks: a rule-based uncertainty model for gene regulatory networks. *Bioinformatics* **18**(2), 261–274 (2002) <https://doi.org/10.1093/bioinformatics/18.2.261>
- [10] Saadatpour, A., Albert, R., Reluga, T.C.: A reduction method for Boolean network models proven to conserve attractors. *SIAM Journal on Applied Dynamical Systems* **12**(4), 1997–2011 (2013) <https://doi.org/10.1137/13090537X>
- [11] Mendoza, L., Alvarez-Buylla, E.R.: Dynamics of the genetic regulatory network for arabidopsis thaliana flower morphogenesis. *Journal of Theoretical Biology* **193**(2), 307–319 (1998) <https://doi.org/10.1006/jtbi.1998.0701>
- [12] Espinosa-Soto, C., Padilla-Longoria, P., Álvarez-Buylla, E.R.: A gene regulatory network model for cell-fate determination during *Arabidopsis thaliana* flower development that is robust and recovers experimental gene expression profiles. *The Plant Cell* **16**(11), 2923–2939 (2004) <https://doi.org/10.1105/tpc.104.021725>
- [13] Benedetto, R.L.: Dynamics in One Non-archimedean Variable. Graduate Studies in Mathematics, vol. 198. American Mathematical Society, Providence, RI (2019). <https://doi.org/10.1090/gsm/198>
- [14] Zúñiga-Galindo, W.A.: p -adic analysis: A quick introduction. In: Galindo, C., Melle Hernández, A., Moyano-Fernández, J., Zúñiga-Galindo, W. (eds.) *p-Adic Analysis, Arithmetic and Singularities*. Contemporary Mathematics, vol. 778, pp. 253–292. American Mathematical Society, Providence, RI (2022). <https://doi.org/10.1090/conm/778/15657> . Mini-Course, L. Santaló Research Summer School 2019, Santander, Spain
- [15] Zúñiga-Galindo, W.A.: p -Adic Analysis: Stochastic Processes and Pseudo-Differential Equations. *Advances in Analysis and Geometry*, vol. 11, p. 162. De Gruyter, Berlin (2025). <https://doi.org/10.1515/9783111578682>
- [16] Gouvêa, F.Q.: *P-adic Numbers: An Introduction*, 3rd edn. Universitext, p. 366. Springer, Cham (2020). <https://doi.org/10.1007/978-3-030-47295-5>
- [17] Alvarez-Buylla, E.R., Benítez, M., Balleza Dávila, E., Chaos, A., Espinosa-Soto, C., Padilla-Longoria, P.: Gene regulatory network models for plant development. *Current Opinion in Plant Biology* **10**(1), 83–91 (2007) <https://doi.org/10.1016/j.pbi.2006.11.008>
- [18] Kauffman, S.A.: Metabolic stability and epigenesis in randomly constructed genetic nets. *Journal of Theoretical Biology* **22**(3), 437–467 (1969) [https://doi.org/10.1016/0022-5193\(69\)90015-0](https://doi.org/10.1016/0022-5193(69)90015-0)

- [19] Glass, L., Kauffman, S.A.: The logical analysis of continuous, non-linear biochemical control networks. *Journal of Theoretical Biology* **39**(1), 103–129 (1973) [https://doi.org/10.1016/0022-5193\(73\)90208-7](https://doi.org/10.1016/0022-5193(73)90208-7)
- [20] Davidich, M.I., Bornholdt, S.: Boolean network model predicts cell cycle sequence of fission yeast. *PLoS ONE* **3**(2), 1672 (2008) <https://doi.org/10.1371/journal.pone.0001672>
- [21] Li, F., Long, T., Lu, Y., Ouyang, Q., Tang, C.: The yeast cell-cycle network is robustly designed. *Proceedings of the National Academy of Sciences* **101**(14), 4781–4786 (2004) <https://doi.org/10.1073/pnas.0305937101>
- [22] Bornholdt, S.: Less is more in modeling large genetic networks. *Science* **310**(5747), 449–451 (2005) <https://doi.org/10.1126/science.1119959>
- [23] Chaves, M., Albert, R., Sontag, E.D.: Robustness and fragility of boolean models for genetic regulatory networks. *Journal of Theoretical Biology* **235**(3), 431–449 (2005) <https://doi.org/10.1016/j.jtbi.2005.01.023>
- [24] Wolfram, S.: Universality and complexity in cellular automata. *Physica D: Nonlinear Phenomena* **10**(1–2), 1–35 (1984) [https://doi.org/10.1016/0167-2789\(84\)90245-8](https://doi.org/10.1016/0167-2789(84)90245-8)
- [25] Cortés-Poza, Y., Padilla-Longoria, P.: A variational approach to morphogenesis: Recovering spatial phenotypic features from epigenetic landscapes. *Bulletin of Mathematical Biology* **84**(3), 33 (2022) <https://doi.org/10.1007/s11538-022-00993-w>
- [26] Avetisov, V.A., Bikulov, A.H., Kozyrev, S.V., Osipov, V.A.: p -adic models of ultrametric diffusion constrained by hierarchical energy landscapes. *Journal of Physics A: Mathematical and General* **35**(2), 177–189 (2002) <https://doi.org/10.1088/0305-4470/35/2/300>
- [27] Pérez-Buendía, J.R., Nopal-Coello, V., Cortés-Poza, Y.: Reproducibility bundle for the hierarchical p -adic framework for gene regulatory networks. Zenodo. Transition tables, analysis scripts, branch-and-bound and saturation logs, and `p-GRN-Suite` source code for the present paper. (2026). <https://doi.org/10.5281/zenodo.20709159>
- [28] Chávez-Hernández, E.C., Quiroz, S., García-Ponce, B., Álvarez-Buylla, E.R.: The flowering transition pathways converge into a complex gene regulatory network that underlies the phase changes of the shoot apical meristem in *Arabidopsis thaliana*. *Frontiers in Plant Science* **13**, 852047 (2022) <https://doi.org/10.3389/fpls.2022.852047>
- [29] Pérez-Buendía, J.R., Cortés-Poza, Y., Padilla-Longoria, P.: Epigenetic forest and flower morphogenesis. *Computational Biology and Chemistry* **98**, 107667 (2022)

<https://doi.org/10.1016/j.compbiochem.2022.107667>

- [30] Weigel, D., Alvarez, J., Smyth, D.R., Yanofsky, M.F., Meyerowitz, E.M.: Leafy controls floral meristem identity in arabidopsis. *Cell* **69**(5), 843–859 (1992) [https://doi.org/10.1016/0092-8674\(92\)90295-N](https://doi.org/10.1016/0092-8674(92)90295-N)
- [31] Blázquez, M.A., Soowal, L.N., Lee, I., Weigel, D.: Leafy expression and flower initiation in arabidopsis. *Development* **124**(19), 3835–3844 (1997) <https://doi.org/10.1242/dev.124.19.3835>
- [32] Chae, E., Tan, Q.K.C., Hill, T.A., Irish, V.F.: An arabidopsis f-box protein acts as a transcriptional co-factor to regulate floral development. *Development* **135**(7), 1235–1245 (2008) <https://doi.org/10.1242/dev.015842>
- [33] Sung, Z.R., Belachew, A., Bai, S., Bertrand-Garcia, R.: Emf, an arabidopsis gene required for vegetative shoot development. *Science* **258**(5088), 1645–1647 (1992) <https://doi.org/10.1126/science.258.5088.1645>
- [34] Shannon, S., Meeks-Wagner, D.R.: A mutation in the arabidopsis *tfl1* gene affects inflorescence meristem development. *The Plant Cell* **3**(9), 877–892 (1991) <https://doi.org/10.1105/tpc.3.9.877>
- [35] Waddington, C.H.: *The Strategy of the Genes*. Allen & Unwin, London, UK (1957). Classic work on developmental biology and epigenetics. Reprint: Routledge, 2015, ISBN 9781138998131. <https://www.routledge.com/The-Strategy-of-the-Genes/Waddington/p/book/9781138998131>
- [36] Huang, S.: The molecular and mathematical basis of waddington’s epigenetic landscape: A framework for post-darwinian biology? *BioEssays* **34**(2), 149–157 (2012) <https://doi.org/10.1002/bies.201100031>
- [37] Trinh, V.-G., Park, K.H., Pastva, S., Rozum, J.C.: Mapping the attractor landscape of Boolean networks with biobalm. *Bioinformatics* **41**(5), 280 (2025) <https://doi.org/10.1093/bioinformatics/btaf280>
- [38] Pérez-Buendía, J.R.: Rational Interpreters for Discrete Dynamics: Existence, Exactness, and Decomposition over p -adic Fields. Companion paper, in preparation. (2026)
- [39] Khrennikov, A.Y., Nilsson, M.: p -Adic Deterministic and Random Dynamics. *Mathematics and Its Applications*, vol. 574. Kluwer Academic Publishers, Dordrecht (2004). <https://doi.org/10.1007/978-1-4020-2660-7>
- [40] Khrennikov, A.Y., Kozyrev, S.V.: Genetic code and deformation of the 2-dimensional 2-adic metric. *p -Adic Numbers, Ultrametric Analysis and Applications* **3**(2), 165–168 (2011) <https://doi.org/10.1134/S2070046611020087>

- [41] Naldi, A., Remy, E., Thieffry, D., Chaouiya, C.: Dynamically consistent reduction of logical regulatory graphs. *Theoretical Computer Science* **412**(21), 2207–2218 (2011) <https://doi.org/10.1016/j.tcs.2010.10.021>
- [42] Cortés-Poza, Y., Pérez-Buendía, J.R.: Topological structure of epigenetic forests in flower morphogenesis. *Bulletin of Mathematical Biology* (2026). to appear (accepted, manuscript BMAB-D-26-00148R1)
- [43] Fabre-Monplaisir, J., Mossé, B., Remy, E.: Isometries of the hypercube: A tool for Boolean regulatory networks analysis. *Physica D: Nonlinear Phenomena* **424**, 132831 (2021) <https://doi.org/10.1016/j.physd.2020.132831>
- [44] Barabási, A.-L., Oltvai, Z.N.: Network biology: Understanding the cell’s functional organization. *Nature Reviews Genetics* **5**(2), 101–113 (2004) <https://doi.org/10.1038/nrg1272>
- [45] Kadelka, C., Butrie, T.-M., Hilton, E., Kinseth, J., Schmidt, A., Serdarevic, H.: A meta-analysis of Boolean network models reveals design principles of gene regulatory networks. *Science Advances* **10**(2), 0822 (2024) <https://doi.org/10.1126/sciadv.adj0822>
- [46] Morone, F., Leifer, I., Makse, H.A.: Fibration symmetries uncover the building blocks of biological networks. *Proceedings of the National Academy of Sciences* **117**(15), 8306–8314 (2020) <https://doi.org/10.1073/pnas.1914628117>
- [47] Rozum, J.C., Marcus, A.M., Sizek, H., Rocha, L.M.: CANA v1.0.0: efficient quantification of canalization in automata networks. *Bioinformatics* **41**(10), 461 (2025) <https://doi.org/10.1093/bioinformatics/btaf461>
- [48] Dimitrova, E., Stigler, B., Kadelka, C., Murrugarra, D.: Revealing the canalizing structure of Boolean functions: Algorithms and applications. *Automatica* **146**, 110630 (2022) <https://doi.org/10.1016/j.automatica.2022.110630>
- [49] Murrugarra, D., Veliz-Cuba, A., Dimitrova, E., Kadelka, C., Wheeler, M., Laubenbacher, R.: Modular control of Boolean network models. *Bulletin of Mathematical Biology* **87**(7), 91 (2025) <https://doi.org/10.1007/s11538-025-01471-9>
- [50] Krämer, A.: Master regulators as order parameters of gene expression states. *Physical Review E* **103**(1), 012409 (2021) <https://doi.org/10.1103/PhysRevE.103.012409>
- [51] Bollig, B., Wegener, I.: Improving the variable ordering of OBDDs is NP-complete. *IEEE Transactions on Computers* **45**(9), 993–1002 (1996) <https://doi.org/10.1109/12.537122>